AD-A100 443 VON KARMAN INST FOR FLUID DYNAMICS RHODE-SAINT-GENESE--ETC F/G 20/4
NONUNIFORM ENERGY TRANSFER IN AXIAL FLOW COMPRESSORS.(U)
JUN 80 G HOLBROOK AFOSR-80-0119
UNCLASSIFIED VKI-PR-1980-16 EOARD-TR-81-4 NL

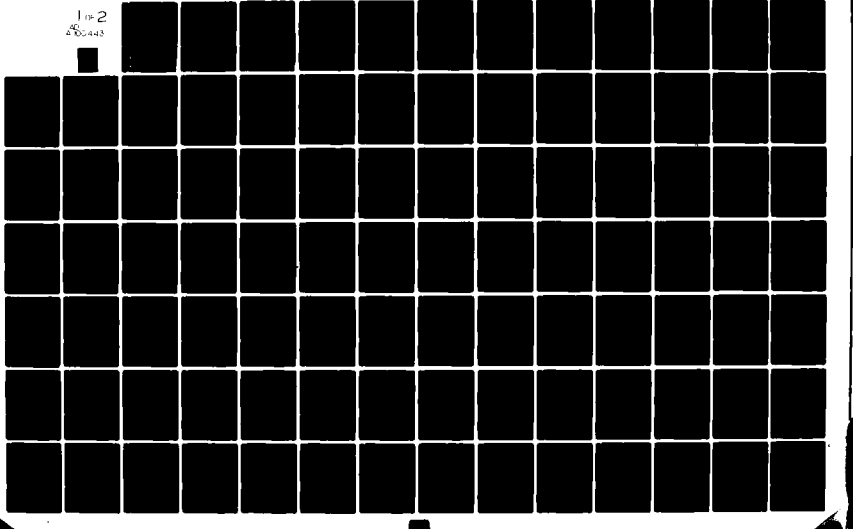

GRANT AFOSR 80-0119
Final Scientific Report
1980 Jan 15-1981 Jan 14

NONUNIFORM ENERGY TRANSFER IN AXIAL FLOW COMPRESSORS

G. Holbrook

REPORT DOCUMENTATION PAGE		READ INSTRUCTIONS BEFORE COMPLETING FORM
1. Report Number EOARD-TR-81-4	2. Govt Accession No. AD-A100 443	3. Recipient's Catalog Number
4. Title (and Subtitle) NONUNIFORM ENERGY TRANSFER IN AXIAL FLOW COMPRESSORS		5. Type of Report & Period Covered Final Scientific Report. 1980 Jan 15-1981 ~~Jan~~ 14 6. Performing Org. Report Number VKI-PR-1980-16
7. Author(s) G. HOLBROOK		8. Contract or Grant Number GRANT AFOSR-80-0119
9. Performing Organization Name and Address von Karman Institute Chaussée de Waterloo 72 B-1640 Rhode Saint Genèse, Belgium		10. Program Element, Project, Task Area & Work Unit Numbers 61102F 2301/D1
11. Controlling Office Name and Address Air Force Office of Scientific Research /PKN Bolling AFB Washington DC 20332		12. Report Date June 1980 13. Number of Pages 109
14. Monitoring Agency Name and Address EOARD / LNE PO Box 14 FPO Box 09510		15.

16. & 17. Distribution Statement

Approved for public release; distribution unlimited.

18. Supplementary Notes

19. Key Words

Axial flow compressors

20. Abstract

Current through flow calculation schemes provide the compressor designer with a 2D inviscid flow analysis of a blade row. Due to blade curvature and viscous effects the flow field is quite 3D. A numerical scheme has been developed to calculate the radial migration of secondary flows in a rotating blade row and the influence of these flows on the energy transfer of the rotor. A simple set of equations for the radial equilibrium and resulting trajectory of these fluid particles is derived. A boundary layer calculation was added to correctly model rotor boundary layer fluid. The calculation scheme was then applied to 2D flow field obtained from an existing through flow analysis of a transonic rotor. The results showed the twisting of the free stream streamsheet due to the blade-to-blade velocity gradient, the magnitude of the boundary layer migration and the influence of the radial shift on the enthalpy rise of these particles. The resulting values of radial velocity and temperature rise are similar to experimentally measured values. Thus, this calculation scheme can provide the compressor designer with a quick first approximation of the influence of 3D and viscous effects on the flow field of a rotating blade row.

This report has been reviewed by the Information Officer (EOARD/CI) and is releasable to the National Technical Information Service (NTIS). At NTIS it will be releasable to the general public, including foreign nations.

This technical report has been reviewed and is approved for publication.

John T. Milton

JOHN T. MILTON
Scientific and Technical
Information Officer

WINSTON K. PENDLETON
Lt Colonel, USAF
Chief, Propulsion & Energy

Gordon L. Hermann

GORDON L. HERMANN
Lt Colonel, USAF
Deputy Commander

A 23
80

ABSTRACT

Current through-flow calculation schemes provide the compressor designer with a 2-dimensional inviscid flow analysis of a blade row. Due to blade curvature and viscous effects the flow field is quite 3-dimensional. A numerical scheme has been developed to calculate the radial migration of secondary flows in a rotating blade row and the influence of these flows on the energy transfer of the rotor. A simple set of equations for the radial equilibrium and resulting trajectory of these fluid particles is derived. A boundary layer calculation was added to correctly model rotor boundary layer fluid. The calculation scheme was then applied to the 2-dimensional flow field obtained from an existing through-flow analysis of a transonic rotor. The results showed the twisting of the freestream streamsheet due to the blade-to-blade velocity gradient, the magnitude of the boundary layer migration and the influence of the radial shift on the enthalpy rise of these particles. The resulting values of radial velocity and temperature rise are similar to experimentally measured values. Thus this calculation scheme can provide the compressor designer with a quick first approximation of the influence of 3-dimensional and viscous effects on the flow field of a rotating blade row.

TABLE OF CONTENTS

LIST OF SYMBOLS

C_f	skin friction coefficeint
F	force
H	stagnation enthalpy
I	calculation station increment
L	Lefoll velocity profile parameter
P	static pressure
R	radial location
t	time
Δt	time increment
u	local velocity
U	wheel speed
U_∞	freestream velocity in Eq. 3.13
V	velocity
y	normal distance to blade
Y	circumferential distance
β	relative flow angle
δ_E	exit boundary layer thickness
η	non-dimensional boundary layer distance, y/δ
ρ	fluid density
σ	velocity ratio factor

Subscripts

FS	freestream
P	particle
R	radial component
u	tangential component
z	axial component

LIST OF FIGURES

1. INTRODUCTION

Current compressor analysis tools include through-flow calculation schemes which provide the compressor designer with an inviscid axisymmetric view of the flow field within a blade row. Such results are useful for determining the radial variations in the flow field for a mean blade-to-blade streamline. Such a meridional streamline network is shown in Figure 1 for a transonic rotor. Blade curvatures and viscous effects however cause considerable distortion of this flow field. The blade curvatures produce a velocity gradient in the blade-to-blade plane creating a non-axisymmetric flow field. This velocity gradient will also cause some warpping or twisting of the blade-to-blade streamsheet (see Figure 2.). Viscosity of the fluid will produce hub and tip casing and blade boundary layers and wakes producing a highly three-dimensional flow. Thus while being a useful engineering tool the through-flow calculation needs to be supplimented with a procedure for determining these additional three-dimensional aspects of the flow field.

Due to the fluid viscosity some of the fluid particles in the flow field will have a deficit or defect in velocity relative to the essentially inviscid free-stream flow. These low momentum fluid particles are subjected to the same pressure forces, both circumferen-

tially and radially, as the freestream but due to their lower momentum their path or trajectory through the blade row will be influenced more by these forces. This momentum deficit is thus the source of some of the secondary flows in the blade row. A classical example of such secondary flows is the migration of endwall boundary layer fluid from the pressure surface to the suction surface of a turbine nozzle vane row. The radial migration of rotor blade boundary layer fluid is another example of these flows.

Several experimentam investigations have presented complete three-dimensional measurements of a rotor exit flow field (REF 1,2,3,4). These studies have shown that radial velocities in a rotor wake (due to the radial migration of boundary layer fluid) can be quite large. Values of these measured radial velocities range from 10% - 15% of the axial velocity in a low speed rotor (REF 2,3) to reportedly as much as 100% of the axial velocity for a transonic rotor (REF 4). It has also been shown that the magnitude of the radial velocity in the wake is influenced by the blade loading (REF 3).

One aspect of these secondary flows that has not recieved much attention is how the energy transfer of the rotating blade row is influenced by these flows. It was originally believed that due to the relative motion of the rotating and stationary blade rows circum-

ferential variations in the flow field would be quickly "mixed out". Measurements (REF 5) have however shown that variations in the total temperature as large as 10% of the overall stage temperature rise can still exist at the exit of a stator row downstream of the rotor. These variations in total temperature could only have been caused by the uneven energy addition of the rotor. It is believed that the secondary flows in the rotating blade row are the source of these temperature variations. The magnitude of these variations is significant when attempting to calculate rotor or stage efficiency from measured exit total temperature. The existing temperature gradient can also be the source of thermally induced secondary flows (REF 6).

Smith (REF 7) showed that the energy transfer to a fluid particle in a turbomachine is proportional to the time the particle remains within the rotating blade row. Thus low momentum particle that, due to their velocity defect, remain within the rotating frame longer will acquire a larger enthalpy increase than freestream fluid. These low momentum particles will also have a tendency to move radially outward due to an imbalance of pressure forces and centrifugal forces. This change in radial location will contribute further to the increased energy transfer to the low momentum particles.

With a simple wake model Kerrebrock and

Mikolajczak (REF 8) showed that blade boundary layer fluid due to a slip velocity of the resulting wake will tend to be separated from the freestream fluid as the flow progresses through the successive blade rows. Thus the low momentum but high total temperature wake fluid of the rotor will tend to be collected by the downstream stator and appear in the wake of the stator blade. Thus areas of concentrated high total temperature rotor wake fluid can occur.

Experimental evidence of circumferential total temperature variations in the flow field has been presented by Keenan (REF 5), Leboeuf (REF 9) and Kool (REF 10). Analytical attempts at predicting the influence of secondary flows on the energy transfer and the resulting temperature field are scarce. Before such an analysis can be made it is important to properly predict the secondary flows themselves. Thus a significant portion of this project is devoted to establishing a simple yet physically correct model for the low momentum particles in a rotating blade row. Such a model should include not only the influence of viscosity but also the effects of blade and meridional flow path curvatures.

Throughout this analysis the author took a "particle" approach for formulating and mentally visualizing the resulting secondary flows. This involved assuming an inviscid fluid particle that for some reason

has a velocity different form that of the freestream is allowed to pass through the pressure field of the rotor blade passage. The presence of the freestream fluid is ignored. Thus no mixing or interaction between the particle and the freestream is considered. However with the technique developed such interactions can be introduced through the specification of the velocity and the relative flow angle evolution of the particle. Generally particles that have a velocity defect (as apposed to a velocity excess) are of the most interest, so the analysis was developed in terms of low momentum particles. The analysis does however apply equally well to particles that have a velocity greater than that of the freestream. This should be kept in mind throughout the explanation of the calculation technique. The particle approach helped a great deal in obtaining an intuitive insight into what parameters were important for the calculation of the particle trajectory. The author relied heavily on this intuitive approach to lead to the correct mathamatical formulation. The importance of correctly modelling the physical behavior of the particle seemed to dictate such an approach, making mathamatical derivations and justifications of secondary importance. Thus few such rigorous mathamatical principles will be presented in this analysis.

2. MECHANISMS OF ENERGY TRANSFER

The fundamental equation for the energy transfer in a turbomachine is the Euler pump equation

$$\Delta H = U_2 V_{u_2} - U_1 V_{u_1} \tag{2.1}$$

The enthalpy addition in a compressor is dependent upon the change in tangential velocity from inlet to exit and on the wheel speed. Basically two different mechanisms for the energy transfer exist. They are the residence time of the particle within the blade row (resulting in tangential velocity changes) and the radial shift of the particle (resulting in changes in the local wheel speed). Due to the associated axial velocity defect of a low momentum particle the time necessary for the particle to pass through the rotor blade passage is greater than that of the freestream fluid. Smith (REF 7) showed that the instantaneous enthalpy addition for an inviscid fluid particle can be expressed as

$$\frac{DH}{Dt} = \frac{1}{\rho} \frac{\partial P}{\partial t} \tag{2.2}$$

where

H : stagnation enthalpy per unit mass

t : time

ρ : density

P : static pressure

In a compressor the right hand side of this equation is positive, so the energy transfer increases as the residence time for a particle becomes greater. This effect can perhaps be seen more clearly by examining the velocity triangles for a low momentum particle and the freestream. Figure 3a is such a velocity triangle for a particle having a defect in the absolute velocity at the enterance of a rotor blade row. Note that the low momentum particle has a smaller absolute tangential velocity than the freestream and also that the relative flow angle of the particle is larger than that of the freestream. Thus the rotor will "see" such low momentum particles as fluid entering the blade row with a high positve incidence. It is assumed throughout this analysis that a particle regardless of the magnitude of the velocity defect or excess will leave the rotor blade row at the same relative flow angle as the mean freestream flow. The rotor exit velocity triangle for the freestream and a low momentum particle is shown in Figure 3b. Here it can be seen that due to associated defect in the axial velocity the low momentum particle has a larger absolute tangential velocity than the freestream. From Eq. 2.1 it can be seen that (assuming equal wheel speeds) the low momentum particle will have a larger enthalpy increase than the freestream. As the magnitude of the velocity defect of the particle becomes greater (i.e. as the axial velocity of the particle is reduced) this difference in the energy transfer for the particle and the freestream will become

larger. The above example was for a particle entering the blade row with an absolute velocity defect. A second possibility exists and that is for a particle entering the blade row with the freestream velocity but due to viscous (or other) effects in the blade passage it leaves the blade row with a defect in the exit relative velocity. The inlet and exit velocity triangles for such a situation are shown in Figure 4. Again due to the velocity defect the particle leaves the blade row with a larger absolute tangential velocity and thus will have a larger enthalpy increase.

Up to this point the influence of changes in the wheel speed has been neglected. From Eq. 2.1 and the velocity triangles of Figure 3. and 4. the influence of the wheel speed can be seen. The wheel speed increases proportionally with the radial location. For two particles with equal inlet and exit tangential velocities the particle with the larger wheel speed will have the larger enthalpy increase. Note that the magnitude of the wheel speed also influences the resulting tangential velocity, thus having a double effect on the enthalpy increase (i.e. enthalpy rise increases with the square of the wheel speed). The influence of changes in wheel speed on the energy transfer is an important aspect of this analysis because the radial pressure field of the blade row will tend to cause low momentum fluid particles to migrate radially outward. Throughout this analysis it is vital

to keep in mind the relationship of the velocity components and the wheel speed to each other in the velocity triangles for the particle and the freestream.

There are two factors that will determine the magnitude of the radial migration of the low momentum fluid particles. First, the magnitude of the imbalance of the pressure forces and the centrifugal forces determines the size of the resultant force on the particle relative to the freestream. The magnitude of this force is dependent upon the difference between the tangential velocity of the particle and the tangential velocity of the freestream at the same radial location. The second parameter influencing the amount of radial shift is the time this net force is applied to the particle. The greater the length of time the force is applied the larger will be the deflection of the particle from a freestream streamline trajectory. This is the so called residence time of the particle and it is directly dependent upon the axial velocity of the particle. Thus the size of the velocity defect effects not only the magnitude of the force imbalance of the particle but also the time this force is applied. The relative flow angle influences the magnitude of the tangential velocity and thus the size of the applied force on the particle.

3. THE COMPUTER PROGRAM

Prior to investing a great deal of time and effort creating an elaborate computational scheme for calculating the trajectory of a low momentum particle a very simple computer program was written to test the feasibility of such a calculation. It was also possible to gain some insight into the assumptions necessary for and the restrictions of this type of calculation from an initial test program.

The calculation of the trajectory of a particle is centered around a radial equilibrium equation. For the initial program the simplest form of the radial equilibrium equation was used

$$\frac{1}{\rho}\frac{\partial \rho}{\partial R} = \frac{V_u^2}{R} \qquad (3.1)$$

This equation is a statement of the assumption that the centrifugal forces generated by the freestream fluid "circling" the compressor axis are in equilibrium with the radial pressure field. Low momentum particles in the flow field are subjected to the same radial pressure field, but due to their lower momentum the trajectory of these particles will be influenced more by the radial pressure field. The low momentum particles will "seek" a radial location where the pressure forces and centrifugal forces are again balanced. For particles with an

excess of tangential velocity (normally associated with low momentum particles) this equilibrium location will occur at a larger radius. This equilibrium equation is the only velocity related equation used in the initial analysis so it is necessary to make two additional assumptions in order to solve for the two remaining velocity components. The first of these assumptions is that the velocity ratio, σ , which is the ratio of the particle axial velocity to the freestream axial velocity is a constant through the entire blade row. The second assumption necessary concerns the evolution of the relative flow angle of the particle. In this initial analysis only defects in entering absolute velocity were considered. From Figure 3.a it can be seen that the inlet relative flow angle, β , is established by the freestream flow direction and the velocity ratio, σ . The resulting relative flow angle for the particle can be considerably larger than the freestream angle at the inlet, but these two angles are assumed to be equal at the blade exit. Thus it is necessary to specify how the relative flow angle of the particle evolves through the blade row. A simple linear variation was used. That is, when the particle is one-half of the way through the blade row the difference between the relative flow angles of the particle and the freestream is assumed to be one-half of what it was at the inlet of the blade row. These two assumptions were made to keep the initial test program as simple as possible. With the equilibrium equation of

3.1 and these assumptions the initial program was written and tested. The freestream velocity field was generated by a Katsanis-McNally through-flow calculation and used as input data for the program. The results of this simplified approach were encouraging and enlightening. There were some discovered limitations of the simple approach but the technique seemed to warrant further improvements and refinements. These improvements would involve the equilibrium equation and the limitations of the velocity and relatve flow angle evolution used.

The final program consists of a MAIN deck and four supplimentary subroutines. All of the trajectory and energy calculation are done in the MAIN deck. Two interpolation subroutines are used to obtain velocity/space interpolations (LININT) and interpolations of various parameters that are a function of one variable only (INTERPOL). The two remaining subroutines are concerned with a boundary layer thickness calculation (BONLAY) and the resulting boundary layer velocity profile (VELRATIO). Because the principle objective of this project was the development of the calculation technique, the procedure will be explained in some detail. For persons interested only in using the program the input and output are explained in Appendix I and II along with a program listing and examples of input and output data.

3.1 MAIN Deck

The results of the initial program indicated a serious limitation of the equilibrium equation used. When a particle was introduced with a velocity ratio equal to unity (i.e. σ = 1.00) the trajectory calculated was that of a straight line in the meridional plane. The slope of this trajectory was determined by the initial radial velocity which then remained constant through the blade row. The equilibrium equation did not take into account the radial acceleration of the freestream (i.e. changes in radial velocity along a freestream streamline). This simple equilibrium equation took into account only the acceleration of the particle relative to the freestream (which is zero for σ = 1.00). The reason for this result can be seen by examining the radial component of the Euler Equations

$$\frac{F_{NET}}{\rho} = -\frac{1}{\rho}\frac{\partial P}{\partial R} + \frac{V_u^2}{R} = \frac{DV_R}{Dt} \qquad (3.2)$$

This equation is Newton's 2nd Law applied to a fluid particle, equating the sum of the forces (per unit mass) to the net acceleration of the particle. It can be seen that use of the initial equation for the radial equilibrium (3.1) assumed that no net acceleration of the freestream existed. This is not the case if the radial velocity of the freestream varies along a streamline (due, for example, to meridional curvatures).

It was also realized that for a velocity ratio of unity (σ = 1.00) the calculation scheme must be able to properly calculate the radial location of a freestream streamline through the blade row. Clearly 3.1 is not capable of doing this because there were large radial variations in the freestream due mainly to the meridional curvatures. Thus a first "test case" for any new calculation scheme will be "can it properly calculate the radial location of a freestream streamline through the blade row".

A brief explanation of the equilibrium equation used in the final program will now be given. The radial equilibrium equation of 3.2 must apply for all particles in the flow field. Writing the equation for a freestream (FS) particle and a low momentum (P) particle yields

$$\frac{DV_R}{Dt}\Big)_{FS} = \frac{V_u^2}{R}\Big)_{FS} - \frac{1}{\rho}\frac{\partial P}{\partial R}\Big)_{FS} \qquad (3.3)$$

$$\frac{DV_R}{Dt}\Big)_{P} = \frac{V_u^2}{R}\Big)_{P} - \frac{1}{\rho}\frac{\partial P}{\partial R}\Big)_{P} \qquad (3.4)$$

The radial pressure field of the freestream is imposed upon the low momentum particles. Therefore,

$$-\frac{1}{\rho}\frac{\partial P}{\partial R}\Big)_{P} = -\frac{1}{\rho}\frac{\partial P}{\partial R}\Big)_{FS} \qquad (3.5)$$

Rewriting the freestream equilibrium equation as

$$-\frac{1}{\rho}\frac{\partial P}{\partial R}\Big)_{FS} = \frac{DV_R}{Dt}\Big)_{FS} - \frac{V_u^2}{R}\Big)_{FS} \qquad (3.6)$$

and substituting in for the pressure gradient term in the equilibrium equation of the low momentum particle yields

$$\frac{DV_R}{Dt}\Big)_{p} = \frac{DV_R}{Dt}\Big)_{FS} + \frac{V_u^2}{R}\Big)_{p} - \frac{V_u^2}{R}\Big)_{FS} \qquad (3.7)$$

From this equation it can be seen that the total radial acceleration of the particle is equal to that of the freestream plus the acceleration of the particle relative to the freestream due to an imbalance of the centrifugal and pressure forces. If the centrifugal terms are of equal magnitude for the particle and freestream, the net radial acceleration of the particle is equal to that of the freestream and thus should follow the same trajectory (or streamline) as a freestream particle.

It was found that a freestream meridional streamline could be satisfactorily approximated by a Taylor series expansion for the radius, R. That is,

$$R(I+1) = R(I) + \frac{dR}{dt}\Big)_I \Delta t + \frac{d^2R}{dt^2}\Big)_I \frac{\Delta t^2}{2} \qquad (3.8)$$

where "I" and "I+1" indicate axial computational stations. This equation can be simplified and solved by recognizing that the first derivative term of Equation 3.8 is the

radial velocity and the second derivative term is the radial acceleration. Approximating the acceleration term by a forward difference scheme and neglecting all terms of the $O(\Delta t^3)$ and smaller yields,

$$R(I+1) = R(I) + V_R(I)\,\Delta t + \left[\frac{V_R(I+1) - V_R(I)}{\Delta t}\right]\frac{\Delta t^2}{2} \qquad (3.9)$$

which can be further simplified to

$$R(I+1) = R(I) + \left[\frac{V_R(I+1) + V_R(I)}{2}\right]\Delta t \qquad (3.10)$$

This trajectory equation states that the new radial location (i.e. at the new axial station) is equal to the old radial location plus the average radial velocity of the particle over the interval times the time the particle is within this interval. The resulting trajectory for a freestream particle (i.e. σ = 1.00) is in very good agreement with the radial location of the meridional streamline calculated by the through-flow calculation. Solving equation 3.10 involves an iterative solution because $V_R(I+1)$ is a function of the new radial location, $R(I+1)$.

The equilibrium equation is again the only equation that relates the trajectory of the particle to the freestream flow field. Thus it is possible to calculate only one new velocity component. Auxilary equations or assumptions are necessary for the two

remaining velocity components. As with the initial program it was decided to specify as input the additional pieces of information but remove some of the limiting restrictions of the initial program. The two additional parameters are again the evolution of the velocity ratio, σ , and the relative flow angle of the particle. Every effort was made to keep this program as flexible as possible by giving the user complete control over these parameters via an easily changed input. The values of the velocity ratio and relative flow angle can be specified as arbitrary functions of the axial distance through the blade row, or for relative velocity defects (such as surface velocity distributions or boundary layer particles) calculated within the program from the surface velocity data or the boundary layer model.

The equilibrium equation of 3.7 is solved using a forward difference scheme yielding

$$\left[\frac{V_R(I+1)-V_R(I)}{\Delta t}\right]_P = \left[\frac{V_R(I+1)-V_R(I)}{\Delta t}\right]_{FS} + \left(\frac{V_u^2}{R}\right)_P - \left(\frac{V_u^2}{R}\right)_{FS} \quad (3.11)$$

A physical interpretation of this equation is easier when equation 3.11 is written as

$$V_R(I+1) = V_R(I) + \left[V_R(I+1)-V_R(I)\right]_{FS}\frac{\Delta t_P}{\Delta t_{FS}} + \left[\left(\frac{V_u^2}{R}\right)_P - \left(\frac{V_u^2}{R}\right)_{FS}\right]\Delta t_P \quad (3.12)$$

The new radial velocity (at the next axial station) $V_R(I+1)$ is equal to the old radial velocity plus the

change in freestream radial velocity "weighted" by the ratio of residence time for a low momentum particle and the freestream plus an additional term due to the difference in centrifugal and pressure forces. From this equation it is easy to see the influence of the residence time and the tangential velocity difference on the rate of change of the radial velocity of the particle.

Equation 3.12 and 3.10 are used to calculate the velocity and radial location of the particle at a new axial calculation station. From the known freestream velocity values the axial velocity, V_z, and the tangential velocity, V_u, of the particle can be determined using the supplied input data for the velocity ratio and relative flow angle evolution. However, because these values are functions of the new radial location it is necessary again to "guess" a new radial location and solve equation 3.12 ans 3.10 iteratively until the guessed radial location and the calculated value are within a specified tolerance.

Once the complete trajectory of the particle is obtained the energy transfer calculations can be made. These calculations are made for the three streamlines shown in Figure 5. Streamline A is the freestream streamline coinciding with the radial location of the particle at the inlet of the blade row. Streamline B is the freestream streamline coinciding with the radial location of

the particle at the exit of the blade. The temperature difference between streamline A and the particle represents the additional energy transfer due to the different velocity evolution of the particle. The temperature difference between streamline B and the particle indicates the size of the temperature variations in the flow field that will exist at the exit of the rotor.

3.2 Subroutine LININT

This subroutine is a three-dimensional interpolation routine used to obtain velocity values of the freestream at a specified meridional location, from the streamline values obtained from the through-flow calculation. The through-flow calculation provides freestream velocity values along seven meridional streamlines (hub, 10%, 30%, 50%, 70%, 90%, and tip) with 10 to 15 values within the blade row for each streamline. This routine was obtain from an existing program.

3.3 Subroutine INTERPOL

This subroutine is also an interpolation routine. It is used to interpolate between values of surface velocity, relative flow angle, and velocity ratio that are supplied as functions of the axial distance only. This interpolation routine was written by the author.

3.4 Subroutine BONLAY

This routine is a simple boundary layer calculation used to obtain the total boundary layer thickness evolution, the skin friction coefficient, and a velocity profile parameter (Lefoll's L) for the rotor blade. Emperical correlations are used for the conventional shape factor (H_{12}) and the skin friction coefficient (REF 11). An additional emperical correlation was used (see REF 12) to obtain the total boundary layer thickness from the calculated momentum thickness. This value is dependent upon the assumed boundary layer velocity profile (Lefoll). Some difficulty arose in defining a starting condition for the calculation. A simple fundamental equation was derived and used to establish a flat plate type starting condition. The boundary layer thickness calculation was a finite differnece scheme (using a central difference) for the intergral boundary layer equation. The calculation procedure assumed the boundary layer to be turbulent and no condition was used to detect separation. Thus care must be used when calculating boundary layers where separation may occur.

3.5 Subroutine VELRATIO

Once the total boundary layer thickness evolution is known it is possible to calculate the velocity

defect of a boundary layer particle at any location within the boundary layer for an assumed velocity profile. To keep the boundary analysis as simple as possible it was decided to use the Lefoll (REF 13) boundary layer profile. This velocity profile can be represented by

$$\frac{u}{U_\infty} = 1 - \sqrt{\frac{c_f}{2}}\left[\frac{\eta^2-1}{2} - \ln(\eta) + L(2\eta^3 - 3\eta^2 + 1)\right] \qquad (3.13)$$

From a specified location within the boundary layer it is possible to obtain the local velocity ratio for a particle at that location in the boundary layer. An assumptions was necessary concerning the shape of the streamline of a boundary layer particle in the blade-to-blade plane. The assumption made was that a boundary layer particle will travel on a streamline that is a constant distance, y, from the surface of the blade. This distance is spcified as a fraction of the exit boundary layer thickness, δ_E . Thus it is possible to choose how "deep" in the boundary layer the particle of interest is. As shown in Figure 6., for y/δ_E = 1.00 the velocity of the particle will be equal to the freestream surface velocity. As y/δ_E becomes smaller the particle enters the boundary layer progressively nearer the blade leading edge and thus the particle will leave the blade row with a larger velocity defect. The velocity defect is not only a function of the specified y/δ_E but also of the evolution of the boundary layer thickness.

3.6 Modes of Operation

The program was developed to handle two distinctly different applications. The specification of the velocity ratio has been separated for absolute velocity ratios and relative velocity ratios (see Figure 3. and Figure 4.). For a defect in the absolute velocity the particle enters the blade row with a relative flow angle different from that of the freestream. This relative flow angle difference does influence the trajectory of the particle because it changes the tangential velocity term in equation 3.12. For this mode of operation it is necessary to supply as input how the relative flow angle progresses from the inlet value to the exit value. In this mode of operation it is possible to model inlet flow nonuniformities such as casing boundary layers and upstream blade wakes entering the blade row and determine the influence of these flows on the energy transfer. Due to a lack of time and the additional complexity of establishing wake or boundary layer decay models this mode of operation was not used during the course of this project. It should be noted however that such entrainment, wake decay and mixing models do exist in the literature and could be incorporated in this calculation procedure. The input format now is such as to allow the user to quickly and easily change the velocity ratio and flow angle evolution data.

The second mode of operation is for velocity ratios in the relative velocity. Here the relative flow direction is not influenced by the velocity ratio, σ. The particle will have the freestream relative flow angle everywhere in the blade row making the specification of the relative flow angle evolution unnecessary. One further simplification was made for this mode of operation. All blade-to-blade streamlines (suction surface to pressure surface) are considered to be the same shape as the mean streamline. That is, the relative flow angle evolution for all blade-to-blade streamlines is assumed equivalent to that of the mean freestream which is essentially the blade camber line. Thus the blades are replaced by their camber lines only as shown in Figure 7. For thin blades away from the leading edge this is a reasonable approximation. The through-flow calculation scheme included a blade-to-blade calculation as well to obtain the blade surface velocity distributions. Because the relative flow angle is assumed equal for all blade-to-blade streamlines the trajectory of a particle becomes dependent only on the relative velocity ratio, σ. This mode of operation is useful for determining the influence of the blade-to-blade velocity gradient and the rotor blade boundary layers on the energy transfer of the blade row. The freestream (out of the boundary layers) blade-to-blade streamline of interest can be specified in the input data (Y/PITCH can range from 0.0 on the suction surface to 1.0 on the pressure surface with the mean streamline

being 0.5). An interpolation routine is used to interpolate between the mean streamline velocities and the surface velocities. This mode of operation was used extensively during the project to obtain freestream and boundary layer particle trajectories and the resulting rotor exit total temperature field variations for a transonic rotor.

4. RESULTS

The flow field of a transonic rotor was used to demostrate the use and capability of the program developed. The program was used to calculate the influence of the blade-to-blade velocity gradient and the boundary layer migration on the rotor exit flow field. The results will first be presented for the freestream (i.e. fluid outside the blade boundary layers) surface particles and then for the blade boundary layer fluid. Results will be shown at span locations of 10%, 50%, and 90% (based of flow area). The calculated trajectories for these particles and the influence of these trajectories on the energy transfer of the rotor will then be shown. All radial shift and energy transfer comparisons are made with respect to the mean blade-to-blade streamline of the through-flow calculation. The analysis was made for clean inlet flow conditions only. No attempt was made to introduce inlet flow field nonuniformities. Finally, a short summary of how these results compare with existing test data will be given.

4.1 Freestream Surface Velocity Evolution

Due to the curvature of the blade channel the surface velocities of the blade will be different than the mean blade-to-blade streamline velocity. The mag-

nitude of these velocity differences depends upon the blade design and loading. In this analysis the axial velocity and tangential velocity are obtain from the freestream velocity values (generated by the through-flow calculation) and the boundary layer calculation. Only the radial velocity component is actually calculated within the program. In Figure 8.a the axial velocity evolution for the mean, suction surface, and pressure surface streamlines is shown for the 50% span location. The velocity distributions are shown versus a nondimensional axial distance, 0% representing the blade leading edge and 100% the blade trailing edge. The suction surface velocity is everywhere greater than that of the mean streamline velocity producing a velocity ratio, σ , larger than one. The opposite is true of the pressure surface velocity, σ is everywhere less than one. The residence time variations of mean, suction surface, and pressure surface particles are a direct result of these axial velocity differences. From the velocity triangles it can be seen that (recall for this analysis the relative flow angles of all blade-to-blade streamlines are assumed equal to the mean streamline flow angle) the suction surface particles will have a smaller absolute tangential velocity and pressure surface particles a larger absolute tangential velocity than the mean streamline. The absolute tangential velocity evolution through the blade row for each of these streamlines is shown in Figure 8.b, again for 50% span.

Because the differences in tangential velocity is an indication of the magnitude of the force imbalance on the particle it is possible to obtain an idea of the evolution of this force on the particle from this figure. The larger tangential velocity for pressure surface particles will tend (see eq. 3.12) to produce a larger radial acceleration of the particle, while the opposite trend occurs for suction surface particles. The resulting calculated radial velocity evolution is shown in Figure 8.c. As expected due to the larger residence time and tangential velocity the pressure surface radial velocity is larger than that of the mean streamline. The suction surface velocity is smaller than the mean. A few remarks can be made concerning these radial velocity evolutions. From 10% to 40% meridional distance the tangential velocity difference between the pressure surface and the mean streamline is the greatest. The resulting rate of change of the pressure surface radial velocity is also the largest. From 40% to 70% meridional distance the tangential velocity difference (indication of force imbalance) becomes smaller, but still non-zero. However the radial velocity of the pressure surface particle actually decreases in this range. This can be explained by noting the rather large rate of change of the radial velocity for the mean streamline. Recall, the change in radial velocity of a particle is related to the change of radial velocity of the freestream "weighted" by the ratio of residence times. Here the

large rate of change of the freestream radial velocity and the increased residence time of the pressure surface particle combine to overcome the centrifugal force imbalance that trys to increase the particles radial velocity. This is essentially the influence of streamline curvature on the low momentum particle. For the suction surface particles all tendencies are to reduce its radial velocity relative to the mean freestream.

Similar axial, tangential, and resulting calculated radial velocity evolutions are shown in Figure 9. and Figure 10. for the 10% (near the hub) span location and the 90% (near the tip) span location. Figure 9.c shows clearly the influence of the high streamline curvature near the hub on lower and higher momentum particles. Again the centrifugal force imbalance tending to push the pressure surface particles upward (thus increasing the radial velocity) is overcome by the strong change in the mean streamline radial velocity. The suction surface particles because of their greater through flow velocity are less effected by the high streamline curvature and thus have a larger radial velocity than the mean streamline through the entire blade row. The higher wheel speed at the tip (Figure 10.) tends to produce larger tangential velocity differences and thus larger differences between the radial velocity for pressure surface, mean, and suction surface particles. The radial velocity of pressure surface particles is beginning to become

significant at the tip.

4.2 Boundary Layer Velocity Evolution

The boundary layer results are presented for four different boundary layer locations. These locations are specified as a ratio of the distance from the blade surface, y, to the exit boundary layer thickness, δ_E . A value of 1.00 corresponds to the edge of the boundary layer region and thus is identical to the surface velocity evolutions presented above. Values of y/δ_E of 0.25, 0.05, and 0.01 indicate streamlines successively closer to the blade surface and thus "deeper" within the boundary layer.

The influence of the boundary layer location on the axial velocity evolution for the suction surface is shown in Figure 11.a for 50% span. Note that over the first 50% axial distance of the blade most of the boundary layer fluid still has an excess of axial velocity relative to the mean streamline. The tangential velocity evolution for these particles is shown in Figure 11.b, and the calculated radial velocity evolution in Figure 11.c. As expected the radial velocities of the suction surface boundary layer particles are smaller than the mean streamline radial velocity over most of the blade.

Similar pressure surface boundary layer data are shown in Figure 12. Again results are shown for four different boundary layer locations. The freestream surface velocity of the pressure surface is already considerably less than that of the mean stramline. As particles deeper within the boundary layer are considered this velocity defect becomes even larger. From the velocity triangles for the boundary layer particles the tangential velocity evolution is obtained and is shown in Figure 12.b. Recall, the axial velocity ratio is an indication of the residence time and the tangential velocity excess is an indication of the radially outward force on the particle. The particle deepest within the boundary layer have not only the largest residence time but also the greatest force imbalance. Thus the high radial velocities shown in Figure 12.c for these particles is not too surprizing. The largest calculated radial velocity in the boundary layer is approximately 10% of the freestream axial velocity.

4.3 Particle Trajectory and Radial Shift

The meridional trajectory for the freestream surface particles and the boundary layer fluid will be presented in this section. The radial location of the particle is dependent not only on the evolution of the radial velocity of the particle through the blade but also on the time the particle remains within the blade

row. The trajectories for freestream suction surface and pressure surface particles are shown in Figure 13. for the 10%, 50%, and 90% span locations. The twisting of the streamsheet as it progress through the blade row can be seen. The amount of twist varies from about 1 mm at the hub to 2.5 mm at the tip with the pressure surface always higher than the suction surface.

The meridional trajectories for suction surface boundary layer particles are shown in Figure 14., also for the 10%, 50%, and 90% span locations. There is very little variation in the particle paths for the suction surface boundary layer fluid. The radial shift is small and nearly constant over the span.

Similar trajectory results are shown in Figure 15. for the pressure surface boundary layer particles. Because of the larger force imbalance and the greater residence time there is a significant radial migration of the pressure surface boundary layer fluid. The magnitude of this radial shift varies over the blade span, from about 4 mm at the hub to over 12 mm at the tip. The deepest boundary layer particle considered (y/δ_E = 0.01) reached the shroud casing radius before leaving the blade row.

4.4 Energy Transfer

As mentioned in Chapter 2 the radial shift can play an important role in determining the magnitude of the energy transfer to a particle. In Figure 16. a circumferential view of the blade-to-blade flow field is shown. The circumferential distance is broken into three small segments showing the suction surface boundary layer, the mean streamline, and the pressure surface boundary layer. Zero, on the horizontal axis, corresponds to the suction surface of the blade and 100% to the pressure surface. Note the different scale used for the suction surface and pressure surface boundary layers. From this view the twisting of the blade-to-blade streamsheet can clearly be seen. Also the radial migration of pressure surface and suction surface boundary layer particles is shown in the figure. The bar graphs represent the temperature increase these fluid particles recieve in addition to that of the mean streamline due to their different velocity evolution. The overall mean freestream temperature rise through the blade row is approximately 22° C.

Figure 16.a shows the circumferential variations in the flow field at 50% span. It can be seen that freestream suction surface fluid recieves the smallest energy addition while pressure surface boundary layer fluid recieves the largest. The temperature variation

is shown to be 4° - 5° C. at this span location. Figure 16.b and Figure 16.c show similar data for 10% span and 90% span. Due to the smaller radial shifts and lower wheel speed at 10% span (Figure 16.b) the circumferential temperature variations are very small. At 90% span however the large radial shifts combine with the high wheel speed to produce the largest circumferential temperature variations in the blade row.

4.5 Relation to Test Data

Unfortunately no test data are available for the transonic rotor used in the analysis above. There are however some experimental results available for similar machines. High speed data are necessary for temperature variation comparisons, but rotor wake radial velocity comparisons can be made for both low speed and high speed rotor data.

Several experimenters (REF 2,3) have reported measuring rotor wake radial velocities on the order of 10% to 15% of the axial velocity downstream of a rotor. This is the order of magnitude of radial velocity obtained for particles deep within the pressure surface boundary layer.

Leboeuf (REF 9) and Kool (REF 10) made circumferential temperature field measurements behind a high

speed rotor at VKI. They reported temperature variations from the freestream flow to the blade wake fluid to be 2° - 3° C at the blade mid-span. The rotor used for these measurements was not as highly loaded as the rotor used in the above analysis. Kerrebrock and Mikolajczak (REF 8) report circumferential temperature variations at the exit of a stator row downstream of a transonic rotor to be on the order of 10% of the overall stage temperature rise. Again the calculated values obtained from the program compare well, on an order of magnitude basis, with these experimental values.

Although it is difficult to draw to many conclusions from this limited comparison it is felt that the calculation technique developed above does produce results that are realistic and are similar to experimentally determined values.

5. CONCLUSIONS

The derivation and development of a technique to calculate the trajectory of low momentum fluid particles and their influence on the energy transfer of a rotating blade row has been presented. The resulting values of radial velocity for the boundary layer fluid and the associated increased temperature rise for these particles agree well with available test data.

A twisting or warpping of a blade-to-blade streamsheet through a rotor blade row was shown to occur due to the velocity gradients in the blade channel. The suction surface freestream fluid tends to go downward while the pressure surface fluid goes radially outward. A quantitative value for this streamsheet twisting was given for a transonic rotor. The amount of twist is greatest at the blade tip.

The radial migration of rotor blade boundary layer fluid was shown to occur. The radial shift of this fluid is more significant in the pressure surface boundary layer than in the suction surface boundary layer. The migration of the boundary layer fluid was shown to be influenced by the wheel speed - increasing the radial shift at the tip and the meridional curvatures - reducing the already small radial shifts near the hub.

The increased residence time and radial shift of the boundary layer particles results in this low momentum fluid obtaining a larger energy transfer from the rotor than the freestream fluid. This nonuniform energy transfer results in circumferential variations in the rotor exit total temperature field. These temperature variations are largest at the tip of the blade due to the influence of the wheel speed on the radial shift and energy transfer.

6. RECOMMENDATIONS FOR FUTURE WORK

Much of this project was devoted to the development of the calculation technique. Only one rotor was analyzed in detail and unfortunately no test data were available for this rotor. The calculation procedure should be applied to a high speed rotor for which reliable velocity and temperature field measurements exist. There is a problem however in comparing the calculation results with measurements. The calculation procedure stops at the blade trailing edge but most measurements are made some distance downstream of the rotor. The calculation should be extended to include some reasonable distance downstream of the rotor. This would entail incorporating a boundary layer - to - wake transition model. This would however make direct comparisons between calculated results and measurement data possible.

The analysis of the transonic rotor was restricted to velocity ratios created within the blade row. The influence of inlet casing boundary layers or upstream blade wakes entering the blade row was not considered. Such an analysis should be made. The program as it exists now is capable of making such an analysis if accompanied by a particle/freestream mixing or interaction model.

Due to the impact the boundary layer model has on the resulting trajectory and energy transfer calculations some thought should be given to incorporating a more elaborate boundary layer calculation.

Finally, the calculation procedure should be extended to include the analysis of centrifugal machines. The radial shift considerations are a little different for this type of application. What might be of particular interest is modelling the inlet casing boundary layers and attempting to determine if there is a relationship between the radial migration of the hub casing boundary layer in the impeller and the separation location.

7. REFERENCES

1. Kool, P., DeRuyck, J., & Hirch, CH., : The Three-Dimensional Flow and Blade Wake in an Axial Plane Downstream of an Axial Compressor Rotor. ASME 78-GT-66

2. Raj, R., & Lakshminarayana, B., : Three Dimensional Characteristics of Turbulent Wakes Behind Rotors of Axial Flow Turbomachinery. ASME 75-GT-1

3. Dring, R., Joslyn, H., & Hardin, L.,: Experimental Investigation of Compressor Rotor Wakes. Tech Report AFAPL-TR-79-2107 (1980)

4. Thompkins, W., & Kerrebrock, J., : Exit Flow From a Transonic Compressor Rotor. MIT Gas Turbine Lab, Report No. 123, 1975

5. Keenan, M., et al.,: Experimental Evaluation of Transonic Stators. NASA CR 54621 19[illegible]

6. Lakshminarayana, B.,: Effects of Inlet Temperature Gradients on Turbomachinery Performance. ASME 74-GT-57

7. Smith, L.,: Wake Dispersion in Turbomachines. ASME Transact. J. of Basic Engr. Sept. 1966

8. Kerrebrock, J., & Mikolajczak, A.,: Intra-Stator Transport of Rotor Wakes and Its Effect on Compressor Performance. ASME 70-GT-39

9. Leboeuf, F., & Breugelmans, F.,: Etude du développement d'un sillage au travers d'un étage de compresseur axial NACA 65-12A_2I_{8b}.
VKI PR 1974-11

10. Kool, P., & Hirsch, CH.,: Blade-to-Blade Pressure, Temperature, and Velocity Profiles Downstream of a Single Rotor Row at High Subsonic Speed.
79-7033

11. NASA SP-36: Aerodynamic Design of Axial Flow Compressors. NASA 1965

12. Papailiou, K.,: Viscous Flows in Centrifugal Compressors.
VKI Lecture Series 95 1977

13. Papailiou, K.,: Blade Optimization Based on Boundary Layer Concepts.
VKI Course Note 60

APPENDIX I. PROGRAM INPUT

The general input format for the program is given in Table I.1 with sample data shown in Table I.2. The program operation is separated for absolute velocity ratios (low momentum fluid entering the blade row) and relative velocity ratios (low momentum fluid generated within the blade row). The input possibilities for these two modes will be explained separately. Common to all of the input data is the freestream velocity field, the hub the shroud contours, and the radial location of the particle or streamline of interest at the inlet of the blade row. The velocity ratio and flow angle data necessary vary with the cases considered (explained below). The program options are selected through the use of a "trigger" card specifying six triggers, I1, I2, I3, I4, I5, and I6. Trigger I3 determines whether absolute velocity ratios (I3=0) or relative velocity ratios (I3=1) are considered.

I.1 Absolute Velocity Ratio

For velocity defects in the inlet flow field it is necessary to specify the velocity ratio and the relative flow angle evolution of the particle through the blade row. The velocity ratio can be specified as a constant or as some function of the axial distance through the blade row. The relative flow angle evolution

is assumed to be a linear variation between the inlet and exit if not otherwise specified in the input. Each of these cases will be briefly outlined below.

Case 1. ("trigger" card: 0 0 0 0 0 0)

For this case the velocity ratio is an input parameter and assumed constant through the blade row. The relative flow angle evolution is assumed linear from the inlet angle to the exit angle.

Case 2. (1 0 0 0 0 0)

This is the same as Case 1 except now the velocity ratio is specified as a function of the axial distance. The relative flow angle evolution is still a linear one.

Case 3. (1 1 0 0 0 0)

For this case both the velocity ratio and the relative flow angle evolution are specified as functions of the axial distance. The blade-to-blade trajectory of the particle can now be arbitrarily specified allowing for freestream/particle mixing or interaction models to be incorporated. Note that the inlet relative flow angle is obtained from the freestream flow direction and the velocity ratio. Thus the relative flow angle evolu-

tion should be specified such that it agrees with this value at the inlet.

I.2 Relative Velocity Ratio

One of the initial goals of this project was to predict the radial migration of blade boundary layer fluid. This mode of operation can consider such flows as well as freestream (i.e. out of the boundary layers) velocity variations. This mode of operation is selected by I3 = 1. For relative velocity ratios it is assumed that the relative flow angle evolution for all blade-to-blade streamlines is (unless otherwise specified) identical to that of the mean streamline. Thus only the velocity ratio needs to be known to obtain the particle trajectory.

Case 1. (0 0 1 0 0 0)

The relative velocity ratio is specified in the input and assumed to be constant through the blade row. This case is not of much importance.

Case 2. (1 0 1 0 0 0)

Here the velocity ratio is specified as a function of the axial distance. The relative flow angle evolution is that of the mean freestream streamline.

Case 3. (1 1 1 0 0 0)

The velocity ratio evolution and the relative flow angle evolution are now specified in the input as functions of the axial distance through the blade row, thus allowing for deviations from the mean streamline relative flow angle evolution.

Case 4. (0 0 1 0 0 1)

Up to this time it has been assumed that the particle follows the mean streamline through the blade row. For this case it is possible to specify the blade-to-blade location of the particle of interest. This is done through the specification of Y/PITCH in the input. A value of 0.0 corresponds to the suction surface, 0.5 to the mean streamline, and 1.0 to the pressure surface of the blade (still assumed out of the boundary layers). For intermediate values of Y/PITCH an interpolation is done between the surface velocities and the mean streamline velocity to obtain a velocity ratio relative to the mean streamline velcity.

Case 5. (0 0 1 1 0 0)

For this case it is possible to consider suction surface boundary layer particles. The desired streamline in the boundary layer in specified as a y/δ_E

value ranging from 1.00 for the streamline coinciding with the edge of the boundary layer at the blade exit (identical to the freestream surface velocity) to 0.0 for particles being "deeper" within the boundary layer (see Figure 6.). The velocity defect is obtained from the boundary layer calculation and the velocity profile model and compared to the mean streamline velocity.

Case 6. (0 0 1 0 1 0)

This is identical to Case 5. except for the pressure surface boundary layer. It is also necessary to input the number of points involved in the boundary layer thickness calculation and the fluid dynamic viscosity for these boundary layer cases.

Table I.1 General Input Format

(all reals read in F10.4 FORMAT)

card 1: rotational speed (rad/s), pitch (m)
card 2: inlet temperature: particle, strm. A, strm. B
card 3: tip LE radius, axial location (m)
card 4: hub LE radius, axial location (m)
card 5: mid-merid. distance tip radius, axial loc.
card 6: mid-merid. distance hub radius, axial loc.
card 7: tip TE radius, axial location
card 8: hub TE radius, axial location
card 9: num. strmlns - IR, num. pts. - IZ (2I4)
card 10: ------- begin reading freestream ----------
card 11: ------- velocity field ----------
" 1 - IZ, 1 - IR
" Read: z,R,W,alpha,beta,Wss,Wps
" from Katsanis Output

then: "trigger" card I1,I2,I3,I4,I5,I6 (6I2)
: Radial location of entering particle on interest

then: input varies depending on the option using

Table I.2 Input Data

100	626.55	0.09541					
200	300.	300.	300.				
300	0.31045	0.019241					
400	0.15397	0.00					
500	0.30843	0.062131					
600	0.16086	0.055896					
700	0.30759	0.095856					
800	0.16351	0.10566					
900	7 17						
1000	-0.015240	0.15073	225.15	13.77	31.79	225.15	225.15
1100	-0.00762	0.15247	225.48	11.96	32.19	225.48	225.48
1200	-0.00	0.15397	228.11	10.41	32.04	250.63	199.56
1300	0.008128	0.15536	231.18	8.96	20.36	276.56	163.60
1400	0.016256	0.15655	224.52	7.81	19.99	291.56	157.46
1500	0.024384	0.15760	216.02	6.91	16.02	262.50	171.13
1600	0.032512	0.15854	213.86	6.27	13.14	249.48	178.24
1700	0.040640	0.15939	215.61	5.72	10.26	250.11	181.12
1800	0.048768	0.16016	216.79	5.16	7.35	254.51	183.06
1900	0.056896	0.16086	222.32	4.64	4.39	259.78	184.85
2000	0.065024	0.16148	224.37	4.11	1.46	263.61	185.06
2100	0.073152	0.16203	225.68	3.60	-1.56	266.76	184.61
2200	0.08128	0.16251	227.49	3.09	-4.60	269.69	185.27
2300	0.059408	0.16291	225.98	2.59	-8.03	252.02	199.95
2400	0.097536	0.16324	221.51	2.11	-8.86	227.12	215.90
2500	0.10566	0.16351	214.42	1.69	-9.06	215.15	213.66
2600	0.11379	0.16373	202.68	1.34	-9.46	212.68	207.68
2700	-0.011835	0.17359	221.13	9.94	35.63	221.13	221.13
2800	-0.003571	0.17477	225.21	9.25	35.22	225.21	225.21
2900	0.0050586	0.17632	232.27	7.67	32.77	271.32	193.38
3000	0.013765	0.17723	228.23	6.58	27.72	296.24	158.57
3100	0.022069	0.17832	219.66	5.87	22.26	266.65	151.95
3200	0.030435	0.17939	212.87	5.177	18.33	260.18	165.80
3300	0.038763	0.18002	212.36	4.43	15.53	248.61	176.16
3400	0.047092	0.18052	213.71	3.73	12.69	250.16	177.51
3500	0.055414	0.18093	215.22	3.07	9.65	253.20	177.50
3600	0.063727	0.18129	215.68	2.45	6.97	254.89	175.51
3700	0.072031	0.18156	218.16	1.90	4.02	255.14	173.47
3800	0.080330	0.18178	213.50	1.44	1.01	250.80	176.50
3900	0.088617	0.18200	216.76	0.99	-1.36	231.36	196.60
4000	0.096897	0.18211	207.55	0.55	-1.92	215.21	200.29
4100	0.10515	0.18221	201.74	0.15	-2.19	206.66	196.98
4200	0.11336	0.18206	191.40	[illegible]	-2.85	191.40	191.40
4300	0.12161	0.18217	192.16	0.13	-2.79	192.16	192.16
4400	-0.008457	0.21180	228.55	5.69	40.62	228.55	228.55
4500	0.0010501	0.21270	234.67	4.53	39.93	234.67	234.67
4600	0.010278	0.21334	237.29	3.81	36.97	281.54	193.19
4700	0.019240	0.21395	230.79	3.13	32.75	300.32	161.46
4800	0.027518	0.21479	219.47	2.58	28.36	291.76	147.39
4900	0.036190	0.21522	212.74	2.15	24.23	267.06	158.58
5000	0.045050	0.21533	209.61	1.60	21.59	248.59	171.10
5100	0.053599	0.21537	208.62	1.01	18.95	217.24	170.20
5200	0.062126	0.21539	206.06	0.47	16.33	246.20	166.02
5300	0.070635	0.21540	202.73	0.02	13.71	243.03	162.46
5400	0.079131	0.21537	199.56	-0.34	11.06	226.49	172.89
5500	0.087605	0.21533	176.59	-0.74	10.28	207.98	155.62
5600	0.096066	0.21519	171.61	-0.87	9.74	203.18	155.16
5700	0.10446	0.21517	159.67	-1.06	9.39	199.19	166.48
5800	0.11286	0.21474	162.09	-1.55	6.65	182.09	182.09
5900	0.12127	0.21462	152.60	-0.97	6.82	182.60	162.60
6000	0.12787	0.21462	183.54	-6.93	6.72	183.54	183.54
6100	-0.000851	0.24450	241.81	1.46	44.26	241.81	291.81

Table I.2 (con't)

6200	0.0067342	0.24498	266.66	0.93	42.68	275.54	217.69
6300	0.017961	0.24494	242.37	0.44	39.09	304.38	180.50
6400	0.026837	0.24547	231.25	0.40	35.49	304.15	156.49
6500	0.035521	0.24560	220.94	0.31	31.76	288.90	153.13
6600	0.044175	0.24559	213.02	0.11	26.42	264.93	161.23
6700	0.052810	0.24532	208.81	-0.33	26.02	219.50	168.27
6800	0.061420	0.24514	204.55	-0.68	23.69	235.35	163.94
6900	0.070009	0.24500	199.73	-0.99	21.36	245.19	164.45
7000	0.078580	0.24474	195.91	-1.18	19.68	215.79	176.26
7100	0.087131	0.24458	193.45	-1.26	19.25	292.41	164.23
7200	0.095660	0.24443	190.17	-1.39	16.83	179.08	161.52
7300	0.10414	0.24437	186.65	-1.50	16.58	194.08	178.88
7400	0.11256	0.24367	180.74	-1.50	16.54	180.71	167.74
7500	0.12097	0.24382	181.07	-1.40	18.46	181.07	181.07
7600	0.12768	0.24364	181.34	-1.38	18.30	181.34	181.34
7700	0.13437	0.24349	181.65	-1.40	18.26	181.65	181.65
7800	0.0085501	0.27324	255.86	-1.46	46.04	255.86	255.86
7900	0.017846	0.27286	255.00	-1.51	43.91	336.44	203.66
8000	0.026768	0.27298	245.92	-1.28	40.71	317.96	172.21
8100	0.035462	0.27285	232.38	-1.20	37.40	310.18	154.71
8200	0.044119	0.27265	220.68	-1.15	33.96	283.83	157.89
8300	0.052748	0.27231	213.56	-1.23	31.74	258.41	160.95
8400	0.061354	0.27262	207.86	-1.39	29.72	248.59	160.88
8500	0.069938	0.27179	202.15	-1.50	27.76	232.20	172.26
8600	0.078501	0.27149	198.45	-1.50	26.92	212.70	184.40
8700	0.087044	0.27137	196.07	-1.44	26.60	206.06	186.28
8800	0.095563	0.27111	192.41	-1.39	26.31	202.49	182.55
8900	0.10404	0.27105	188.68	-1.43	26.20	195.15	182.41
9000	0.11248	0.27061	183.86	-1.31	26.53	183.86	183.86
9100	0.12089	0.27054	183.89	-1.32	26.49	183.89	183.89
9200	0.12761	0.27037	183.60	-1.33	26.46	183.60	183.60
9300	0.13432	0.27022	183.38	-1.38	26.42	183.38	183.38
9400	0.14100	0.27005	183.16	-1.49	26.36	183.16	183.16
9500	0.0094078	0.29896	267.42	-3.22	49.41	267.42	267.42
9600	0.018606	0.29841	267.02	-2.90	47.00	313.16	221.89
9700	0.027454	0.29810	257.83	-2.59	44.19	330.25	185.65
9800	0.036082	0.29776	241.13	-2.35	41.30	324.77	163.54
9900	0.044673	0.29741	230.56	-2.12	38.31	300.12	161.08
10000	0.053237	0.29706	221.37	-1.95	36.19	271.72	171.07
10100	0.061776	0.29673	214.65	-1.86	34.37	255.37	173.59
10200	0.070292	0.29646	208.38	-1.71	32.81	234.95	181.87
10300	0.078785	0.29620	204.98	-1.48	32.37	217.55	192.48
10400	0.087259	0.29603	202.51	-1.27	32.03	215.18	189.90
10500	0.095709	0.29584	198.09	-0.99	31.78	212.34	183.89
10600	0.10413	0.29561	193.94	-0.91	31.58	201.01	186.91
10700	0.11254	0.29555	189.96	-0.88	32.23	189.96	189.96
10800	0.12092	0.29546	187.80	-0.74	32.23	189.80	189.80
10900	0.12763	0.29539	188.99	-0.73	32.34	188.99	188.99
11000	0.13434	0.29531	188.30	-0.75	32.44	188.30	188.30
11100	0.14103	0.29522	187.46	-0.84	32.56	187.46	187.46
11200	0.010174	0.31103	273.81	-3.68	50.40	273.81	273.81
11300	0.019241	0.31045	273.69	-3.45	46.36	318.12	229.67
11400	0.028018	0.30995	263.83	-3.11	45.65	337.51	196.15
11500	0.036591	0.30956	249.77	-2.83	42.67	332.54	167.00
11600	0.045130	0.30910	235.70	-2.55	39.97	308.04	163.36
11700	0.053643	0.30874	225.97	-2.28	37.76	278.35	173.60
11800	0.062131	0.30843	218.72	-1.99	36.15	258.92	178.53
11900	0.070546	0.30815	217.57	-1.71	34.86	233.45	197.70
12000	0.079038	0.30792	209.22	-1.42	34.39	223.02	195.41
12100	0.087456	0.30773	205.67	-1.13	34.00	221.30	192.03
12200	0.095856	0.30759	201.92	-0.84	33.72	221.34	182.50

Table I.2 (concluded)

```
12300    0.10424    0.30748    197.45    -0.61    33.11    197.45    197.45
12400    0.11261    0.30741    193.72    -0.42    33.79    193.72    193.72
12500    0.12097    0.30736    193.47    -0.30    33.82    193.47    193.47
12600    0.12767    0.30733    192.50    -0.23    34.00    192.50    192.50
12700    0.13437    0.30730    191.67    -0.20    34.15    191.67    191.67
12800    0.14107    0.30728    190.64    -0.21    34.35    190.64    190.64
12900     1 1 0 0 0 0
13000      50
13100     4
13200    1.00          0.09
13300    0.90          0.04
13400    0.80          0.08
13500    0.70          0.12          Set 1
13600     4
13700    40.0          0.09
13800    30.0          0.04
13900    20.0          0.08
14000    10.0          0.12
```

```
12300    0.10424    0.30748    197.45    -0.61    33.11    197.45    197.45
12400    0.11261    0.30741    193.72    -0.42    33.79    193.72    193.72
12500    0.12097    0.30736    193.47    -0.30    33.82    193.47    193.47
12600    0.12767    0.30733    192.50    -0.23    34.00    192.50    192.50
12700    0.13437    0.30730    191.67    -0.20    34.15    191.67    191.67
12800    0.14107    0.30728    190.64    -0.21    34.35    190.64    190.64
12900     0 0 1 0 0 1
13000      50                          Set 2
13100    0.25
13200      50
13300    0.75
```

```
12300    0.10424    0.30748    197.45    -0.61    33.11    197.45    197.45
12400    0.11261    0.30741    193.72    -0.42    33.79    193.72    193.72
12500    0.12097    0.30736    193.47    -0.30    33.82    193.47    193.47
12600    0.12767    0.30733    192.50    -0.23    34.00    192.50    192.50
12700    0.13437    0.30730    191.67    -0.20    34.15    191.67    191.67
12800    0.14107    0.30728    190.64    -0.21    34.35    190.64    190.64
12900     0 0 1 1 0 0
13000      50
13100    31
13200    0.0000157
13300    0.50                        Set 3
13400      50
13500    31
13600    0.0000157
13700    0.25
```

Sample Data Sets

Set 1

card 129: "trigger" card (6I2)
card 130: radial location, % span (I4)
card 131: num. pts. in velocity ratio distribution (I2)
card 132: velocity ratio, axial location
card 133: " " " "
card 134: " " " "
card 135: " " " "
card 136: num. pts. in flow angle distribution (I2)
card 137: relative flow angle, axial distance
card 138: " " " " "
card 139: " " " " "
card 140: " " " " "
card 141: start next data set with new span location

Set 2

card 129: "trigger" card (6I2)
card 130: radial location, % span (I4)
card 131: Y/PITCH
card 132: start next data set with new span location

Set 3

card 129: "trigger" card (6I2)
card 130: radial location, % span (I4)
card 131: num. pts. used in boundary layer calc. (I2)
card 132: fluid dynamic viscosity - SI units
card 133: y/δ_E , b. l. streamline of interest
card 134: start next data set with new span location

APPENDIX II. PROGRAM OUTPUT

Examples of the program output are shown in Table II.1. The headings identify the mode of operation and general inlet conditions. The particles radial location and velocity is calculated at 12 axial locations through the blade row at increments based on the blade axial chord at the specified inlet radius. The axial and radial location of the particle is given at each station, as well as the velocity ratio and the velocity components of the particle and the freestream. The span (here based on the blade height) is also given at each axial location to gain a quick appreciation for the magnitude of radius variations calculated.

The blade inlet conditions are then summarized for three different streamlines, the particle streamline, streamline A, and streamline B (see Figure 5.). The velocity components and flow angles are given for each of these streamlines. The blade exit conditions are likewise given. Lastly the energy transfer for the three different streamlines is summarized. Given is the radial shift of each streamline, the inlet total temperature, the exit total temperature, the temperature rise, and the exit temperature difference between the particle streamline and streamline B.

Two additional parameters are included in the output that have not yet been explained. They are labeled "Q/VZB" and "E/P". These parameters estimate the "cross-flow" of a particle and the resulting displacement in the blade-to-blade plane. Q/VZB is the ratio of the component of the particle velocity that is perpendicular to the relative freestream velocity direction and the freestream axial velocity. E/P is the fraction of the blade pitch the particle will be displaced as it flows through the blade row. Such a displacement will occur only for particles that have at some time a relative flow angle different then that of the freestream. These parameters were included mainly out of the curiousity of the author.

Table II.1 Sample Output.

Results From Data Set 1.

PATH OF PARTICLE INTRODUCED UPSTREAM

AT SPAN = 50% OF MASS FLOW

WITH VELOCITY RATIO, SIGMA = 0.99 IN ABSOLUTE VELOCITY

ARBITRARY SIGMA DISTRIBUTION GIVEN

ARBITRARY BETA DISTRIBUTION GIVEN

BLADE-TO-BLADE POSITION OF THE PARTICLE IS, Y/PITCH = 0.50

					********** PARTICLE **********				********** FREESTREAM **********			
CHORD	RADIUS	SPAN	Z	SIGMA	VZ	VU	VR	W	VZFS	VUFS	VRFS	WFS
-.100	0.24581	0.58	0.00226	0.994	174.50	33.99	3.65	243.10	175.50	34.18	3.67	243.68
0.000	0.24600	0.58	0.01120	0.972	177.81	68.36	2.61	223.24	182.93	39.11	2.33	245.83
0.100	0.24612	0.58	0.02012	0.950	178.59	78.51	2.09	217.35	183.04	54.14	1.21	240.10
0.200	0.24624	0.58	0.02903	0.927	174.43	91.37	2.64	207.39	180.06	73.15	1.11	228.85
0.300	0.24636	0.58	0.03795	0.905	169.78	103.58	2.79	197.09	187.56	90.83	0.72	218.87
0.400	0.24651	0.58	0.04687	0.883	165.26	114.83	2.28	187.88	187.20	104.85	-0.19	211.81
0.500	0.24661	0.58	0.05579	0.861	161.06	125.08	1.22	179.26	187.16	114.43	-1.57	207.42
0.600	0.24666	0.58	0.06470	0.838	156.21	134.90	0.53	170.76	186.36	123.93	-2.67	202.60
0.700	0.24668	0.58	0.07362	0.816	150.79	144.21	0.25	162.17	184.81	132.26	-3.50	196.23
0.800	0.24671	0.58	0.08254	0.794	145.24	152.87	0.65	153.95	183.00	137.17	-3.94	189.83
0.900	0.24678	0.58	0.09146	0.771	139.39	161.00	1.71	145.86	180.71	139.34	-4.20	181.95
1.000	0.24695	0.58	0.10038	0.749	133.00	168.71	3.34	137.67	177.55	141.43	-4.46	188.35

BLADE INLET CONDITIONS

	R	Z	VZ	VU	VR	W	ALPHA	BETA	THETA
PARTICLE	0.24584	0.00226	174.50	33.99	3.65	243.10	11.02	44.12	1.20
FREESTREAM A	0.24584	0.00228	175.50	34.18	3.67	243.68	11.02	43.92	1.20
FREESTREAM B	0.24571	0.01128	183.04	39.24	2.38	245.68	12.10	41.83	0.74

BLADE EXIT CONDITIONS

	R	Z	VZ	VU	VR	W	ALPHA	BETA	THETA
PARTICLE	0.24695	0.10038	133.00	168.71	3.34	137.67	51.75	14.91	1.44
FREESTREAM A	0.24632	0.10038	177.75	141.48	-4.47	188.34	38.52	19.26	-1.44
FREESTREAM B	0.24695	0.10038	177.55	141.43	-4.46	188.35	38.54	19.45	-1.44

ENERGY TRANSFER

	DEL P	T01	T02	DEL T	T DIF	G/VZ0	E/P
PARTICLE	0.00111	300.00	327.39	27.39	4.25	0.003	0.003
FREESTREAM A	0.00078	300.00	321.75	21.75			
FREESTREAM B	0.00124	300.00	320.79	20.79			

Table II.1 (con't)

Results From Data Set 2.

PATH OF PARTICLE INTRODUCED UPSTREAM

AT SPAN = 50% OF MASS FLOW

WITH VELOCITY RATIO, SIGMA = 1.00 IN RELATIVE VELOCITY

BLADE-TO-BLADE POSITION OF THE PARTICLE IS, YZPITCH = 0.75

					********** PARTICLE **********				********** FREESTREAM **********			
CHORD	RADIUS	SPAN	Z	SIGMA	VZ	VU	VR	W	VZFS	VUFS	VRFS	WFS
-.100	0.24584	0.58	0.00228	1.000	175.50	34.18	3.67	243.68	175.50	34.18	3.67	243.68
0.000	0.24600	0.58	0.01120	0.924	169.11	51.51	2.40	227.27	162.93	39.11	2.33	245.63
0.100	0.24610	0.58	0.02012	0.866	162.80	74.18	1.55	207.86	158.05	54.14	1.21	240.09
0.200	0.24621	0.58	0.02903	0.843	158.62	93.57	2.12	193.00	156.08	73.15	1.12	226.84
0.300	0.24633	0.58	0.03795	0.855	160.33	107.26	2.42	187.07	157.59	90.88	0.72	216.65
0.400	0.24645	0.58	0.04687	0.886	165.78	115.99	2.01	187.57	161.21	104.84	-0.16	211.81
0.500	0.24653	0.58	0.05579	0.923	168.94	123.14	0.95	187.19	163.16	114.43	-1.57	207.41
0.600	0.24656	0.58	0.06470	0.956	168.87	131.43	0.16	183.72	166.36	123.93	-2.66	202.79
0.700	0.24656	0.58	0.07362	0.978	171.51	137.43	-0.40	183.69	164.64	132.28	-3.49	196.22
0.800	0.24653	0.58	0.08254	0.991	175.43	139.77	-0.65	187.21	163.05	137.16	-3.94	194.62
0.900	0.24649	0.58	0.09146	0.996	176.53	140.91	-0.82	187.36	160.80	139.39	-4.21	191.95
1.000	0.24645	0.58	0.10038	0.979	173.94	142.79	-1.01	184.30	177.71	141.47	-4.47	186.34

BLADE INLET CONDITIONS

	R	Z	VZ	VU	VR	W	ALPHA	BETA	THETA
PARTICLE	0.24584	0.00228	175.50	34.18	3.67	243.68	11.02	43.92	1.20
FREESTREAM A	0.24584	0.00228	175.50	34.18	3.67	243.68	11.02	43.92	1.20
FREESTREAM B	0.24517	0.01121	163.16	39.14	2.50	245.49	12.07	41.77	0.76

BLADE EXIT CONDITIONS

	R	Z	VZ	VU	VR	W	ALPHA	BETA	THETA
PARTICLE	0.24645	0.10038	173.94	142.79	-1.01	184.30	39.38	19.30	-0.36
FREESTREAM A	0.24632	0.10038	177.75	141.48	-4.47	188.34	38.52	19.26	-1.44
FREESTREAM B	0.24645	0.10038	177.71	141.47	-4.47	188.34	38.52	19.30	-1.44

ENERGY TRANSFER

	DEL R	T01	T02	DEL T	T DIF	U/VZB	E/P
PARTICLE	0.00060	300.00	322.03	22.03	1.25	0.000	0.000
FREESTREAM A	0.00048	300.00	321.75	21.75			
FREESTREAM B	0.00127	300.00	320.78	20.78			

Table II.1 (concluded)

Results From Data Set 3.

PATH OF PARTICLE INTRODUCED UPSTREAM

AT SPAN = 50% OF MASS FLOW

WITH VELOCITY RATIO, SIGMA = 1.00 IN RELATIVE VELOCITY

PARTICLE IS IN SUCTION SURFACE BOUNDARY LAYER, WITH Y/DEL = 0.250 EXIT BOUNDARY LAYER THICKNESS = 0.005461

					********** PARTICLE **********				********** FREESTREAM **********			
CHORD	RADIUS	SPAN	Z	SIGMA	VZ	VU	VR	W	VZFS	VUFS	VRFS	WFS
-.100	0.24564	0.58	0.00228	1.000	175.50	34.18	3.67	243.68	175.50	34.18	3.67	243.68
0.000	0.24598	0.56	0.01120	1.152	210.80	14.09	2.30	283.28	162.93	39.11	2.33	245.83
0.100	0.24605	0.58	0.02012	1.270	236.77	13.99	1.06	304.81	158.05	54.15	1.22	240.07
0.200	0.24607	0.58	0.02903	1.314	247.22	32.22	0.47	300.70	160.10	73.16	1.13	228.79
0.300	0.24607	0.58	0.03795	1.291	242.27	58.12	-0.51	282.49	167.63	90.84	0.76	218.78
0.400	0.24603	0.58	0.04687	1.229	230.19	82.02	-1.92	260.21	167.31	104.62	-0.14	211.74
0.500	0.24592	0.58	0.05579	1.178	220.71	98.58	-3.08	244.30	167.34	114.40	-1.52	207.36
0.600	0.24574	0.57	0.06470	1.157	215.84	111.55	-5.15	234.51	166.61	123.95	-2.83	202.72
0.700	0.24549	0.57	0.07362	1.090	201.84	120.05	-6.29	216.07	165.14	132.40	-3.47	195.13
0.800	0.24519	0.57	0.08254	1.004	184.26	130.98	-6.89	195.73	163.44	137.28	-3.93	189.78
0.900	0.24484	0.57	0.09146	0.965	174.97	141.70	-7.13	185.34	161.30	139.51	-4.23	191.94
1.000	0.24447	0.56	0.10038	0.955	170.24	144.38	-7.28	179.90	176.33	141.64	-4.51	188.34

BLADE INLET CONDITIONS

	R	Z	VZ	VU	VR	W	ALPHA	BETA	THETA
PARTICLE	0.24564	0.00228	175.50	34.18	3.67	243.68	11.02	43.92	1.20
FREESTREAM A	0.24564	0.00228	175.50	34.18	3.67	243.68	11.02	43.92	1.20
FREESTREAM B	0.24304	0.01095	183.20	38.75	3.16	244.66	11.94	41.51	0.99

BLADE EXIT CONDITIONS

	R	Z	VZ	VU	VR	W	ALPHA	BETA	THETA
PARTICLE	0.24447	0.10038	170.24	144.38	-7.28	179.90	40.30	18.72	-2.49
FREESTREAM A	0.24432	0.10038	177.75	141.48	-4.47	188.34	38.52	19.26	-1.41
FREESTREAM B	0.24447	0.10038	178.33	141.64	-4.51	188.34	38.46	18.72	-1.45

ENERGY TRANSFER

	DEL R	T01	T02	DEL T	T DIF	Q/VZ0	E/P
PARTICLE	-0.00137	300.00	322.12	22.12	1.39	0.000	0.000
FREESTREAM A	0.00048	300.00	321.75	21.75			
FREESTREAM B	0.00143	300.00	320.73	20.73			

APPENDIX III. PROGRAM LISTING

A listing og the final program is included for the readers convenience.

```
C       THIS PROGRAM WILL CALCULATE THE PATH OF A LOW MOMENTUM FLUID
C       PARTICLE THROUGH A ROTOR BLADE ROW AND GIVE ROTOR INLET
C       AND EXIT CONDITIONS.   GREG HOLBROOK  FEBRUARY 1980
C
C       ABSOLUTE VELOCITY RATIO, SIGMA
C             I1,I2,I3,I4,I5,I6 = 0:  SIGMA IS CONSTANT, AND BETA DIFFERENCE
C                  DECREASES LINEARLY.
C             I1 = 1:  ARBITRARY SIGMA DISTRIBUTION INPUT
C             I2 = 1:  ARBITRARY BETA DISTRIBUTION INPUT
C             I3 = 1:  RELATIVE VELOCITY RATIO
C
C       RELATIVE VELOCITY RATIO, SIGMA
C             I1,I2,I4,I5,I6 = 0,I3 = 1:  SIGMA IS CONSTANT, BETA PARTICLE
C                  IS EQUAL TO BETA OF THE FREESTREAM.
C             I1 = 1:  ARBITRARY SIGMA DISTRIBUTION INPUT
C             I2 = 1:  ARBITRARY BETA DISTRIBUTION INPUT
C             I3 = 1:  RELATIVE VELOCITY RATIO
C             I4 = 1:  PARTICLE IN SUCTION SURFACE BOUNDARY LAYER
C             I5 = 1:  PARTICLE IN PRESSURE SURFACE BOUNDARY LAYER
C             I6 = 1:  PARTICLE BETWEEN MEAN AND PRESSURE OR SUCTION SURFACES
C
      DIMENSION R(25),Z(25),VZ(25),VU(25),VR(25),WU(25),BETA(25)
      DIMENSION THETA(25),CX(25),AR(25),ARB(25),WUFS(25),BETAF(25)
      DIMENSION THETF(25),VRB(25),VZB(25),DZ(25),RF(20,20),SIGMAG(25)
      DIMENSION ZF(20,20),VZF(20,20),VRF(20,20),VUF(20,20)
      DIMENSION VZFS(25),VUFS(25),VRFS(25),W(25),WFS(25),VUB(25)
      DIMENSION VZSL(25),VRSL(25),ARSL(25),ARBSL(25),VUSL(25)
      DIMENSION VZBSL(25),VRBSL(25),PSL(25),SIGMA(25),VUBSL(25)
      DIMENSION BETAIO(25),ZSIG(25),ZBETA(25),WSS(20,20),WPS(20,20)
      DIMENSION UOUB(60),WSURF(60),CP(60),GAM(60),DEL(60)
      DIMENSION BETAS(60),ZBL(60),P(3),V(3)
C
      CP=1005.
      PI=3.14159
C
      READ(5,100) OMEGA,PITCH
      READ(5,100) T01,T01A,T01B
      READ(5,100) R10,Z10
      READ(5,100) R1L,Z1L
      READ(5,100) R50U,Z50U
      READ(5,100) R50L,Z50L
      READ(5,100) R20,Z20
      READ(5,100) R2L,Z2L
      READ(5,101) IR,IZ
  100 FORMAT(8F10.4)
  101 FORMAT(3I4)
  102 FORMAT(8F10.4)
  103 FORMAT(6I2)
  104 FORMAT(2F10.5)
C
      DO 5 J=1,IR
      DO 4 I=1,IZ
      READ(5,102) ZF(I,J),RF(I,J),WIN,AIN,BIN,WSS(I,J),WPS(I,J)
      UIN=RF(I,J)*OMEGA
      WRIN=WIN*COS(BIN/180.*PI)
      WUIN=WIN*SIN(BIN/180.*PI)
      WZIN=WRIN*COS(AIN/180.*PI)
      WRIN=WRIN*SIN(AIN/180.*PI)
      VZF(I,J)=WZIN
      VUF(I,J)=UIN-WUIN
      VRF(I,J)=WRIN
```

```
      4 CONTINUE
      5 CONTINUE
C
      READ(5,103) I1,I2,I3,I4,I5,I6
    1 READ(5,101,END=11) ISPAN
      IF((I1+I4+I5+I6).GT.0) GO TO 51
      READ(5,100) SIGMAI
   51 CONTINUE
      IF(I1.EQ.0) GO TO 6
      READ(5,103) ISIG
      READ(5,104) (SIGMAG(I),ZSIG(I),I=1,ISIG)
    6 CONTINUE
      IF(I2.EQ.0) GO TO 7
      READ(5,103) IBETA
      READ(5,104) (BETAIN(I),ZBETA(I),I=1,IBETA)
    7 CONTINUE
      IF((I4+I5).EQ.0) GO TO 35
      READ(5,103) KBL
      READ(5,100) VIS
      READ(5,100) YUBELZ
   35 CONTINUE
      IF(I6.EQ.0) GO TO 37
      READ(5,100) YUPII
   37 CONTINUE
C
C        APPROXIMATION:  HUB AND SHROUD CURVATURES BY A SECOND ORDER CURVE
C
      CU=((R2U-R1U)/(Z2U-Z1U)-(R2U-R50U)/(Z2U-Z50U))/(Z1U-Z50U)
      BU=(R2U-R1U-CU*(Z2U*Z2U-Z1U*Z1U))/(Z2U-Z1U)
      AU=R1U-BU*Z1U-CU*Z1U*Z1U
      CL=((R2L-R1L)/(Z2L-Z1L)-(R2L-R50L)/(Z2L-Z50L))/(Z1L-Z50L)
      BL=(R2L-R1L-CL*(Z2L*Z2L-Z1L*Z1L))/(Z2L-Z1L)
      AL=R1L-BL*Z1L-CL*Z1L*Z1L
C
      IZG=1
      JRG=4
      SPAN=ISPAN*0.01
      R(2)=SQRT((R1U*R1U-R1L*R1L)*SPAN+R1L*R1L)
      Z(2)=Z1L+(R(2)-R1L)*(Z1U-Z1L)/(R1U-R1L)
      R2A=SQRT((R2U*R2U-R2L*R2L)*SPAN+R2L*R2L)
      Z2A=Z2L+(R2A-R2L)*(Z2U-Z2L)/(R2U-R1L)
      CHORD=Z2A-Z(2)
      Z(1)=Z(2)-CHORD/10.
      RMAX=AU+BU*Z(1)+CU*Z(1)*Z(1)
      RMIN=AL+BL*Z(1)+CL*Z(1)*Z(1)
      R(1)=SQRT((RMAX*RMAX-RMIN*RMIN)*SPAN+RMIN*RMIN)
C
      IF(I1.EQ.1) GO TO 40
      IF((I4+I5).GT.0) GO TO 52
      IF(I6.EQ.1) GO TO 59
C
C        SIGMA IS CONSTANT
C
      SIGMA(1)=SIGMAI
      GO TO 72
C
C        SIGMA FROM DISTRIBUTION GIVEN AS INPUT
C
   40 CALL INTERPOL (ZSIG,SIGMAG,ISIG,25,Z(1),SIGMA(1))
      GO TO 72
C
```

```
C           SIGMA DISTRIBUTION FROM BOUNDARY LAYER MODEL
C
   52 ZBL(1)=Z(2)
      NBLM1=NBL-1
      DO 58 I=1,NBL
      ZBL(I)=ZBL(1)+CHORD*(I-1)/NBLM1
      RBLMAX=AU+BU*ZBL(I)+CU*ZBL(I)*ZBL(I)
      RBLMIN=AL+BL*ZBL(I)+CL*ZBL(I)*ZBL(I)
      RBL=SQRT((RBLMAX*RBLMAX-RBLMIN*RBLMIN)*SPAN+RBLMIN*RBLMIN)
C
      CALL LININT (ZF,RF,VZF,IZ,IR,20,20,ZBL(I),RBL,VZBL,IZG,JRG)
      CALL LININT (ZF,RF,VUF,IZ,IR,20,20,ZBL(I),RBL,VUBL,IZG,JRG)
C
      IF(IS.EQ.1) GO TO 54
      CALL LININT (ZF,RF,WSS,IZ,IR,20,20,ZBL(I),RBL,WSURF(I),IZG,JRG)
      GO TO 56
   54 CALL LININT (ZF,RF,WPS,IZ,IR,20,20,ZBL(I),RBL,WSURF(I),IZG,JRG)
   56 CONTINUE
C
      UBL=RBL*OMEGA
      WUBL=UBL-VUBL
      BETAS(I)= ATAN(WUBL/VZBL)
C
   58 CONTINUE
C
      REC=WSURF(1)*CHORD/VIS
C
      CALL BOUNLAY (WSURF,BETAS,ZBL,REC,60,NBL,CF,GAM,DEL)
C
      Y=(DEL2*DEL(NBL)
C
      CALL VELRATIO (CF,GAM,DEL,ZBL,Y,60,NBL,UGGE)
C
      IZG=1
      JRG=4
C
      SIGMA(1)=1.00
      GO TO 72
C
C           SIGMA DISTRIBUTION FROM INTERPOLATING IN BLADE-TO-BLADE PLANE
C
   59 CALL LININT (ZF,RF,VZF,IZ,IR,20,20,Z(1),R(1),V(2),IZG,JRG)
      CALL LININT (ZF,RF,VUF,IZ,IR,20,20,Z(1),R(1),VUF1,IZG,JRG)
      CALL LININT (ZF,RF,VRF,IZ,IR,20,20,Z(1),R(1),VRF1,IZG,JRG)
      CALL LININT (ZF,RF,WSS,IZ,IR,20,20,Z(1),R(1),WSS1,IZG,JRG)
      CALL LININT (ZF,RF,WPS,IZ,IR,20,20,Z(1),R(1),WPS1,IZG,JRG)
C
      U1=R(1)*OMEGA
      WUF1=U1-VUF1
      BETF1= ATAN(WUF1/V(2))
      IF((WSS1*WSS1-VRF1*VRF1).LT.0.00) GO TO 71
      V(1)=SQRT(WSS1*WSS1-VRF1*VRF1)*COS(BETF1)
      GO TO 712
   71 V(1)=1.00
  712 IF((WPS1*WPS1-VRF1*VRF1).LT.0.00) GO TO 714
      V(3)=SQRT(WPS1*WPS1-VRF1*VRF1)*COS(BETF1)
      GO TO 716
  714 V(3)=1.00
  716 CONTINUE
C
      F(1)=0.0
```

```
      P(2)=0.5
      P(3)=1.00
C
      CALL INTERPOL (P,V,3,3,IOPIT,VAA1)
C
      SIGMA(1)=1.00
C
   72 CONTINUE
C
      CALL LININT (ZF,RF,VZF,IZ,IR,20,20,Z(1),R(1),VZFS(1),IZO,IRO)
      CALL LININT (ZF,RF,VOF,IZ,IR,20,20,Z(1),R(1),VOFS(1),IZO,IRO)
      CALL LININT (ZF,RF,VRF,IZ,IR,20,20,Z(1),R(1),VRFS(1),IZO,IRO)
C
      VZ(1)=SIGMA(1)*VZFS(1)
      VR(1)=SIGMA(1)*VRFS(1)
      U=OMEGA*R(1)
C
      IF(I3.EQ.1) GO TO 74
C
C        IF ABSOLUTE VELOCITY RATIO:  VO=SIGMA*VOFS
C
      VO(1)=SIGMA(1)*VOFS(1)
      GO TO 76
C
C        IF RELATIVE VELOCITY RATIO:  WO=SIGMA*WOFS
C
   74 VO(1)=SIGMA(1)*VOFS(1)+U*(1.-SIGMA(1))
C
   76 CONTINUE
C
      WOFS(1)=U-VOFS(1)
      WFS(1)=SQRT(VZFS(1)*VZFS(1)+WOFS(1)*WOFS(1)+VRFS(1)*VRFS(1))
      BETAF(1)= ATAN(VOFS(1)/VZFS(1))*180./PI
      INCIF(1)= ATAN(VRFS(1)/VZFS(1))*180./PI
      WO(1)=U-VO(1)
      W(1)=SQRT(VZ(1)*VZ(1)+WO(1)*WO(1)+VR(1)*VR(1))
      BETA(1)= ATAN(WO(1)/VZ(1))*180./PI
      INCTA(1)= ATAN(VR(1)/VZ(1))*180./PI
      DBETA=(BETA(1)-BETAF(1))*PI/180.
C
      CA(1)=-0.100
      RSL(1)=R(1)
      ZMAA=AO+BO*Z(1)+CO*Z(1)*Z(1)
      RMIN=AL+BL*Z(1)+CL*Z(1)*Z(1)
      SPANCA=(R(1)-RMIN)/(RMAX-RMIN)
      VZSL(1)=VZFS(1)
      VOSL(1)=VOFS(1)
      VRSL(1)=VRFS(1)
C
      WRITE(6,230)
  230 FORMAT(1H1,///,2X,36HPATH OF PARTICLE INTRODUCED UPSTREAM,/)
      WRITE(6,231) ISPAN
  231 FORMAT(8X,10HAT SPAN = ,I2,'%',13H OF MASS FLOW,/)
      IF(I3.EQ.1) GO TO 82
      WRITE(6,232) SIGMA(1)
  232 FORMAT(8X,29HRATIO VELOCITY RATIO, SIGMA = ,F4.2,21H IN ABSOLUTE VE
     1LOCITY,/)
      GO TO 83
   82 WRITE(6,233) SIGMA(1)
  233 FORMAT(8X,29HRATIO VELOCITY RATIO, SIGMA = ,F4.2,21H IN RELATIVE VE
     1LOCITY,/)
```

```
      63 CONTINUE
         IF(II.EQ.0) GO TO 64
         WRITE(6,234)
234   FORMAT(5X,34HARBITRARY SIGMA DISTRIBUTION GIVEN,/)
      64 IF(IZ.EQ.0) GO TO 65
         WRITE(6,235)
235   FORMAT(5X,33HARBITRARY BETA DISTRIBUTION GIVEN,/)
      65 IF(IT.EQ.0) GO TO 66
         WRITE(6,237) TUBLAZ,DEL(NBL)
237   FORMAT(5X,30HPARTICLE IS IN SUCTION SURFACE BOUNDARY LAYER, WITH Y
     1/PEL = ,F5.3,5X,32HEXIT BOUNDARY LAYER THICKNESS = ,F8.6)
      66 IF(IS.EQ.0) GO TO 67
         WRITE(6,238) TUBLAZ,DEL(NBL)
238   FORMAT(5X,31HPARTICLE IS IN PRESSURE SURFACE BOUNDARY LAYER, WITH
     1Y/PEL = ,F5.3,5X,32HEXIT BOUNDARY LAYER THICKNESS = ,F8.6)
      67 IF(IB.EQ.0) GO TO 68
         WRITE(6,239) IBPIT
239   FORMAT(5X,54HBLADE-TO-BLADE POSITION OF THE PARTICLE IS, Y/PITCH =
     1 ,F4.2)
      68 IF((IA+IS+IB).GT.0) GO TO 69
         WRITE(6,251)
251   FORMAT(5X,53HBLADE-TO-BLADE POSITION OF THE PARTICLE IS, Y/PITCH =
     1 0.50)
      69 CONTINUE
         WRITE(6,230)
230   FORMAT(5X,/)
         WRITE(6,201)
201   FORMAT(53X,'************ PARTICLE ************',9X,'************
     1 PRESSURE ************',/)
         WRITE(6,202)
202   FORMAT(5X,5HCHORD,4X,6HRADIUS,5X,4HSPAN,7X,1HZ,7X,5HSIGMA,6X,2HVZ,
     1 8X,2HVU,8X,2HVR,8X,1HM,8X,4HVZPS,8X,4HVUPS,8X,4HVRPS,8X,3HALPS,/)
         WRITE(6,203) (A(I),R(I),SPAN(A,Z(I),SIGMA(I),VZ(I),VU(I),VR(I),
     1A(I),VZPS(I),VUPS(I),VRPS(I),ALPS(I)
203   FORMAT(5X,F5.3,F11.5,F8.2,F11.5,F9.3,8F10.2)
C
C        START DO-LOOP TO CALCULATE NEW RADIAL POSITION
C
         DO 30 I=1,11
         II=0
         IIRGL=0
         Z(I+1)=Z(1)+I*CHORD*0.10
         DZ(I)=Z(I+1)-Z(I)
         CA(I+1)=(Z(I+1)-Z(I))/CHORD-0.100
         RMAX=AU+BU*Z(I+1)+CU*Z(I+1)*Z(I+1)
         RMIN=AL+BL*Z(I+1)+CL*Z(I+1)*Z(I+1)
C
C        APPROXIMATION:  FREESTREAM STREAMLINES BY THE FOLLOWING EQ'N;
C             RSL(I+1)=RSL(I)+VRSL(I)*TSL
C
         TEMP=SQRT((RMAX*RMAX-RSL(N)*RMIN)*SPACA+RMIN*RMIN)
C
C        E=1E-9 IS RSL(I+1) LOOP
C
      8 CONTINUE
C
         IIRGL=IIRGL+1
C
         CALL BLADE (ZP,RP,VZP,IZ,IR,ZU,Z ,Z(I+1),IP ,VRSL(I+1),IGS,DRG)
         CALL BLADE (ZP,TP,VUP,IZ,IR,ZU,ZP,Z(I+1),IPP,VUSL(I+1),IZS,DUG)
         CALL BLADE (ZP,RP,VRP,IZ,IP,ZU,ZP,Z(I+1),IP ,VRSL(I+1),IZS,DUG)
```

```
C
      VZBSL(I)=(VZSL(I+1)+VZSL(I))/2.
      TSL=DZ(I)/VZBSL(I)
      VRBSL(I)=(VRSL(I+1)+VRSL(I))/2.
C
      RSL(I+1)=RSL(I)+VRBSL(I)*TSL
C
      IF(ABS(RSL(I+1)-TEMP).LT.0.00001) GO TO 9
      IF(TEMP.GT.25) GO TO 70
      TEMP=RSL(I+1)
      GO TO 8
C
    9 CONTINUE
C
      ARSL(I)=VOSL(I)*VOSL(I)/RSL(I)
      ARSL(I+1)=VOSL(I+1)*VOSL(I+1)/RSL(I+1)
      ARBSL(I)=(ARSL(I+1)+ARSL(I))/2.
C
C        GUESS AT VZ(I+1)
C
      VZ(I+1)=VZ(I)*VZSL(I+1)/VZSL(I)
      VZB(I)=(VZ(I+1)+VZ(I))/2.
      TF=DZ(I)/VZB(I)
C
C        GUESS AT VR(I+1)
C
      VR(I+1)=VRSL(I+1)+VR(I)-VRSL(I)
      VRB(I)=(VR(I+1)+VR(I))/2.
C
C        INITIAL GUESS FOR R(I+1)
C
      TEMP=R(I)+VRB(I)*TF
C
C        10-TO-25 IS R(I+1) LOOP
C
   10 CONTINUE
C
      II=II+1
C
      CALL DIFINT (ZF,RF,VZF,IZ,IR,20,20,Z(I+1),TEMP,VZFS(I+1),IZG,JRG)
      CALL DIFINT (ZF,RF,VOF,IZ,IR,20,20,Z(I+1),TEMP,VOFS(I+1),IZG,JRG)
      CALL DIFINT (ZF,RF,VRF,IZ,IR,20,20,Z(I+1),TEMP,VRFS(I+1),IZG,JRG)
C
      U=UREGA*TEMP
      WOFS(I+1)=U-VOFS(I+1)
      VFS(I+1)=SQRT(VZFS(I+1)*VZFS(I+1)+WOFS(I+1)*WOFS(I+1)+VRFS(I+1)*VR
     1FS(I+1))
      MBIAF(I+1)= ATAN(WOFS(I+1)/VZFS(I+1))
      THETF(I+1)= ATAN(VRFS(I+1)/VZFS(I+1))*180./PI
C
      IF(II.EQ.1) GO TO 14
      IF((14+15).GT.0) GO TO 15
      IF(16.EQ.1) GO TO 16
C
C        SIGMA IS CONSTANT
C
      SIGMA(I+1)=SIGMA(I)
      GO TO 165
C
C        SIGMA FROM DISTRIBUTION GIVEN AS INPUT
C
```

```
      14 CALL INTERPOL (ZSIG,SIGMAG,ISIG,25,Z(I+1),SIGMA(I+1))
         GO TO 165
C
C           SIGMA DISTRIBUTION FROM BOUNDARY LAYER MODEL
C
      15 CALL INTERPOL (ZBL,WSURF,NBL,80,Z(I+1),WREL)
         CALL INTERPOL (ZBL,BETAS,NBL,80,Z(I+1),BETREL)
         SIGMA(I+1)=UUBL(I+1)*WREL*COS(BETREL)/VZFS(I+1)
         GO TO 165
C
C           SIGMA DISTRIBUTION FROM INTERPOLATING IN BLADE-TO-BLADE PLANE
C
      16 CALL LININT (ZF,RF,WSS,IZ,IR,20,20,Z(I+1),TRW,WSSIP1,IZG,JRG)
         CALL LININT (ZF,RF,WPS,IZ,IR,20,20,Z(I+1),TRW,WPSIP1,IZG,JRG)
C
         IF((WSSIP1*WSSIP1-VRFS(I+1)*VRFS(I+1)).LT.0.00) GO TO 161
         V(1)=SQRT(WSSIP1*WSSIP1-VRFS(I+1)*VRFS(I+1))*COS(BETAF(I+1))
         GO TO 162
  161 V(1)=1.00
  162 V(2)=VZFS(I+1)
         IF((WPSIP1*WPSIP1-VRFS(I+1)*VRFS(I+1)).LT.0.00) GO TO 163
         V(3)=SQRT(WPSIP1*WPSIP1-VRFS(I+1)*VRFS(I+1))*COS(BETAF(I+1))
         GO TO 164
  163 V(3)=1.00
  164 CONTINUE
C
         CALL INTERPOL (P,V,3,3,YOPIT,VAXIP1)
C
         SIGMA(I+1)=VAXIP1/VZFS(I+1)
C
  165 CONTINUE
C
         VZ(I+1)=SIGMA(I+1)*VZFS(I+1)
C
         IF(IZ.EQ.1) GO TO 17
C
C           ASSUMPTION:  DBETA DECREASES LINEARLY WITH Z
C                NOTE:  IF DBETA = 0, BETA PARTICLE = BETA FREESTREAM
C
         BETA(I+1)=BETAF(I+1)+DBETA*(1.-CX(I+1))
         GO TO 18
C
C           ELSE:  USE THE BETA DISTRIBUTION GIVEN AS INPUT
C
      17 CALL INTERPOL (ZBETA,BETAIN,IBETA,25,Z(I+1),BETA(I+1))
         BETA(I+1)=BETA(I+1)*PI/180.
C
      18 CONTINUE
C
         BETAF(I+1)=BETAF(I+1)*180./PI
         THETA(I+1)= ATAN(VR(I+1)/VZ(I+1))*180./PI
         W(I+1)=VZ(I+1)*TAN(BETA(I+1))
         BETA(I+1)=BETA(I+1)*180./PI
         VU(I+1)=U-WU(I+1)
         W(I+1)=SQRT(VZ(I+1)*VZ(I+1)+VU(I+1)*WU(I+1)+VR(I+1)*VR(I+1))
C
         VZB(I)=(VZ(I+1)+VZ(I))/2.
         TP=DZ(I)/VZB(I)
         VRB(I)=(VR(I+1)+VR(I))/2.
         AR(I)=VU(I)*VU(I)/R(I)
         AR(I+1)=VU(I+1)*VU(I+1)/TIP
```

```
      AR5(I)=(AR(I+1)+AR(I))/2.
C
      VR(I+1)=VR(I)+(VRSL(I+1)-VRSL(I))/TSL*TP+(ARB(I)-ARBSL(I))*TP
C
      VRB(I)=(VR(I+1)+VR(I))/2.
C
      R(I+1)=R(I)+VRB(I)*TP
C
      IF(ABS(R(I+1)-TEMP).LT.0.00001) GO TO 25
      IF(IT.EQ.25) GO TO 90
      TEMP=R(I+1)
      GO TO 10
C
   25 CONTINUE
C
      IF(R(I+1).GT.RMAX) GO TO 50
      IF(R(I+1).LT.RMIN) GO TO 60
      SPANCA=(R(I+1)-RMIN)/(RMAX-RMIN)
      RSL(I+1)=R(I+1)
      J=I+1
      WRITE(6,203) CX(J),R(J),SPANCA,Z(J),SIGMA(J),VZ(J),VB(J),VR(J),
     1R(J),VZFS(J),VOFS(J),VRFS(J),WFS(J)
C
   30 CONTINUE
C
      CALL LININT (ZF,RF,VZF,IZ,IR,Z0,Z0,Z2A,R2A,VZ2A,IZG,JFG)
      CALL LININT (ZF,RF,VUF,IZ,IR,Z0,Z0,Z2A,R2A,VU2A,IZG,JFG)
      CALL LININT (ZF,RF,VRF,IZ,IR,Z0,Z0,Z2A,R2A,VR2A,IZG,JFG)
C
      WU2A=SIGMGA*R2A-VU2A
      V2A=SQRT(VZ2A*VZ2A+WU2A*WU2A+VR2A*VR2A)
      ALPHZA= ATAN(VU2A/VZ2A)*180./PI
      DELTZA= ATAN(WU2A/VZ2A)*180./PI
      THETZA= ATAN(VR2A/VZ2A)*180./PI
      R1B=SQRT(((R(J)*R(J)-R2L*R2L)*(R1U+R1U-R1L+R1L)/(R2U*R2U-R2L*R2L
     1))+R1L*R1L)
      Z1B=Z1L+(R1B-R1L)*(Z1U-Z1L)/(R1U-R1L)
      IZG=2
C
      CALL LININT (ZF,RF,VZF,IZ,IR,Z0,Z0,Z1B,R1B,VZ1B,IZG,JFG)
      CALL LININT (ZF,RF,VUF,IZ,IR,Z0,Z0,Z1B,R1B,VU1B,IZG,JFG)
      CALL LININT (ZF,RF,VRF,IZ,IR,Z0,Z0,Z1B,R1B,VR1B,IZG,JFG)
C
      WU1B=SIGMGA*R1B-VU1B
      V1B=SQRT(VZ1B*VZ1B+WU1B*WU1B+VR1B*VR1B)
      ALPH1B= ATAN(VU1B/VZ1B)*180./PI
      DELA1B= ATAN(WU1B/VZ1B)*180./PI
      THETA1B= ATAN(VR1B/VZ1B)*180./PI
      ALPHA1= ATAN(VU(1)/VZ(1))*180./PI
      ALPHAJ= ATAN(VU(J)/VZ(J))*180./PI
      ALPH1F= ATAN(VUFS(1)/VZFS(1))*180./PI
      ALPH2B= ATAN(VUFS(J)/VZFS(J))*180./PI
C
      WRITE(6,204)
  204 FORMAT(5X,///)
      WRITE(6,205)
  205 FORMAT(6X,22HBLADE INLET CONDITIONS)
      WRITE(6,206)
  206 FORMAT(3X,1HR,10X,1HZ,9X,2HVZ,8X,2HVU,8X,2HVR,8X,1HW,7X,5HALPHA,
     1X,4HDELA,5X,5HTHETA,/)
      WRITE(6,207) R(1),Z(1),VZ(1),VB(1),VR(1),W(1),ALPHA1,DELA(1),THETA
```

```
     1(1)
207  FORMAT(13X,8HPARTICLE,7X,F8.5,F11.5,4F10.2,3F9.2)
     WRITE(6,208) R(1),Z(1),VZFS(1),VUFS(1),VRFS(1),WFS(1),ALPHA1A,BETAF
     1(1),THETF(1)
208  FORMAT(13X,12HFREESTREAM A,3X,F8.5,F11.5,4F10.2,3F9.2)
     WRITE(6,209) R1B,Z1B,VZ1B,VU1B,VR1B,W1B,ALPHA1B,BETA1B,THETA1B
209  FORMAT(13X,12HFREESTREAM B,3X,F8.5,F11.5,4F10.2,3F9.2,///)
     WRITE(6,210)
210  FORMAT(6X,21HBLADE EXIT CONDITIONS)
     WRITE(6,205)
     WRITE(6,207) R(J),Z(J),VZ(J),VU(J),VR(J),W(J),ALPHAJ,BETA(J),THETA
     1(J)
     WRITE(6,208) R2A,Z2A,VZ2A,VU2A,VR2A,W2A,ALPHA2A,BETA2A,THETA2A
     WRITE(6,209) R(J),Z(J),VZFS(J),VUFS(J),VRFS(J),WFS(J),ALPHA2B,
     1BETAF(J),THETF(J)
C
     BETA(1)=BETA(1)*PI/180.
     BETAF(1)=BETAF(1)*PI/180.
     DRM=R(J)-R(1)
     T02=T01+OMEGA*(R(J)*VU(J)-R(1)*VU(1))/CP
     T01F=OMEGA*R(J)*((F1B*VU1B/R(J)-R(1)*VU(1)/F(J))+VZFS(J)*((1.-SIGM
     1A(J))*TAN(BETAF(J)*PI/180.)))/CP
     XEU=VZ2A/VZFS(J)
     TR77=VZ2A/VZFS(1)
     GUVZ2F=((1.-SIGMA(1))**2+(SIGMA(1)*TAN(BETA(1))-TAN(BETAF(1)))**2-
     1(1./COS(BETAF(1))-SIGMA(1)*COS(BETA(1)-BETAF(1))/COS(BETA(1)))**2)
     2*XEU/2./TAUA
     IF(ABS(GUVZ2F).LT.0.00001) GUVZ2F=0.0
     GUVZ2F=SQRT(GUVZ2F)
     EFF=CP*T01*GUVZ2F*(2.*TAUA/(TAUA+XEU))/PITOT
     DRM=R2A-R(1)
     T02=T01A+OMEGA*(R2A*VU2A-R(1)*VUFS(1))/CP
     DT2=T02A-T01A
     DRM=R(J)-R1B
     T02=T01B+OMEGA*(R(J)*VUFS(J)-F1B*VU1B)/CP
     D1F=T02-T01B
     DELT=T02-T01
C
     WRITE(6,221)
221  FORMAT(6X,15HFREESTREAM TRANSFER)
     WRITE(6,222)
222  FORMAT(3X,5HROTL I,6X,3HT01,7X,3HT02,6X,5HDELT,4X,5HT DIF,4X,5HGUV
     1Z2F,5X,3HEFF,/)
     WRITE(6,223) IFF,T01,T02,DELT,T01F,GUVZ2F,EFF
223  FORMAT(13X,6HPARTICLE,7X,F8.5,2F10.2,2F9.2,2F9.3)
     WRITE(6,224) DRM,T01A,T02A,D1A
224  FORMAT(13X,12HFREESTREAM A,3X,F8.5,2F10.2,F9.2)
     WRITE(6,225) DRM,T01B,T02B,D1B
225  FORMAT(13X,12HFREESTREAM B,3X,F8.5,2F10.2,F9.2)
     GO TO 1
C
  50 WRITE(6,240)
240  FORMAT(10X,/,10X,40HRADIUS OF PARTICLE IS GREATER THAN OUTER RADI
     1US)
     GO TO 1
  60 WRITE(6,241)
241  FORMAT(10X,/,10X,42HRADIUS OF PARTICLE IS LESS THAN HUB RADIUS)
     GO TO 1
  70 WRITE(6,242)
242  FORMAT(10X,/,10X,45HSOL LOOP DID NOT CONVERGE AFTER 25 ITERATIONS)
     GO TO 1
```

```
55000        90 WRITE(6,244)
55100       244 FORMAT(10X,/,10X,45HR(I+1) LOOP DID NOT CONVERGE AFTER 25 ITERATIO
55200          1NS)
55300           GO TO 1
55400     C
55500        11 CONTINUE
55600           WRITE(6,200)
55700       200 FORMAT(1H1)
55800           END
55900     C-------------------------------------------------------------------------
```

```
      SUBROUTINE LININT(X,Y,Z,NX,NY,NDIMX,NDIMY,X0,Y0,Z0,I,J)
C
C--LININT LOCATES THE POINT (X0,Y0) IN A 2-D  MESH WITH
C--COORDINATES STORED IN THE X AND Y ARRAYS.  THEN THE VALUE OF Z0 AT
C--(X0,Y0) IS INTERPOLATED FROM THE Z ARRAY VALUES CORRESPONDING
C--TO THE X AND Y ARRAYS
C
      DIMENSION X(NDIMX,NDIMY),Y(NDIMX,NDIMY),Z(NDIMX,NDIMY)
      DIMENSION EXTRAP(2)
      INTEGER ABOVE,RIGHT
C--FIND I,J SUCH THAT (X0,Y0) IS IN COLUMN I FROM THE LEFT AND IN ROW J
C--FROM THE BOTTOM
      IF(NX.LT.2.OR.NY.LT.2) STOP
      IF(I.LE.0) I = 1
      IF(I.GE.NX) I = NX-1
      IF(J.LE.0) J = 1
      IF(J.GE.NY) J = NY-1
   10 ABOVE = -1
      RIGHT = -1
      IF(Y0.GE.Y(I,J)+(X0-X(I,J))/(X(I+1,J)-X(I,J))*(Y(I+1,J)-Y(I,J)))
     1   ABOVE = ABOVE+1
      IF(Y0.GE.Y(I,J+1)+(X0-X(I,J+1))/(X(I+1,J+1)-X(I,J+1))*
     1   (Y(I+1,J+1)-Y(I,J+1)))  ABOVE = ABOVE+1
      IF(X0.GE.X(I,J)+(Y0-Y(I,J))/(Y(I,J+1)-Y(I,J))*(X(I,J+1)-X(I,J)))
     1   RIGHT = RIGHT+1
      IF(X0.GE.X(I+1,J)+(Y0-Y(J+1,J))/(Y(J+1,J+1)-Y(I+1,J))*
     1   (X(I+1,J+1)-X(I+1,J)))  RIGHT = RIGHT+1
      II = I+RIGHT
      JJ = J+ABOVE
      IF(II.LT.1.OR.II.GE.NX) RIGHT = 0
      IF(JJ.LT.1.OR.JJ.GE.NY) ABOVE = 0
      IF(ABOVE**2+RIGHT**2.EQ.0) GO TO 20
      I = I+RIGHT
      J = J+ABOVE
      GO TO 10
   20 IJFX = 1
C-- SET EXTRAP TO INDICATE EXTRAPOLATION
      EXTRAP(1) = 0.
      EXTRAP(2) = 0.
      IF(I0.LT.1) EXTRAP(2) = -1.
      IF(I.GE.NX) EXTRAP(2) = 1.
      IF(JJ.LT.1) EXTRAP(1) = -1.
      IF(JJ.GE.NY) EXTRAP(1) = 1.
C--CALCULATE CONSTANTS TO CALCULATE FY
      Y13 = Y(I,J)-Y(I,J+1)
      X13 = X(I,J)-X(I,J+1)
      Y42 = Y(I+1,J+1)-Y(I+1,J)
      X42 = X(I+1,J+1)-X(I+1,J)
      Y01 = Y0-Y(I,J)
      X01 = X0-X(I,J)
      Y02 = Y0-Y(I+1,J)
      X02 = X0-X(I+1,J)
      Y21 = Y(I+1,J)-Y(I,J)
      X21 = X(I+1,J)-X(I,J)
C--CALCULATE COEFFICIENTS OF QUADRATIC EQUATION FOR FRACTIONAL DISTANCE
C--IN QUADRILATERAL
   30 QA = Y13*X42-X13*Y42
      QB = X13*Y02-Y13*X02+Y01*X42-X01*Y42
      QC = Y01*X21-X01*Y21
      DISCR = QB**2-4.*QA*QC
      IF(DISCR.LT.0.) GO TO 110
```

```
C--CHECK TO SEE IF QUADRATIC EQUATION IS CLOSE TO LINEAR
      IF(ABS(4.*QA*QC).LE.QB**2*.01) GO TO 80
      FA = -QB/2./QA
      FB = SQRT(DISCR)/2./QA
      F1 = FA+FB
      F2 = FA-FB
C--CHECK TO DETERMINE WHETHER F1 OR F2 IS THE PROPER SOLUTION
      CASE = -1.
      IF(EXTRAP(IJEX)) 40,50,60
C--EXTRAPOLATION BELOW OR TO LEFT (FF LESS THAN 0.)
   40 IF(F1.LT..01) CASE = CASE+1.
      IF(F2.LT..01) CASE = CASE+2.
      IF(CASE.LT.1.5) GO TO 70
      CASE = CASE-1.
      IF(F2.LT.F1) CASE = CASE-1.
      GO TO 70
C--NO EXTRAPOLATION
   50 IF(ABS(F1-.5).LT..51) CASE = CASE+1.
      IF(ABS(F2-.5).LT..51) CASE = CASE+2.
      GO TO 70
C--EXTRAPOLATION ABOVE OR TO RIGHT (FF GREATER THAN 1.)
   60 IF(F1.GT..99) CASE = CASE+1.
      IF(F2.GT..99) CASE = CASE+2.
      IF(CASE.GT.1.5) GO TO 70
      CASE = CASE-1.
      IF(F1.GT.F2) CASE = CASE-1.
   70 IF(ABS(CASE-.5).GT..6) GO TO 110
      FF = (1.-CASE)*F1+CASE*F2
      GO TO 90
C--IF QUADRATIC EQUATION IS NEAR LINEAR, USE BINOMIAL EXPANSION FOR FF
   80 ACB2 = QA/QB*QC/QB
      IF(ABS(ACB2).LT.1.E-8) ACB2=0.
      FF = -QC/QB*(1.+ACB2+2.*ACB2**2)
   90 IF(IJEX.EQ.2) GO TO 100
      IJEX = IJEX+1
      FY = FF
C--INTERCHANGE CORNER POINTS TO GET FX
      Y13 = Y(I,J)-Y(I+1,J)
      X13 = X(I,J)-X(I+1,J)
      Y42 = Y(I+1,J+1)-Y(I,J+1)
      X42 = X(I+1,J+1)-X(I,J+1)
      Y02 = Y0-Y(I,J+1)
      X02 = X0-X(I,J+1)
      Y21 = Y(I,J+1)-Y(I,J)
      X21 = X(I,J+1)-X(I,J)
      GO TO 30
C--CALCULATE INTERPOLATED VALUE
  100 FX = FF
      Z0 = Z(I,J)*(1.-FX)*(1.-FY)+Z(I+1,J)*FX*(1.-FY)+Z(I,J+1)*(1.-FX)
     1    *FY+Z(I+1,J+1)*FX*FY
      RETURN
C-- PRINT ERROR MESSAGE IF THERE IS A PROBLEM IN OBTAINING A SOLUTION
  110 Z0 = 0.
      WRITE(6,1000) I,J
      RETURN
 1000 FORMAT(38H1LINT CANNOT FIND INTERPOLATED VALUE/4H I =,I6,4H J =,
     1I6)
      END
C-------------------------------------------------------------------------------
      SUBROUTINE INTERPOL (X,Y,GP,NDIM,X0,Y0)
C
```

```
C
C        THIS IS AN INTERPOLATION ROUTINE USING A SECOND ORDER FIT OF
C        THE FUNCTION Y=F(X).  IT WILL ALSO EXTRAPOLATE TO THE LEFT
C        AND THE RIGHT A DISTANCE OUT GREATER THAN THE FIRST (TO THE
C        LEFT) OR THE LAST (TO THE RIGHT) DELTA X INCREMENT.
C
      DIMENSION X(NDIM),Y(NDIM)
C
      IF(X0.LE.X(1)) GO TO 40
      IF(X0.GE.X(NP)) GO TO 50
C
C        INTERPOLATION
C
      I=0
C
   10 CONTINUE
      I=I+1
      IF(X(I).GT.X0) GO TO 20
      IF(I.GT.NP) GO TO 70
      GO TO 10
   20 CONTINUE
C
      IF((X0-X(I-1)).LT.(X(I)-X0)) I=I-1
C
      IF(I.EQ.1) I=2
      IF(I.EQ.NP) I=NP-1
C
      C=((Y(I+1)-Y(I))/(X(I+1)-X(I))-(Y(I)-Y(I-1))/(X(I)-X(I-1)))/(X(I+1
     1)-X(I-1))
      B=(Y(I)-Y(I-1)-C*(X(I)*X(I)-X(I-1)*X(I-1)))/(X(I)-X(I-1))
      A=Y(I)-B*X(I)-C*X(I)*X(I)
      Y0=A+B*X0+C*X0*X0
      RETURN
C
C        EXTRAPOLATION TO THE LEFT
C
   40 CONTINUE
      DX=X(2)-X(1)
      XM1=X(1)-DX
      IF(X0.LT.XM1) GO TO 80
      I=2
      C=((Y(I+1)-Y(I))/(X(I+1)-X(I))-(Y(I)-Y(I-1))/(X(I)-X(I-1)))/(X(I+1
     1)-X(I-1))
      B=(Y(I)-Y(I-1)-C*(X(I)*X(I)-X(I-1)*X(I-1)))/(X(I)-X(I-1))
      A=Y(I)-B*X(I)-C*X(I)*X(I)
      Y0=A+B*X0+C*X0*X0
      RETURN
C
C        EXTRAPOLATION TO THE RIGHT
C
   50 CONTINUE
      J=NP-1
      DX=X(NP)-X(J)
      XP1=X(NP)+DX
      IF(X0.GT.XP1) GO TO 90
      I=J
      C=((Y(I+1)-Y(I))/(X(I+1)-X(I))-(Y(I)-Y(I-1))/(X(I)-X(I-1)))/(X(I+1
     1)-X(I-1))
      B=(Y(I)-Y(I-1)-C*(X(I)*X(I)-X(I-1)*X(I-1)))/(X(I)-X(I-1))
      A=Y(I)-B*X(I)-C*X(I)*X(I)
      Y0=A+B*X0+C*X0*X0
      RETURN
```

```
C
   70 WRITE(6,201)
  201 FORMAT(5X,30HSOMETHING IS WRONG IN INTERPOL)
      RETURN
   80 WRITE(6,202)
  202 FORMAT(5X,25HX0 IS TOO FAR TO THE LEFT)
      RETURN
   90 WRITE(6,203)
  203 FORMAT(5X,26HX0 IS TOO FAR TO THE RIGHT)
      RETURN
      END
C-----------------------------------------------------------------------
      SUBROUTINE BOUNDAY (W,BETA,ZBL,REC,NDIM,ABL,CF,GAM,DEL)
C
C        THIS SUBROUTINE WILL CALCULATE THE SKIN FRICTION COEFF, CF,
C        THE LEHOLL COEFF, GAMMA, AND THE BOUNDARY LAYER MOMENTUM
C        THICKNESS, DEL.
C
      DIMENSION W(NDIM),BETA(NDIM),ZBL(NDIM)
      DIMENSION CF(NDIM),GAM(NDIM),DEL(NDIM)
      DIMENSION THETA(80)
C
      CHORD=ZBL(NBL)-ZBL(1)
      VIS=W(1)*CHORD/REC
C
C        INITIAL STARTING CONDITIONS
C
      H12=1.45
      CF(1)=0.0025
      DS=(ZBL(2)-ZBL(1))/COS((BETA(2)+BETA(1))/2.)
      L=0
C
      TEMP0=CF(1)*DS/(2.+(4.+2.*H12)*(W(2)/W(1)-1.))
    2 CONTINUE
      L=L+1
      REDZ=W(1)*TEMP0/VIS
      H12=1.63+0.9775*ALOG10(REDZ)
      CF(1)=0.246*EXP(-1.561*H12)*(REDZ)**(-0.268)
      THETA(1)=CF(1)*DS/(2.+(4.+2.*H12)*(W(2)/W(1)-1.))
      IF(ABS(THETA(1)-TEMP0).LT.(0.01*THETA(1))) GO TO 3
      IF(L.GT.50) GO TO 30
      TEMP0=THETA(1)
      GO TO 2
    3 CONTINUE
C
      G=(H12-1.)/H12/SQRT(CF(1)/2.)
C
      A=0.3714
      B=1.15-G*0.41/2.
      C=1.2414-2.*G*0.41/3.
C
      GAMP=(-B-SQRT(B*B-4.*A*C))/2./A
      GAMM=(-B+SQRT(B*B-4.*A*C))/2./A
C
C        ASSUME THAT GAM(1) IS POSITIVE TERM OF QUAD.
C
      GAM(1)=GAMP
C
      H1=1.535*(H12-0.7)**(-2.715)+3.3
      DEL(1)=THETA(1)*(H1+H12)
C
```

```
      THETA(2)=THETA(1)+(CF(1)*(ZBL(2)-ZBL(1))/COS((BETA(2)+BETA(1))/2.)
     1/2.-(2.+H12)*THETA(1)*(W(2)-W(1))/W(1))
      RED2=W(2)*THETA(2)/VIS
      H12=1.63-0.0775*ALOG10(RED2)
      CF(2)=0.246*EXP(-1.561*H12)*(RED2)**(-0.268)
C
      G=(H12-1.)/H12/SQRT(CF(2)/2.)
C
      A=0.3714
      B=1.15-G*0.41/2.
      C=1.2444-2.*G*0.41/3.
C
      GAMM=(-B-SQRT(B*B-4.*A*C))/2./A
      GAMP=(-B+SQRT(B*B-4.*A*C))/2./A
C
      GAM(2)=GAMP
C
      H1=1.535*(H12-0.70)**(-2.715)+3.3
      DEL(2)=THETA(2)*(H1+H12)
C
      NBL1=NBL-1
C
C     LOOP TO CALCULATE BOUNDARY LAYER PARAMETERS
C
      DO 10 I=2,NBL1
C
      BETAA=(BETA(I+1)+BETA(I))/2.
C
      THETA(I+1)=THETA(I-1)+(CF(I)*(ZBL(I+1)-ZBL(I))/COS(BETAA)-(2.+H12)
     1*THETA(I)*(W(I+1)-W(I-1))/W(I))
      RED2=W(I+1)*     A(I+1)/VIS
      H12=1.63-0.07    ALOG10(RED2)
      CF(I+1)=0.246    EXP(-1.561*H12)*(RED2)**(-0.268)
C
      G=(H12-1.)/H12/     (CF(I+1)/2.)
C
      A=0.3714
      B=1.15-G*0.41/2.
      C=1.2444-2.*G*0.41/3.
C
      GAMM=(-B-SQRT(B*B-4.*A*C))/2./A
      GAMP=(-B+SQRT(B*B-4.*A*C))/2./A
C
      GAM(I+1)=GAMP
C
      H1=1.535*(H12-0.70)**(-2.715)+3.3
      DEL(I+1)=THETA(I+1)*(H1+H12)
C
   10 CONTINUE
      RETURN
C
   30 WRITE(6,200) L
  200 FORMAT(10X,34HSOMETHING IS WRONG IN BOUNDAY, L = ,I3)
      RETURN
      END
C-----------------------------------------------------------------------------
      SUBROUTINE VELRATIO (CF,GAM,DEL,ZBL,Y,NDIM,NBL,UOUT)
C
C     THIS SUBROUTINE WILL CALCULATE THE BOUNDARY LAYER VELOCITY
C     PROFILE USING COFFELL'S METHOD.
C
```

```
      DIMENSION CF(NDIM),GAM(NDIM),DEL(NDIM),ZBL(NDIM)
      DIMENSION GOOF(NDIF)
C
      CHORD=ZBL(NBL)-ZBL(1)
C
      DO 10 I=2,12
C
      Z=ZBL(1)+(I-2)*CHORD/10.
C
      CALL INTERPOL (ZBL,CF,NBL,NDIM,Z,CFVR)
      CALL INTERPOL (ZBL,GAM,NBL,NDIM,Z,GAMVR)
      CALL INTERPOL (ZBL,DEL,NBL,NDIF,Z,DELVR)
C
      YOO=1/DELVR
C
      IF(YOO.GE.1.00) GO TO 5
C
      TERM1=((YOO)**2-1.)/2.
      TERM2=ALOG(YOO)
      TERM3=2.*(YOO)**3-3.*(YOO)**2+1.
C
      GOOF(I)=1.-SQRT(CFVR/2.)*(TERM1-TERM2+GAMVR*TERM3)
      GO TO 10
C
    5 GOOF(I)=1.00
C
   10 CONTINUE
C
      RETURN
      END
```

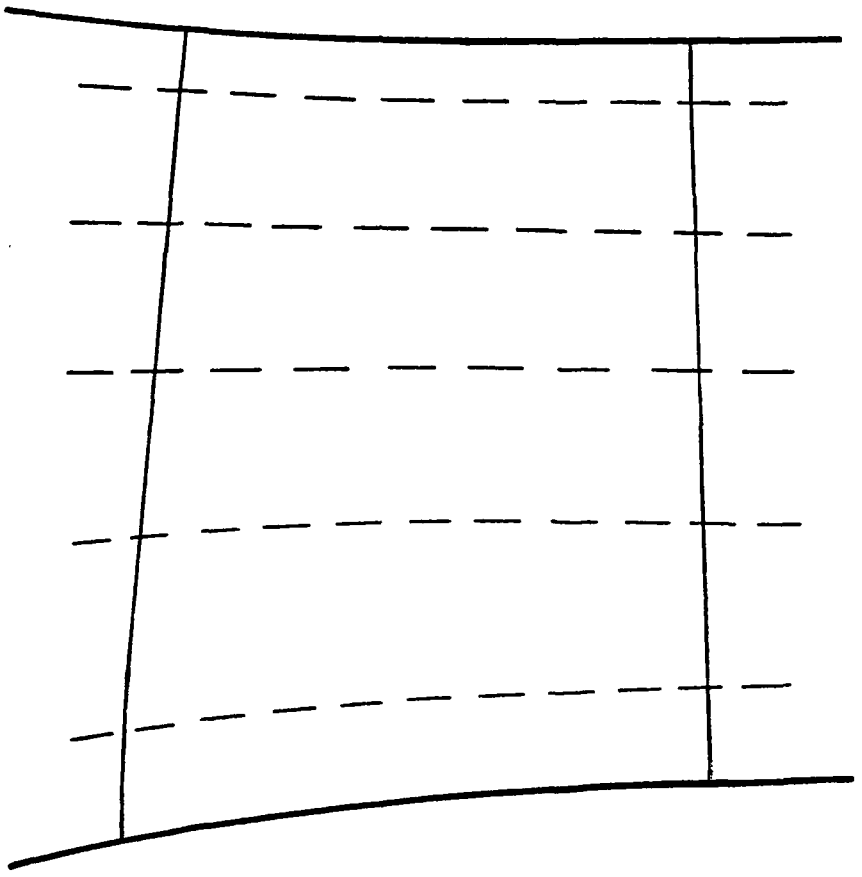

Figure 1. Meridional Streamline Network.

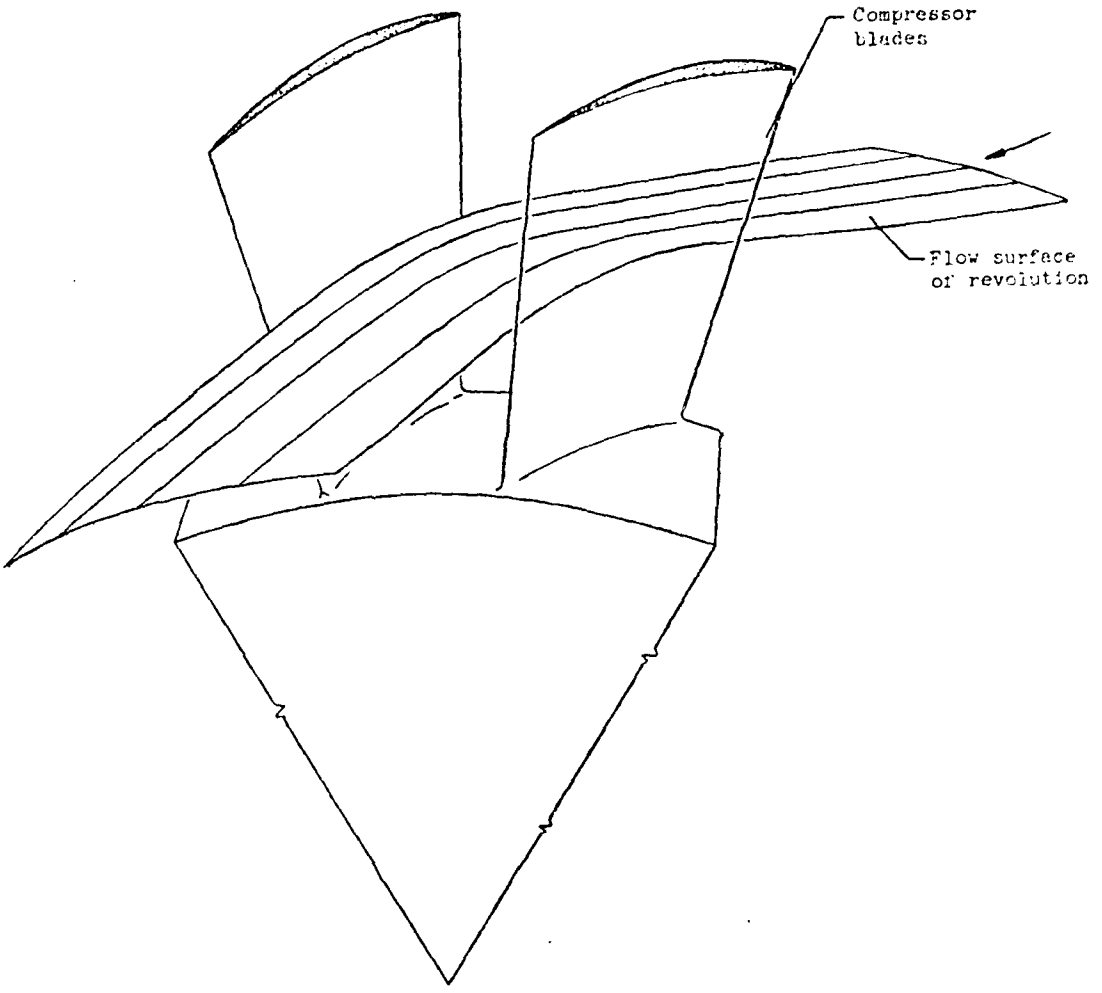

Figure 2. Inviscid Through-Flow Streamsheet.

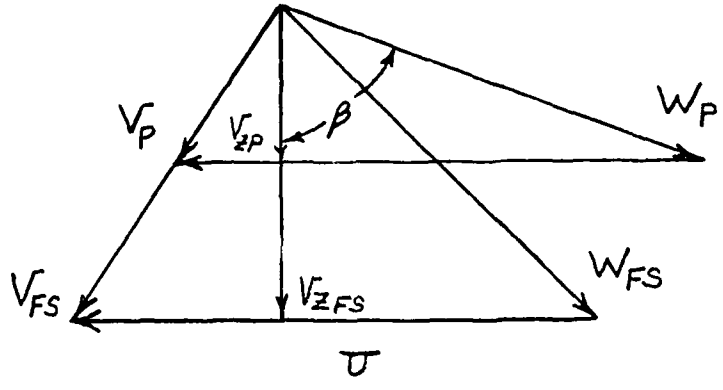

a). Rotor Inlet.

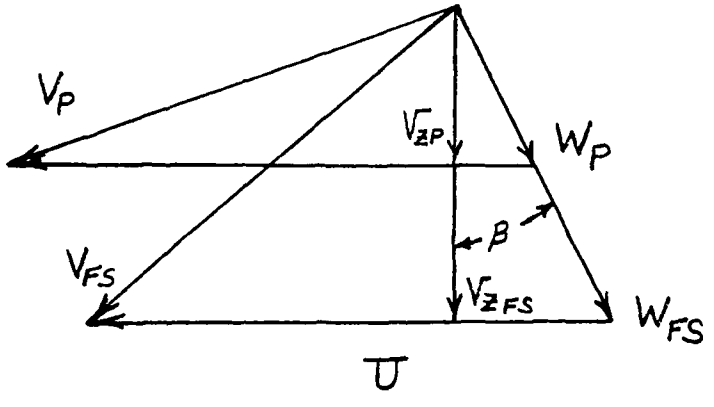

b). Rotor Exit.

Figure 3. Rotor Velocity Triangles For Absolute Velocity Defect.

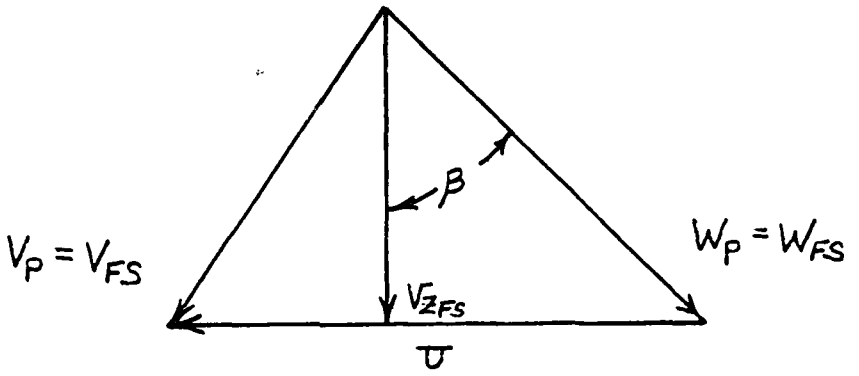

a). Rotor Inlet.

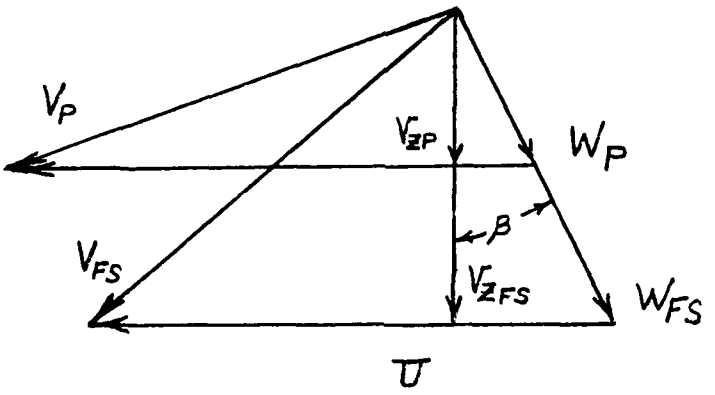

b). Rotor Exit.

Figure 4. Rotor Velocity Triangles For Relative Velocity Defect.

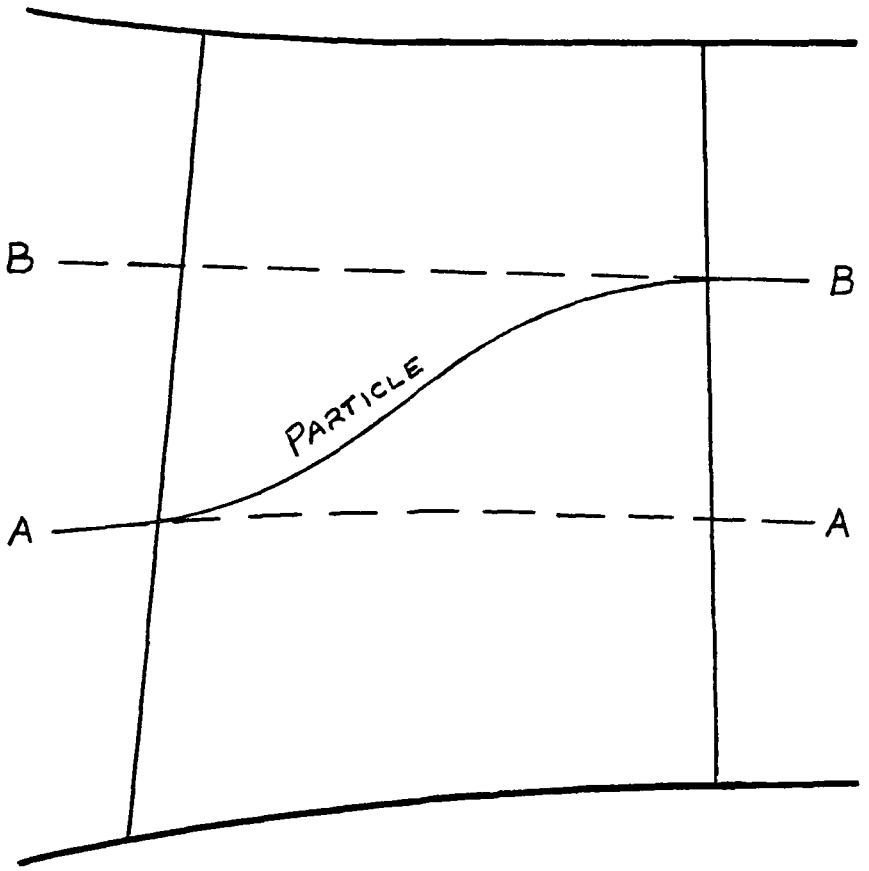

Figure 5. Meridional Streamline Nomenclature.

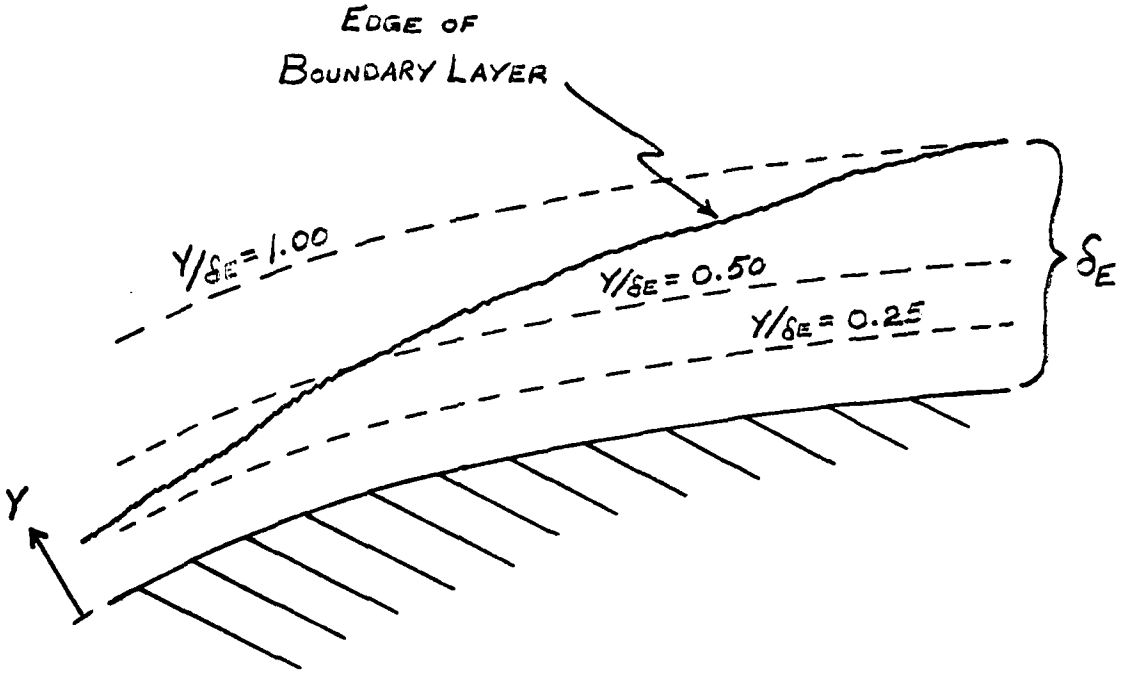

Figure 6. Boundary Layer Streamline Specification.

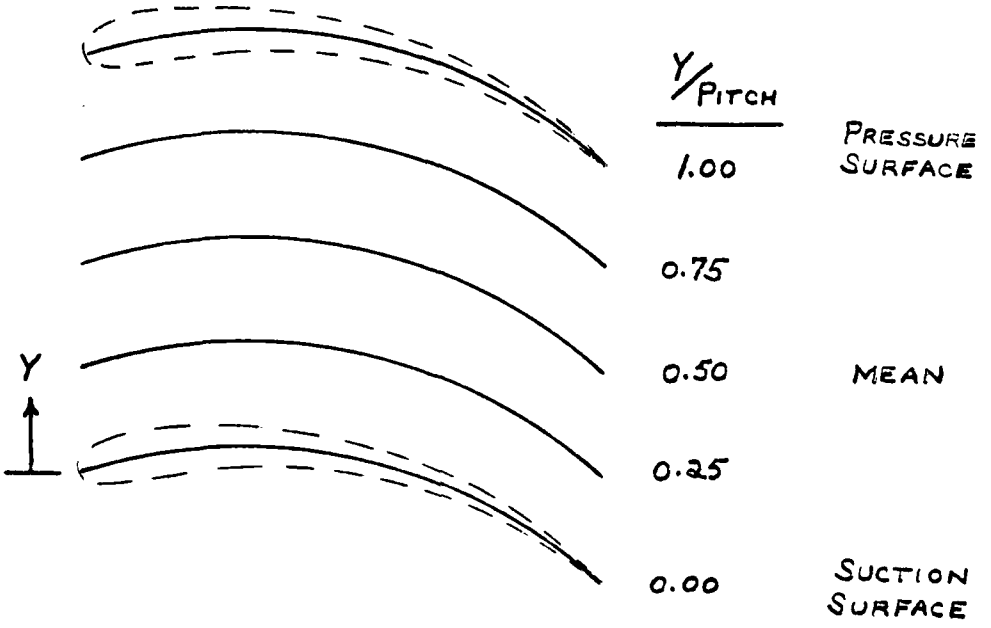

Figure 7. Blade-to-Blade Streamline Approximation and Notation.

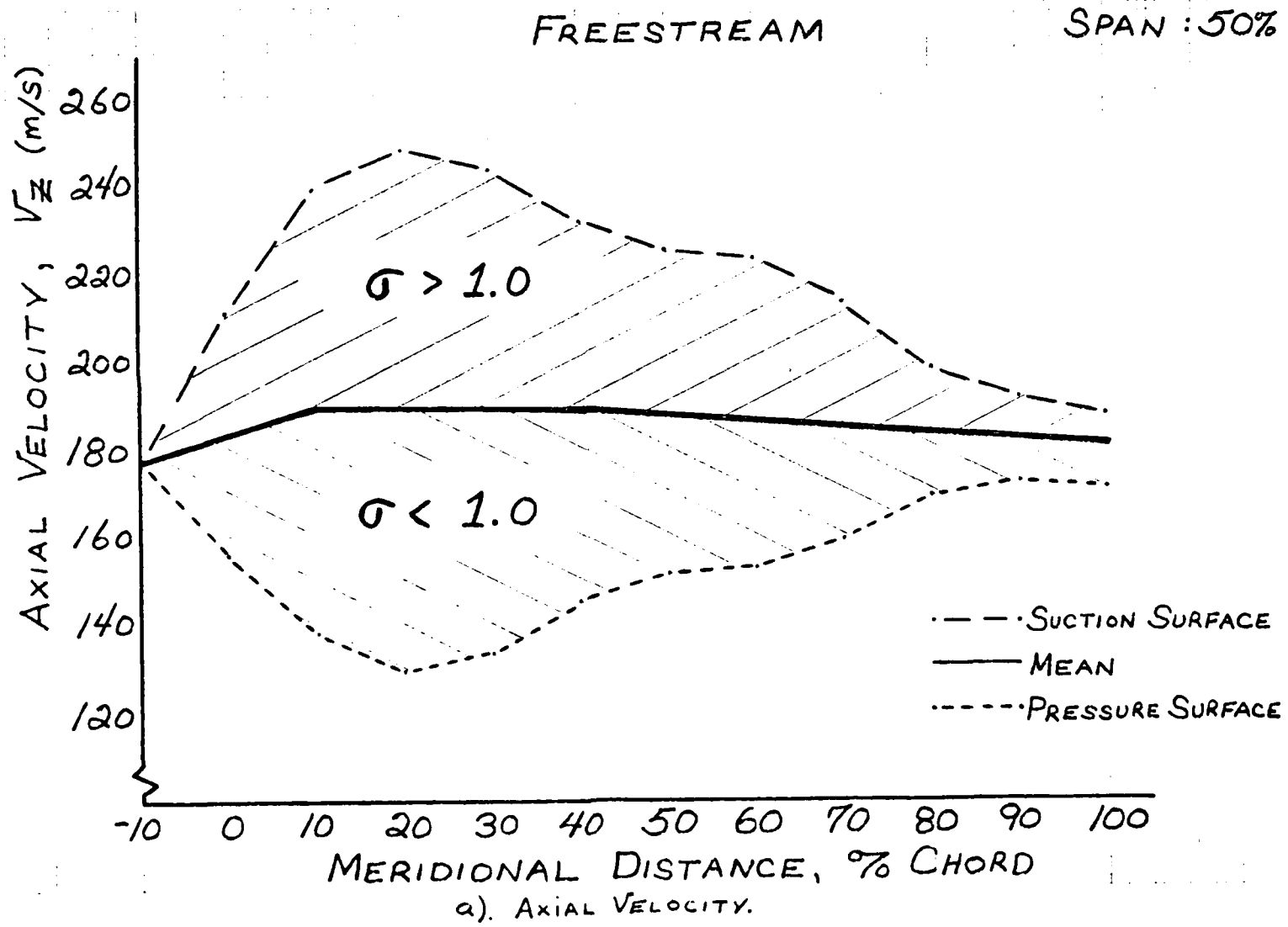

a). AXIAL VELOCITY.

FIGURE 8. FREESTREAM VELOCITY EVOLUTION, 50% SPAN.

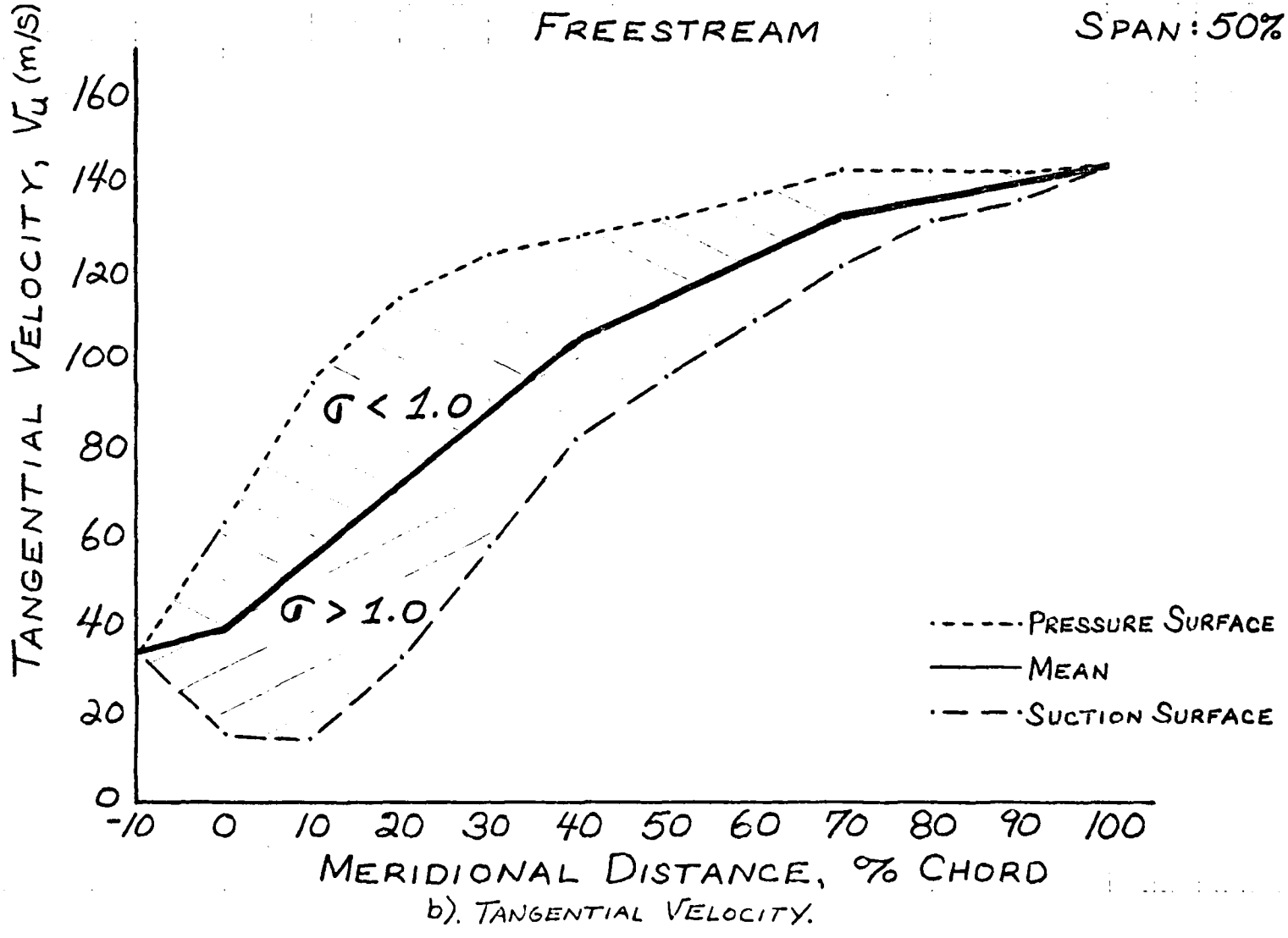

b). TANGENTIAL VELOCITY.

FIGURE 8. FREESTREAM VELOCITY EVOLUTION, 50% SPAN.

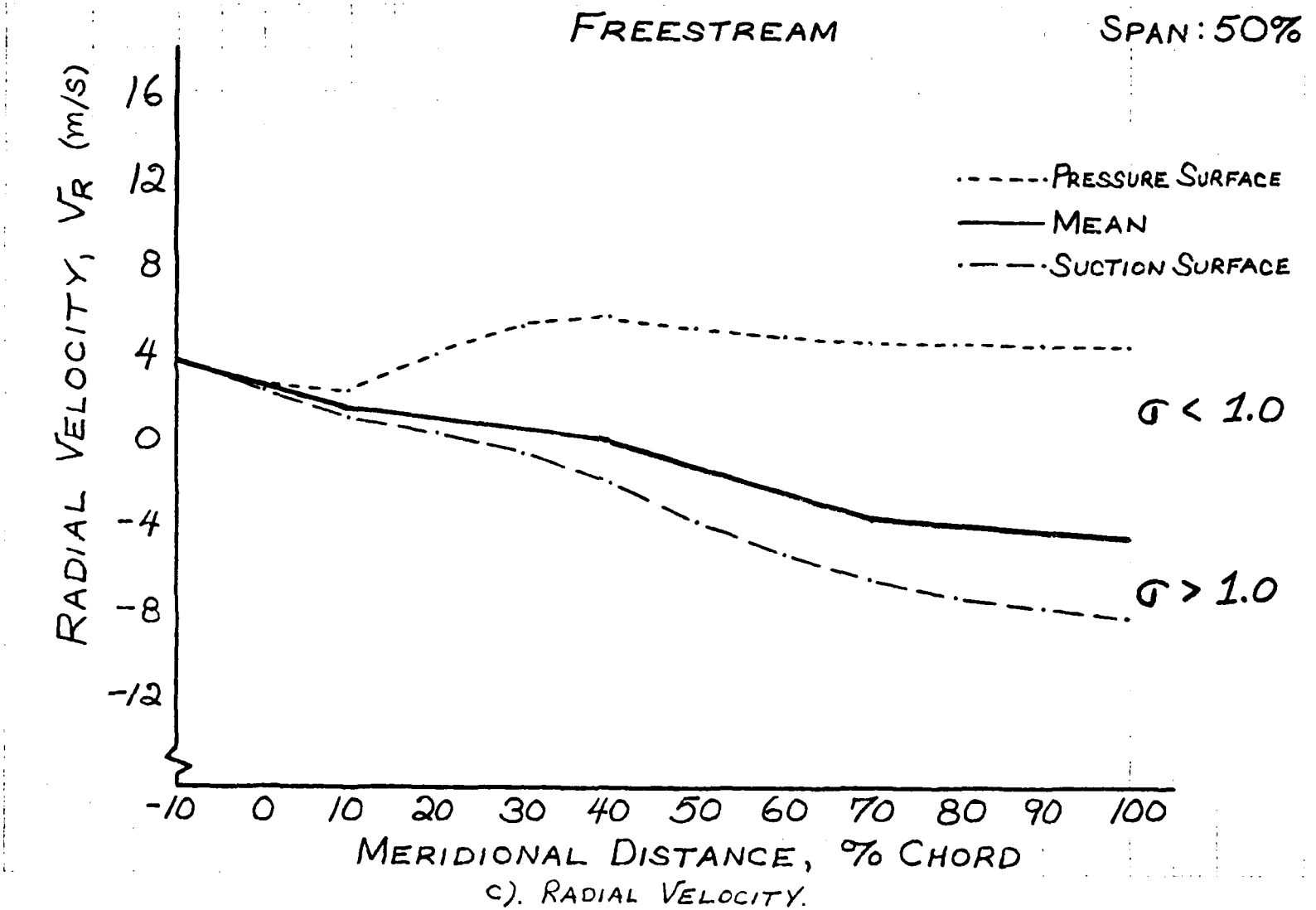

c). RADIAL VELOCITY.

FIGURE 8. FREESTREAM VELOCITY EVOLUTION, 50% SPAN.

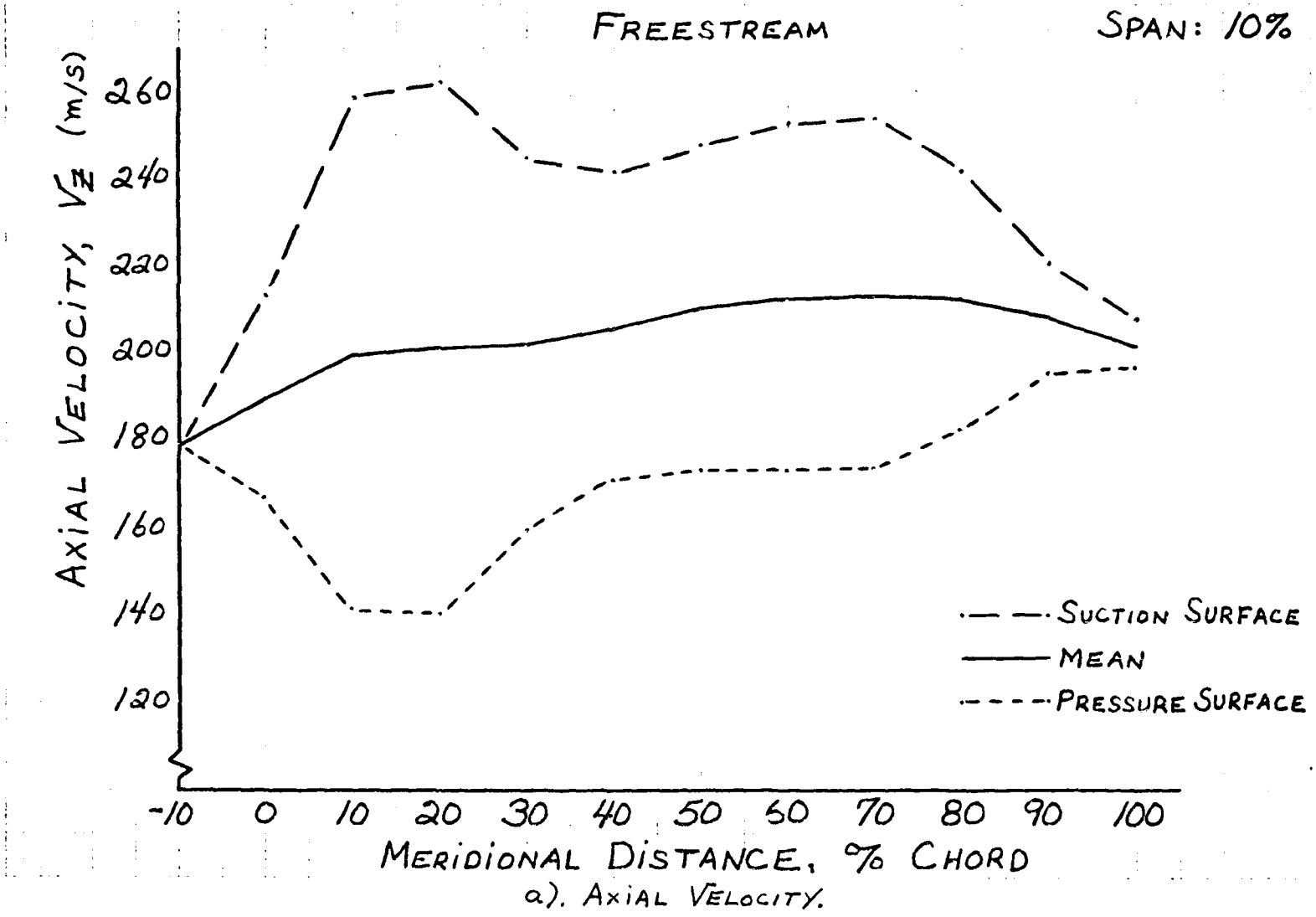

a). AXIAL VELOCITY.

FIGURE 9. FREESTREAM VELOCITY EVOLUTION, 10% SPAN.

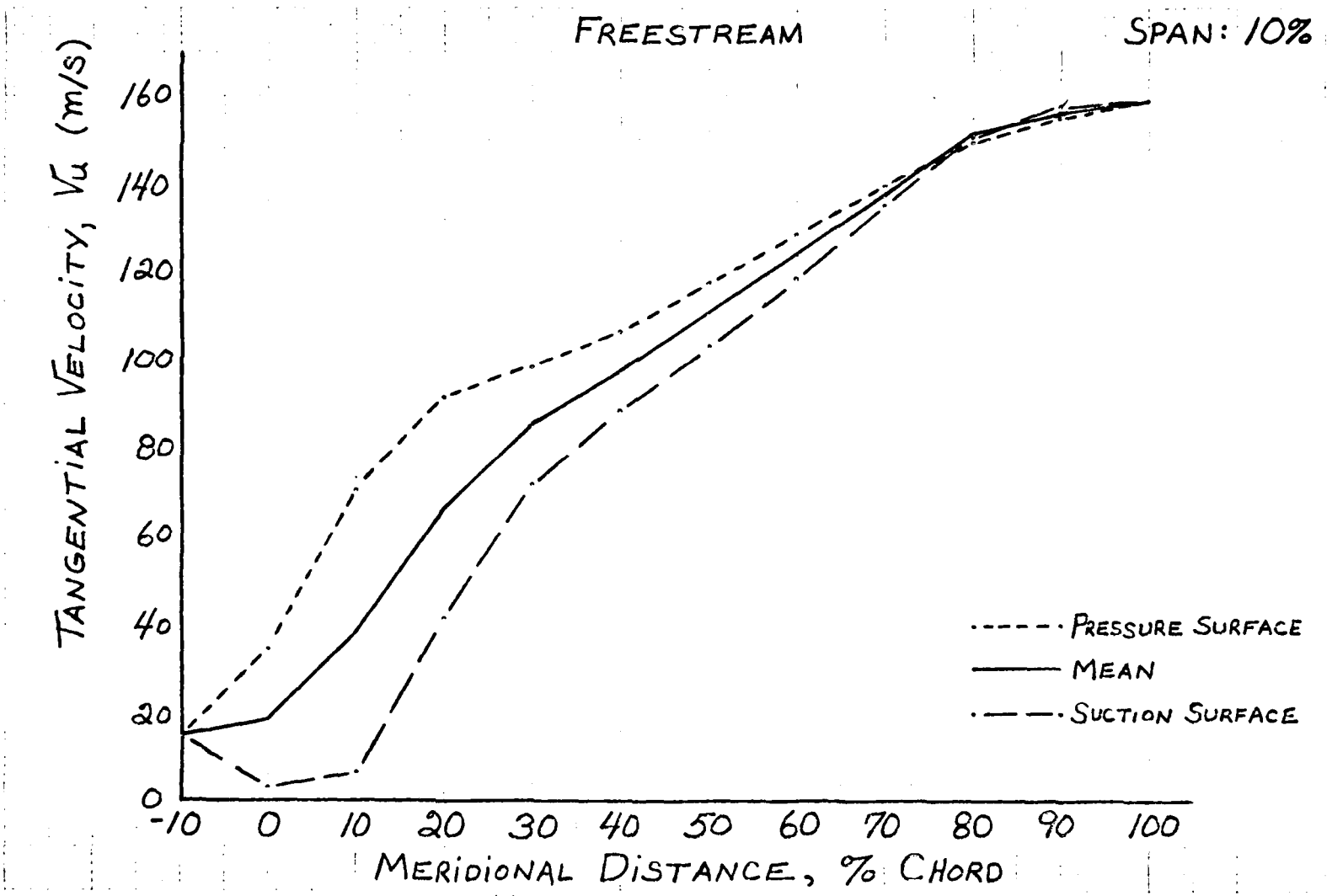

b). TANGENTIAL VELOCITY.

FIGURE 9. FREESTREAM VELOCITY EVOLUTION, 10% SPAN.

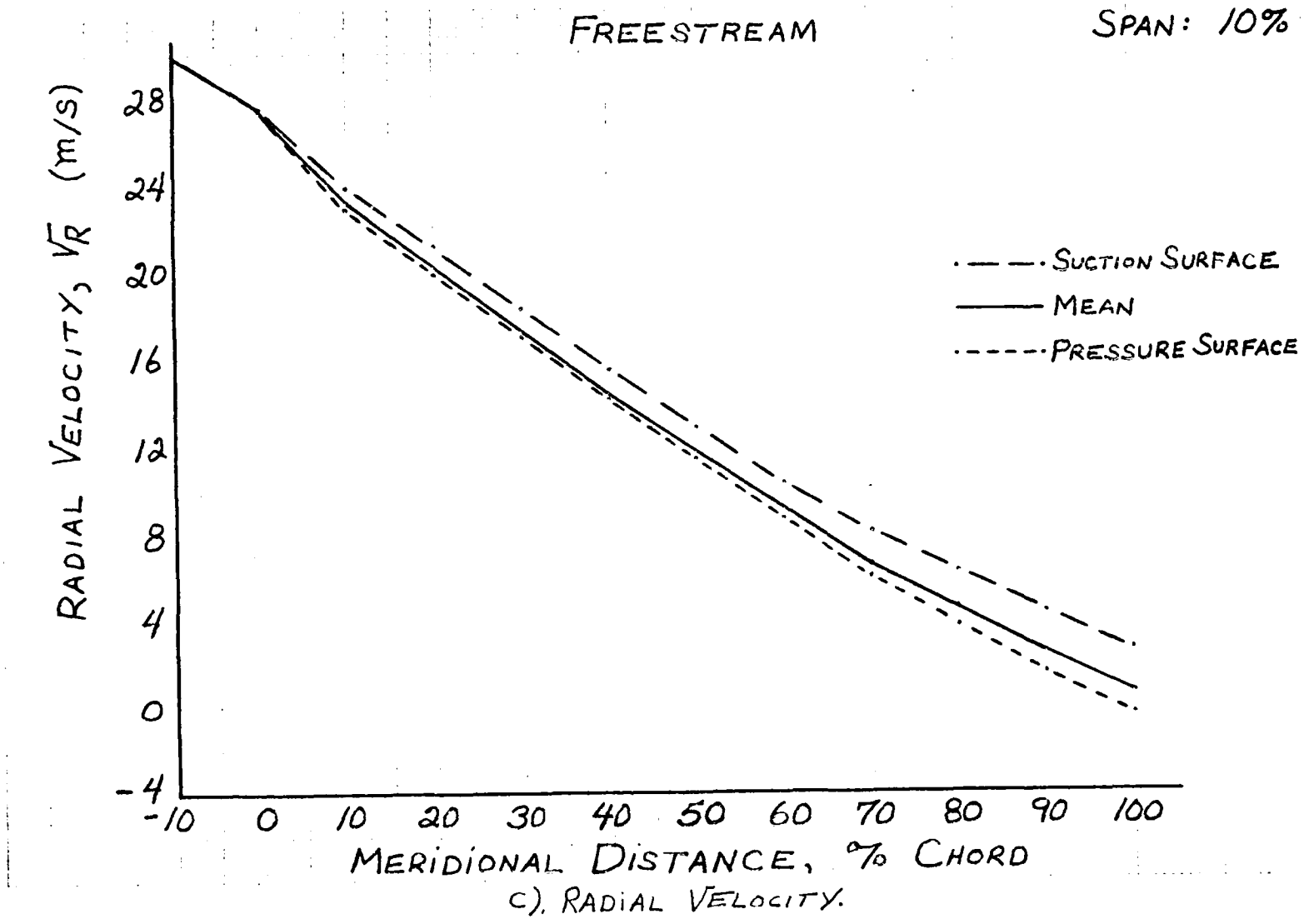

c). RADIAL VELOCITY.

FIGURE 9. FREESTREAM VELOCITY EVOLUTION, 10% SPAN.

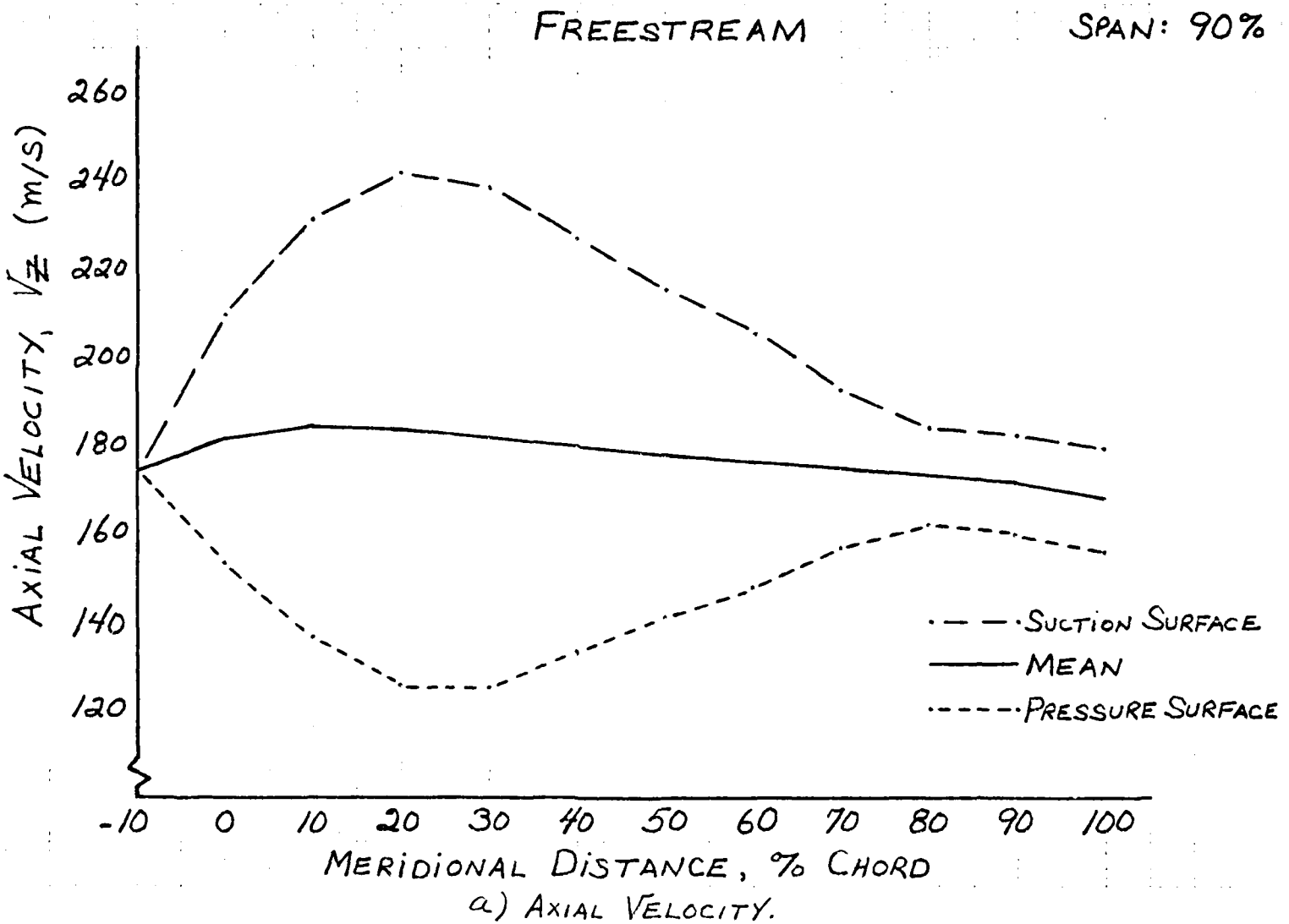

a) AXIAL VELOCITY.

FIGURE 10. FREESTREAM VELOCITY EVOLUTION, 90% SPAN.

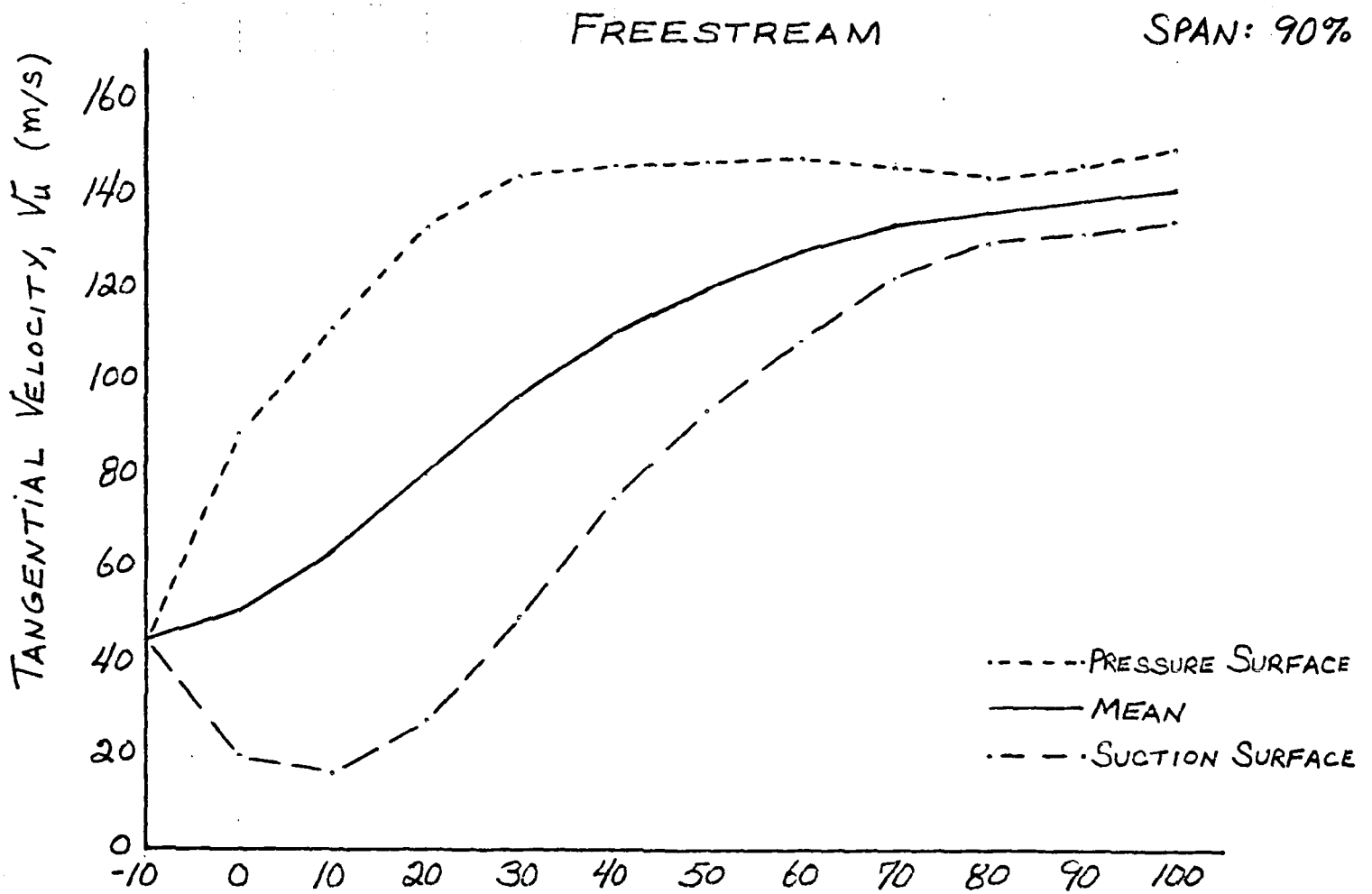

b). TANGENTIAL VELOCITY.

FIGURE 10. FREESTREAM VELOCITY EVOLUTION, 90% SPAN.

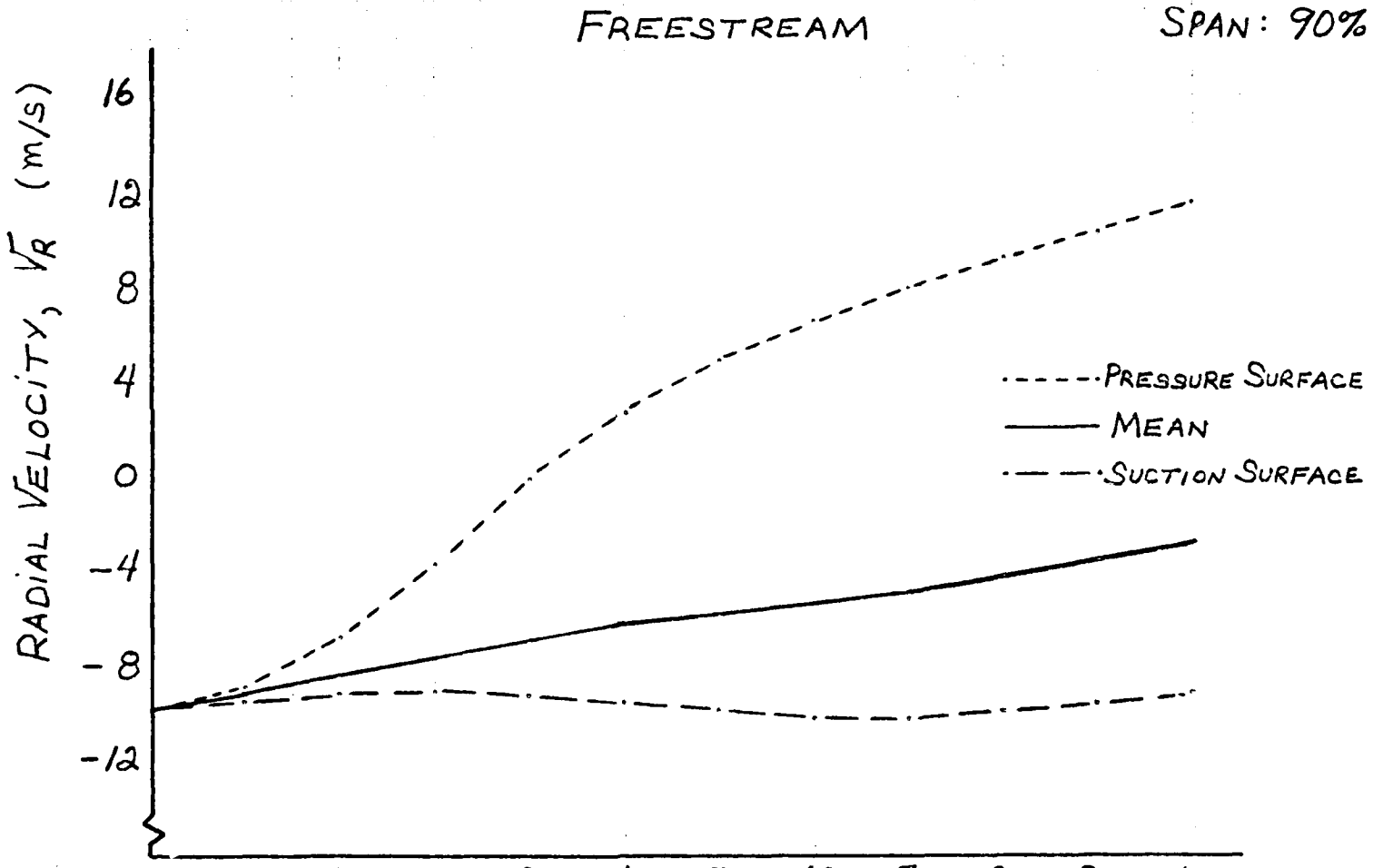

c). RADIAL VELOCITY.

FIGURE 70. FREESTREAM VELOCITY EVOLUTION, 90% SPAN.

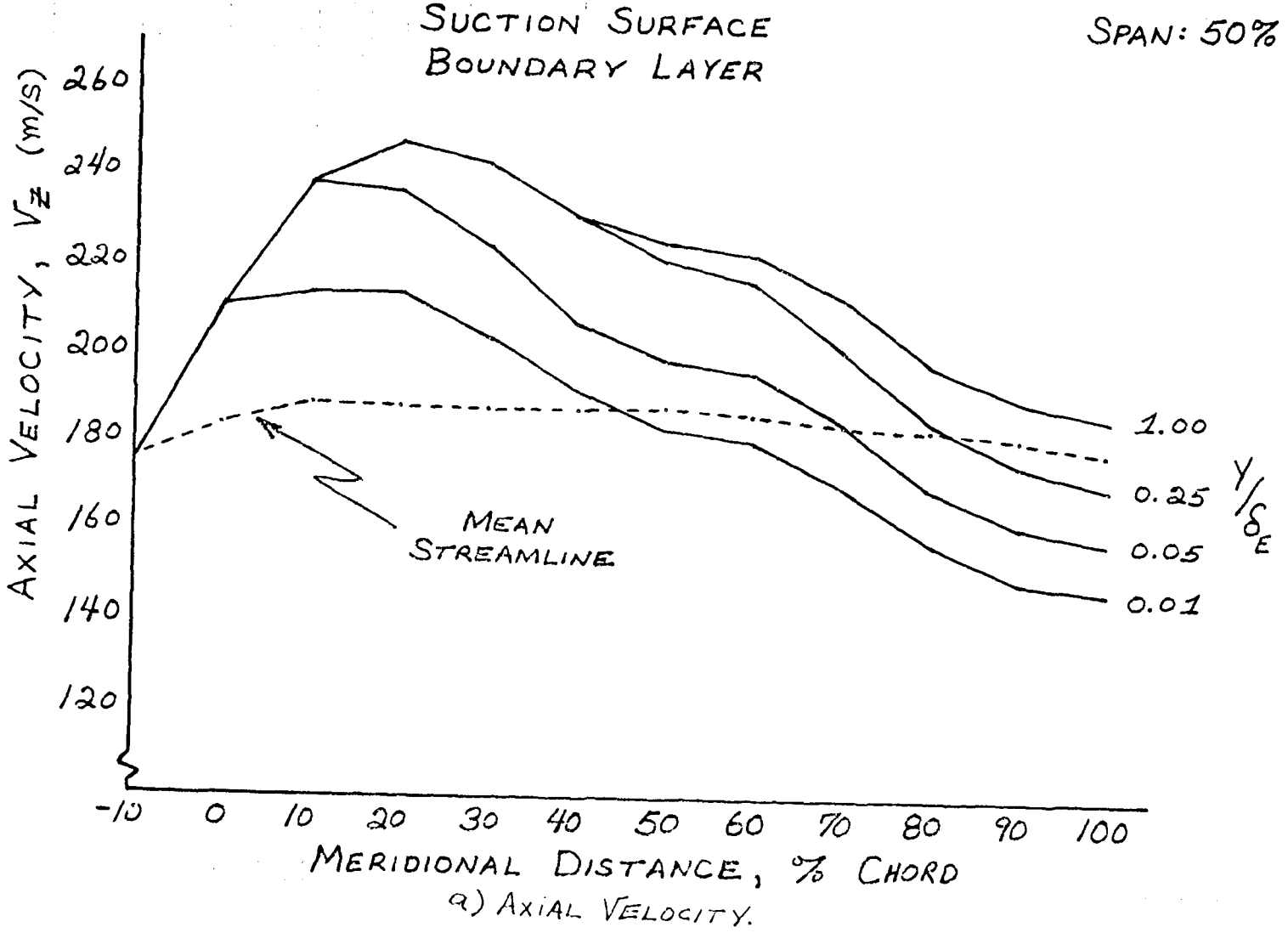

a) AXIAL VELOCITY.

FIGURE 11. SUCTION SURFACE BOUNDARY LAYER VELOCITY EVOLUTION, 50% SPAN.

AD-A100 443 VON KARMAN INST FOR FLUID DYNAMICS RHODE-SAINT-GENESE--ETC F/G 20/4
NONUNIFORM ENERGY TRANSFER IN AXIAL FLOW COMPRESSORS.(U)
JUN 80 G HOLBROOK AFOSR-80-0119
UNCLASSIFIED VKI-PR-1980-16 EOARD-TR-81-4 NL

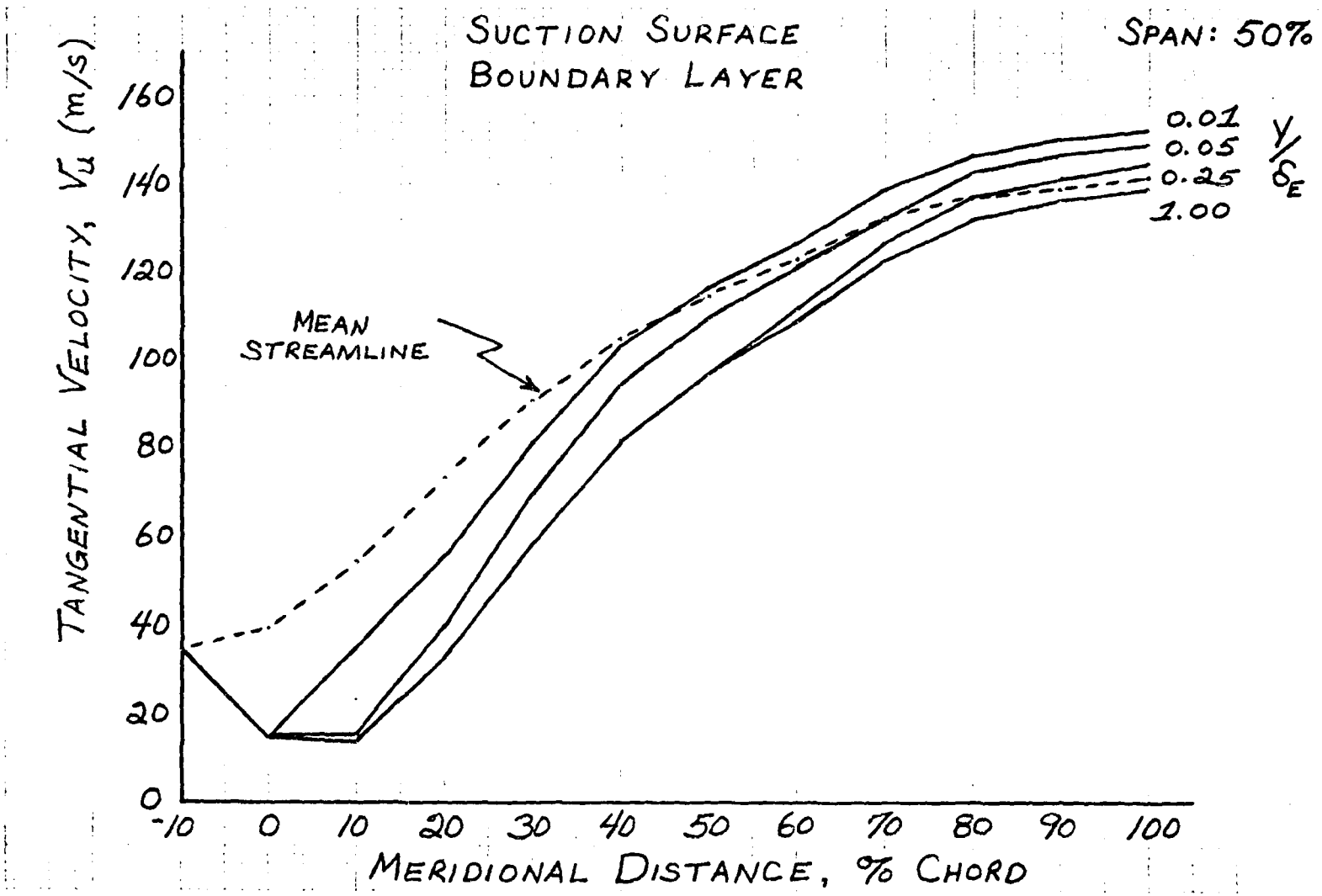

b) TANGENTIAL VELOCITY.

FIGURE 11. SUCTION SURFACE BOUNDARY LAYER VELOCITY

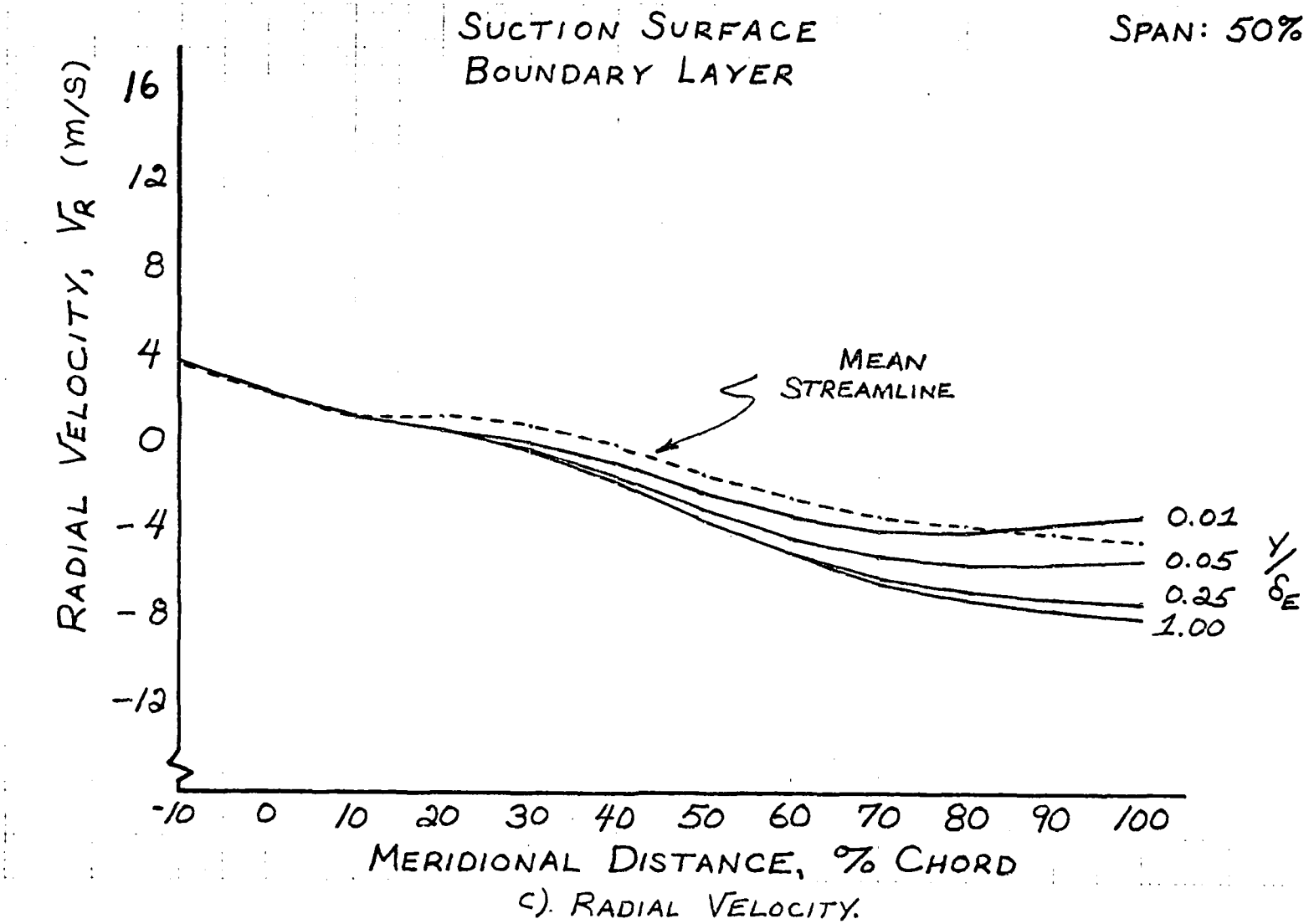

c). RADIAL VELOCITY.

FIGURE 11. SUCTION SURFACE BOUNDARY LAYER VELOCITY EVOLUTION, 50% SPAN.

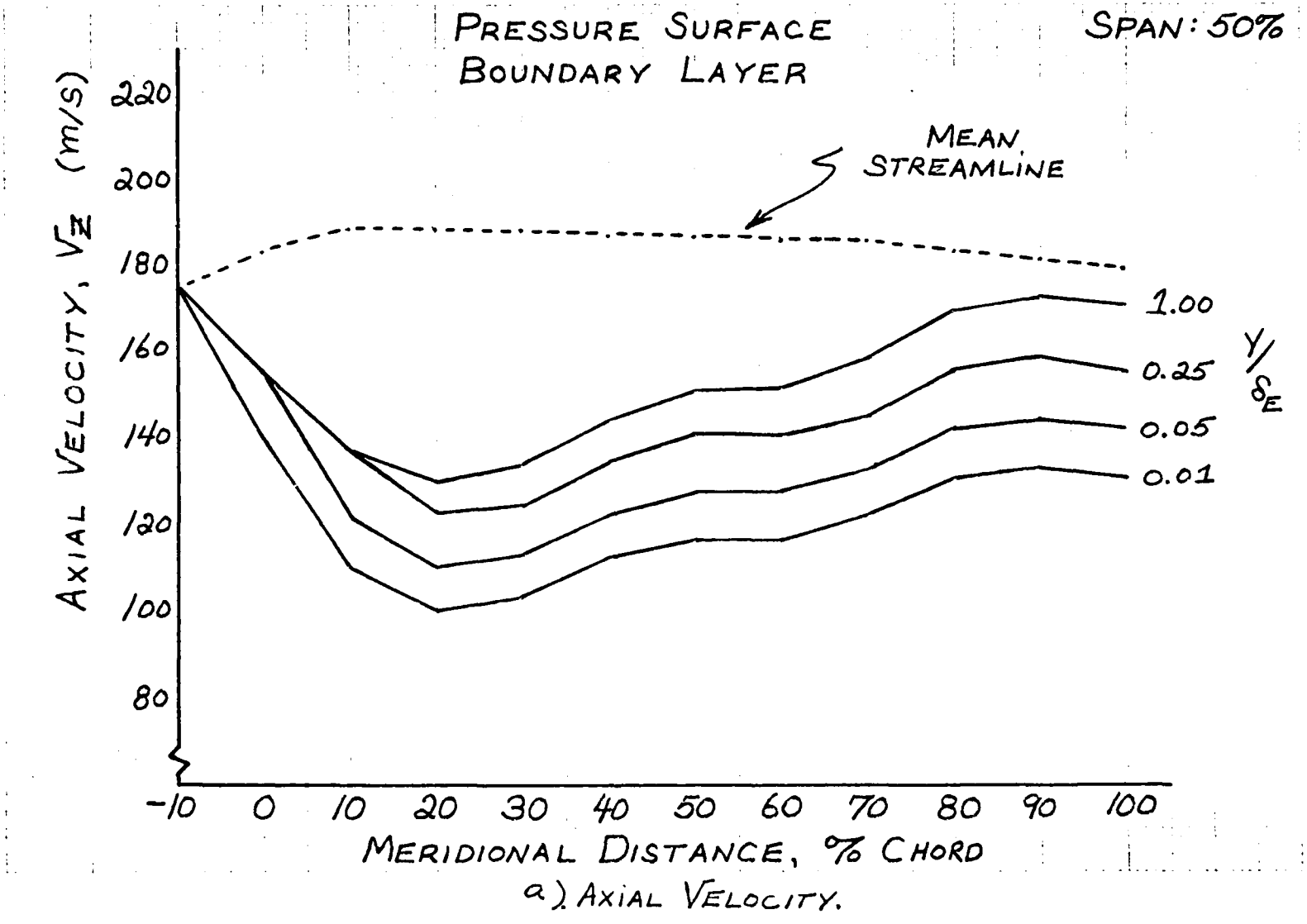

a) AXIAL VELOCITY.

FIGURE 12. PRESSURE SURFACE BOUNDARY LAYER VELOCITY

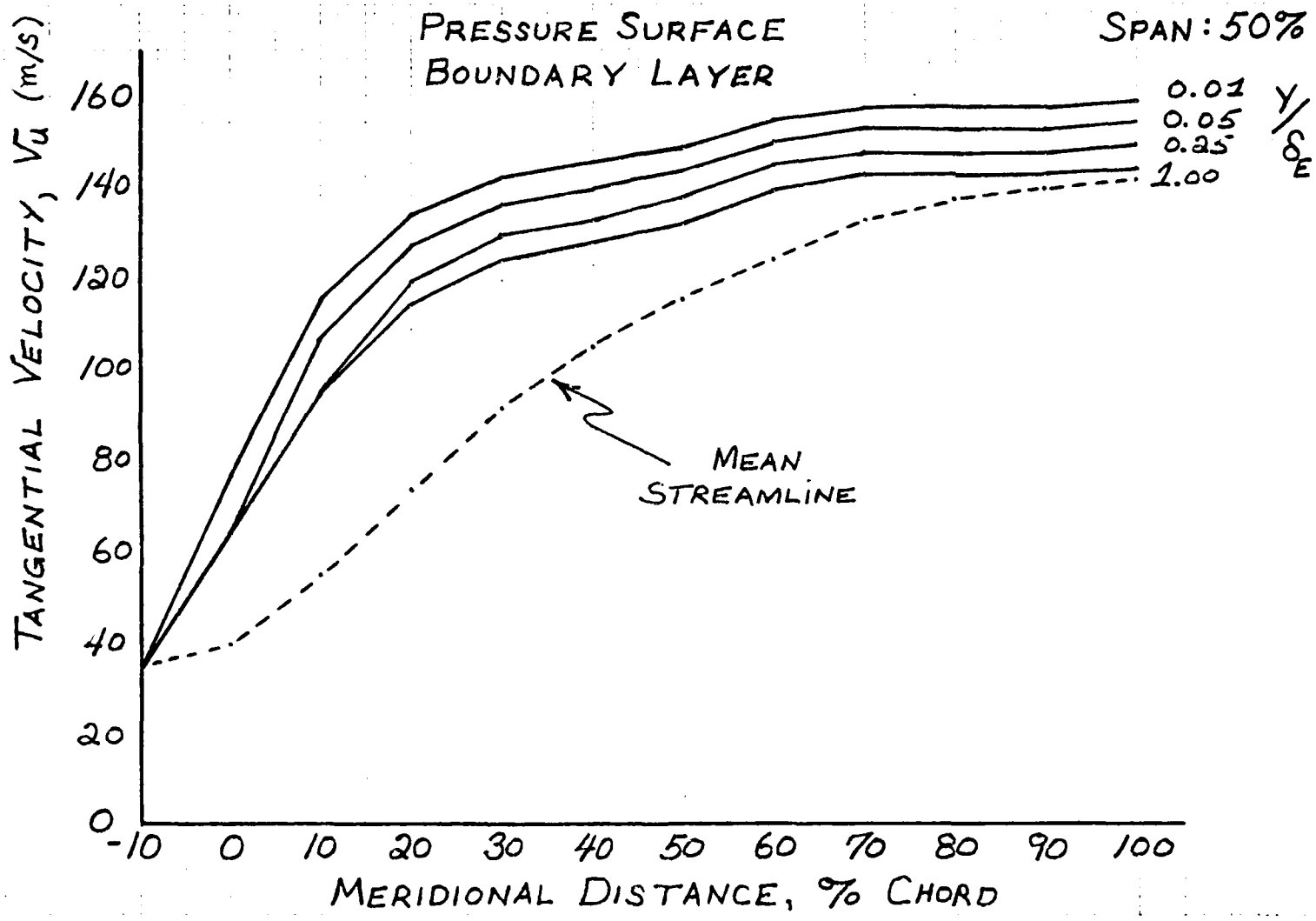

b). TANGENTIAL VELOCITY.

FIGURE 12. PRESSURE SURFACE BOUNDARY LAYER VELOCITY EVOLUTION, 50% SPAN.

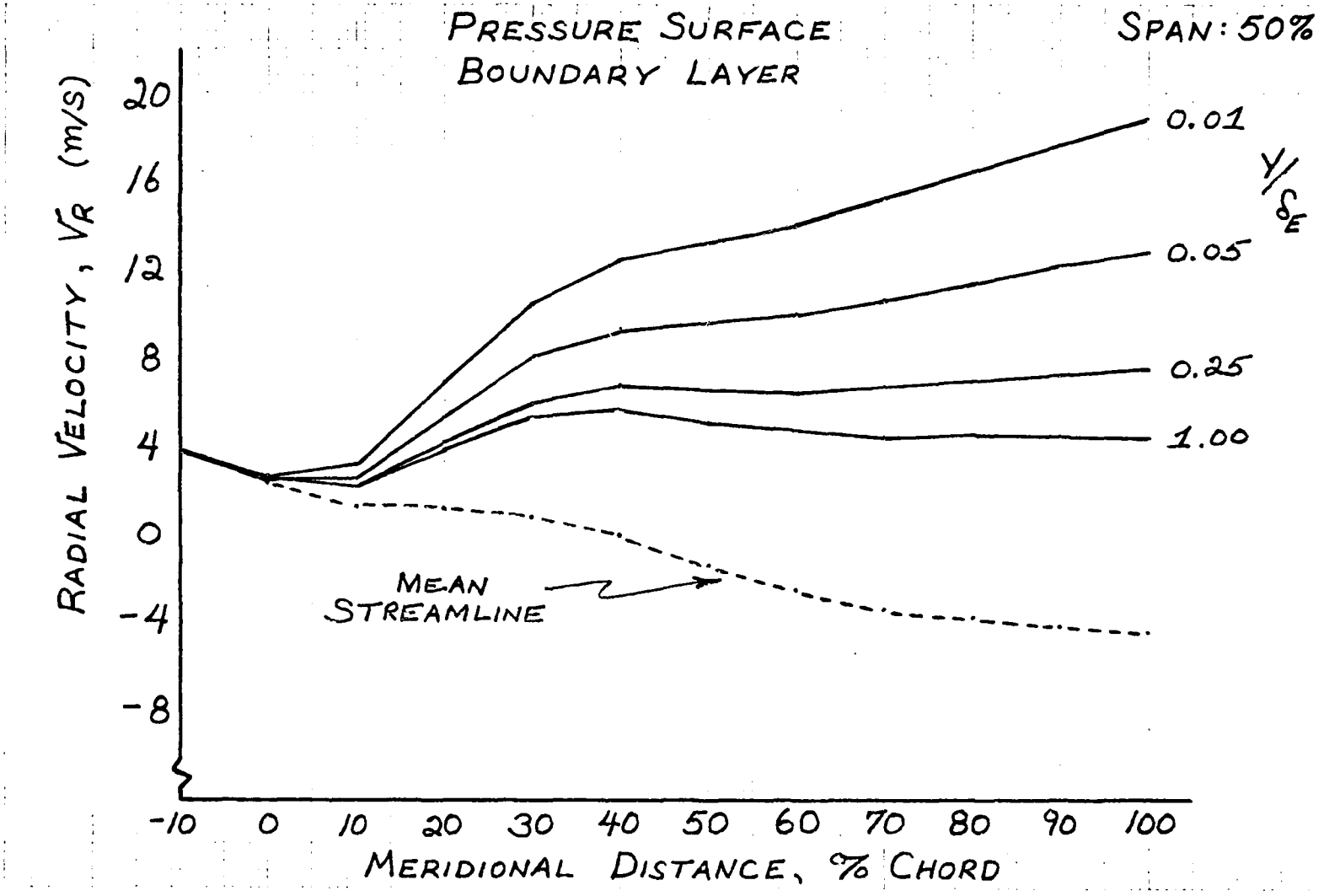

c). RADIAL VELOCITY.

FIGURE 12. PRESSURE SURFACE BOUNDARY LAYER VELOCITY

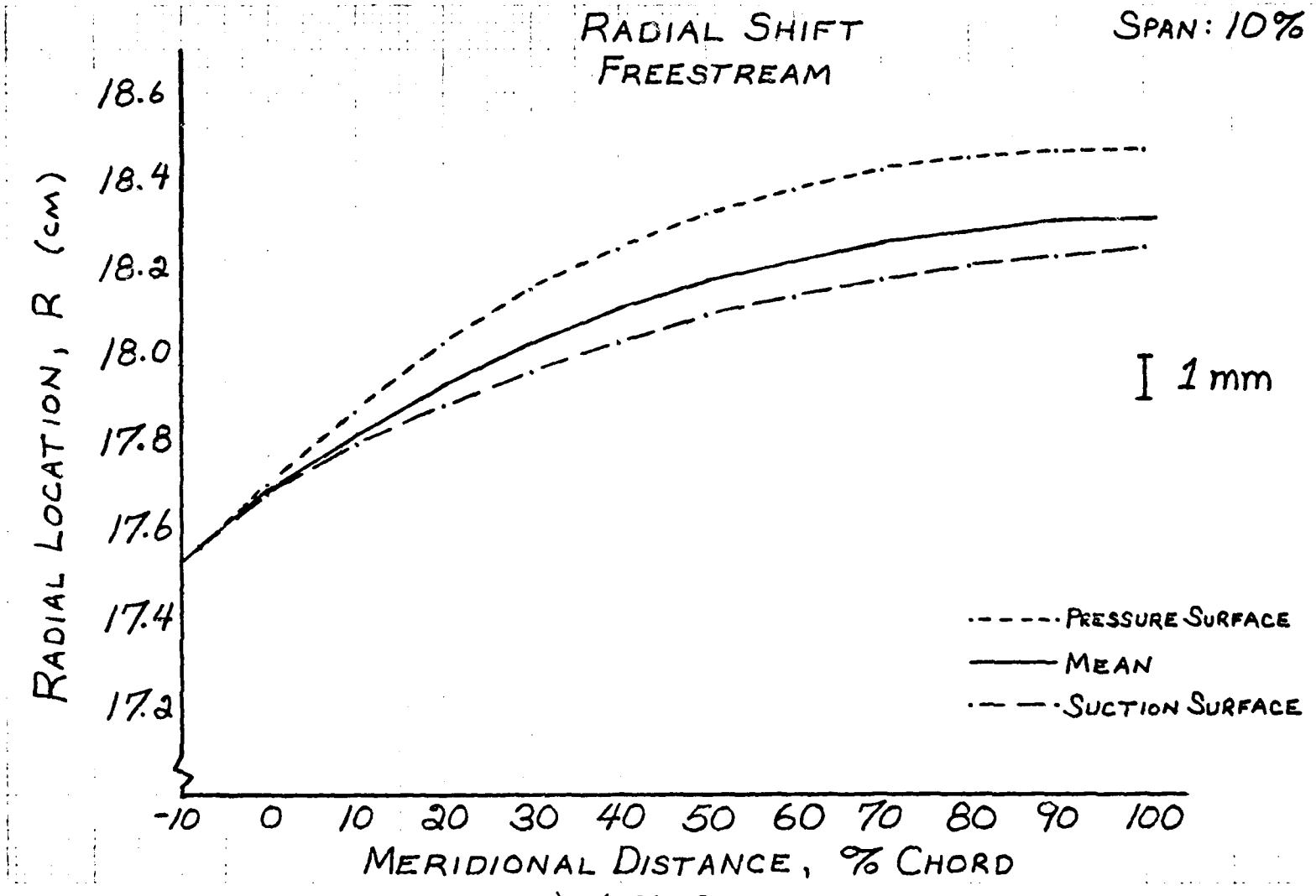

a). 10% SPAN.

FIGURE 13. FREESTREAM MERIDIONAL TRAJECTORY.

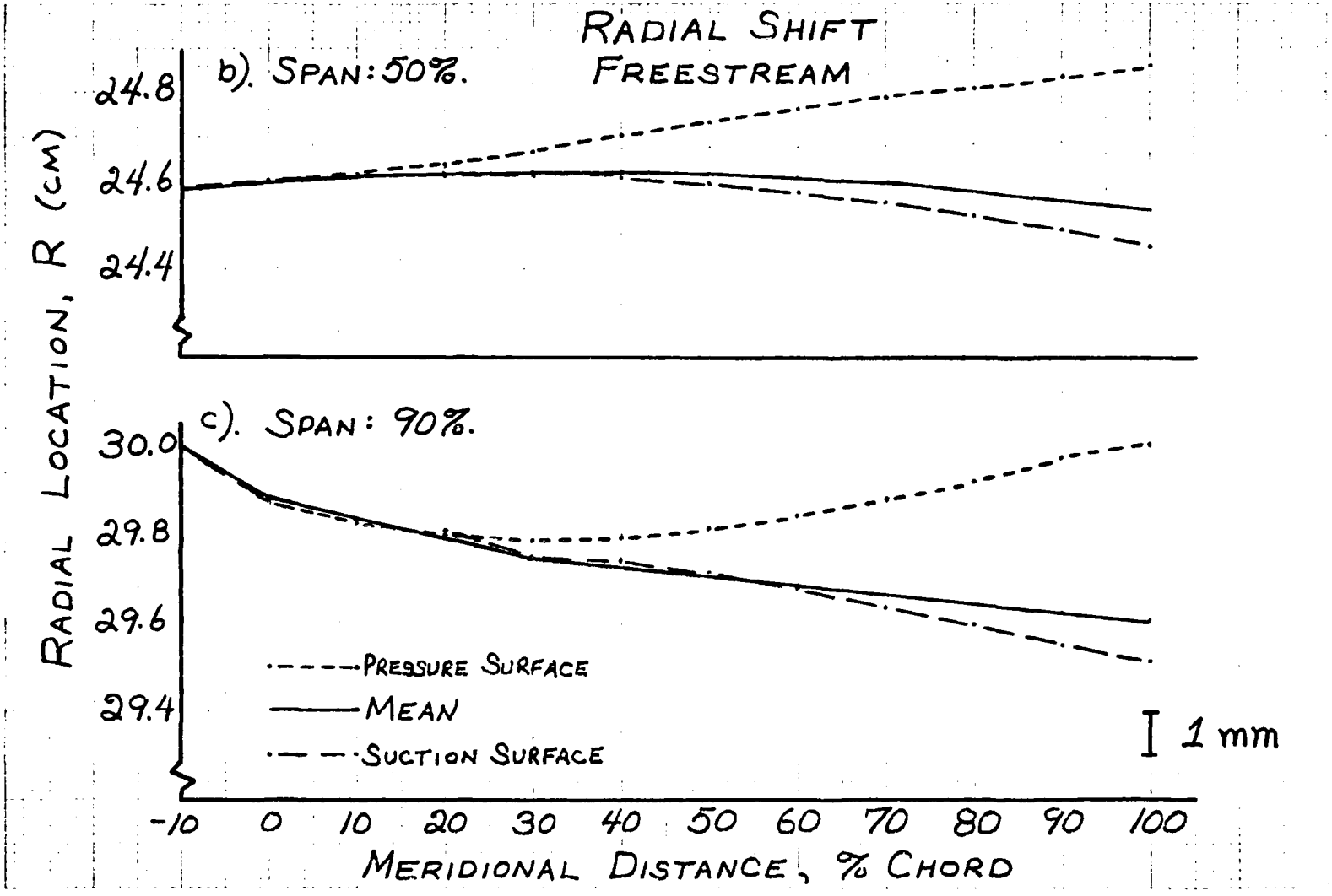

FIGURE 13. FREESTREAM MERIDIONAL TRAJECTORY.

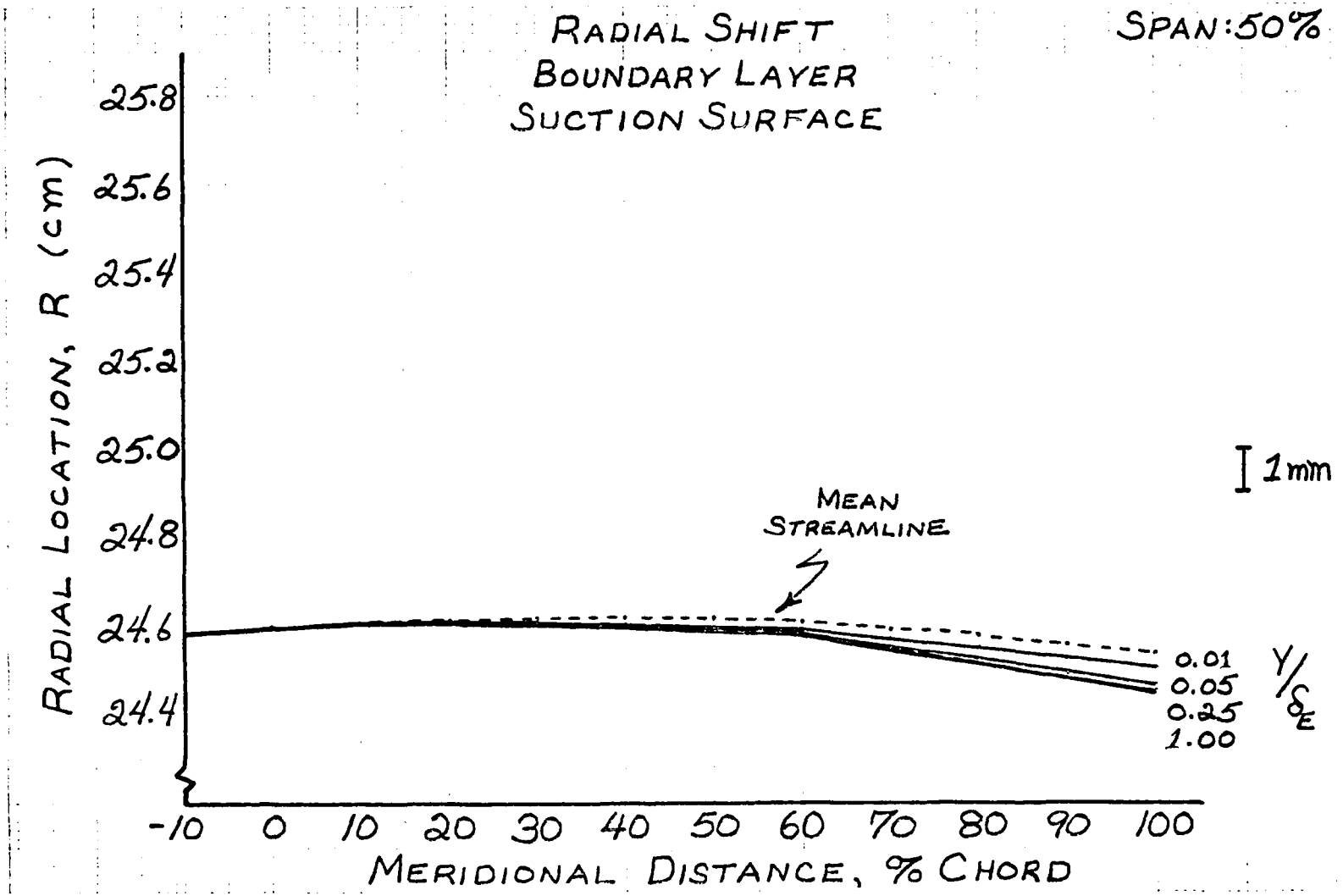

a). 50% SPAN.

FIGURE 14. SUCTION SURFACE BOUNDARY LAYER MERIDIONAL TRAJECTORY.

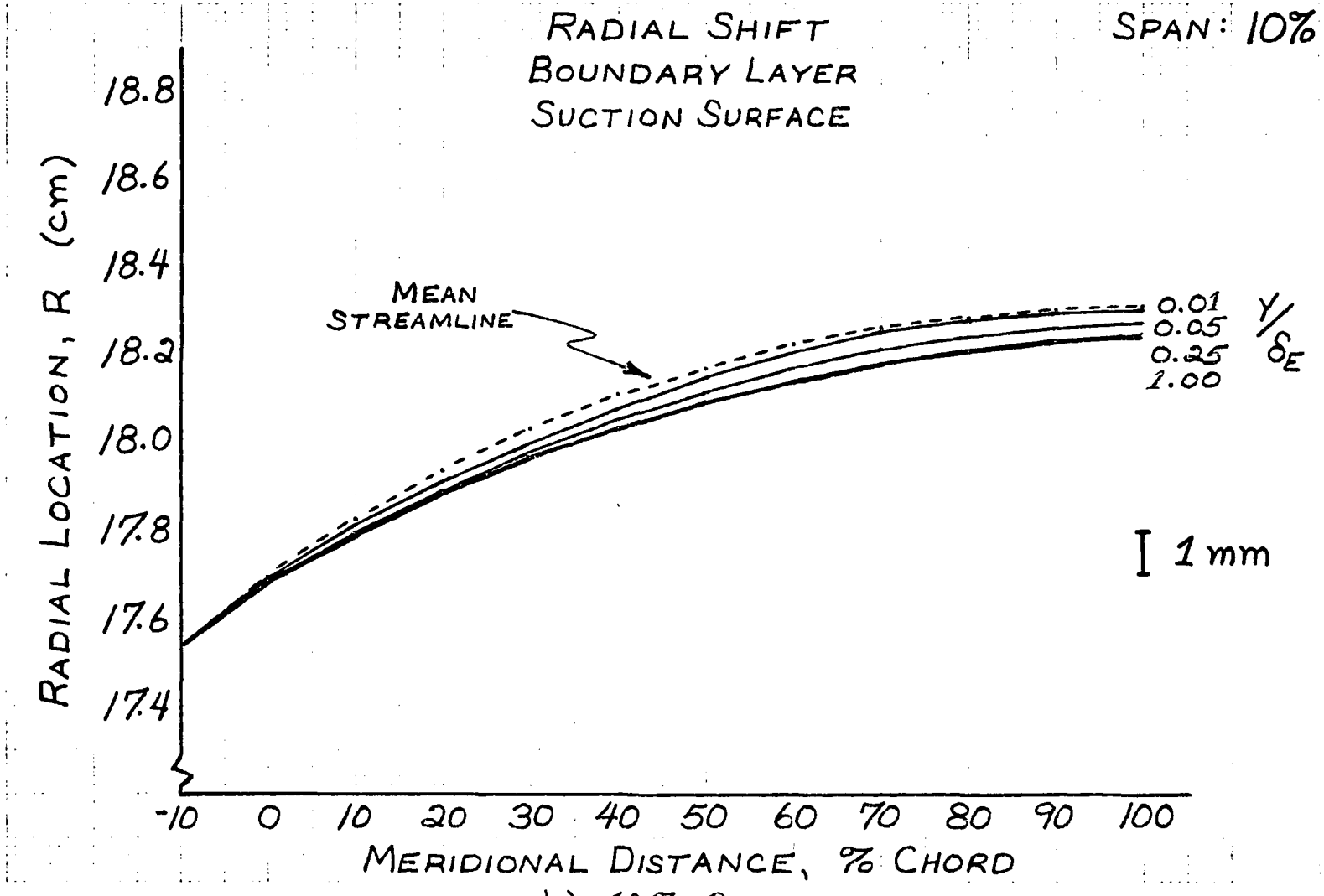

b). 10% SPAN.

FIGURE 14. SUCTION SURFACE BOUNDARY LAYER

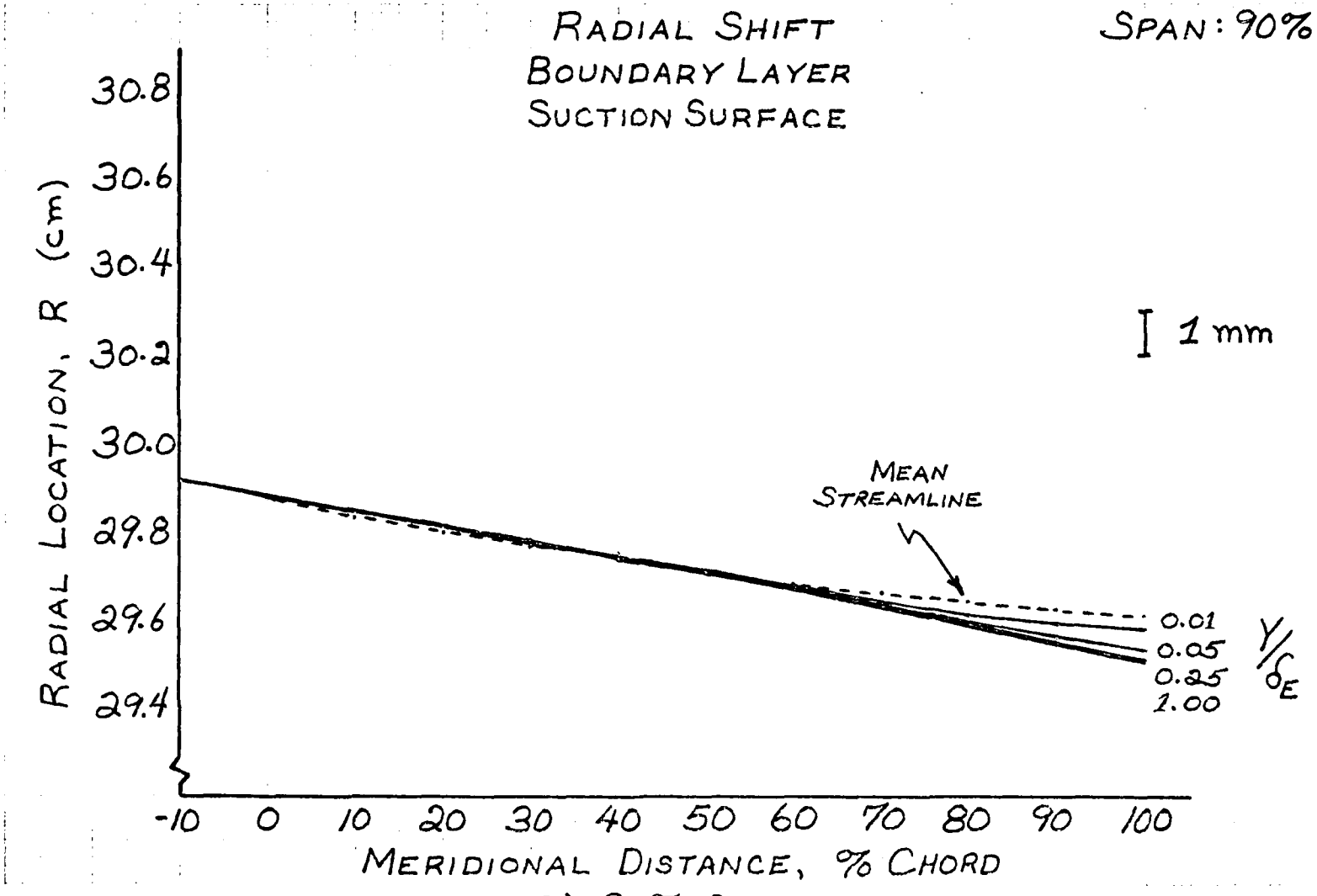

c). 90% SPAN.

FIGURE 14. SUCTION SURFACE BOUNDARY LAYER MERIDIONAL TRAJECTORY.

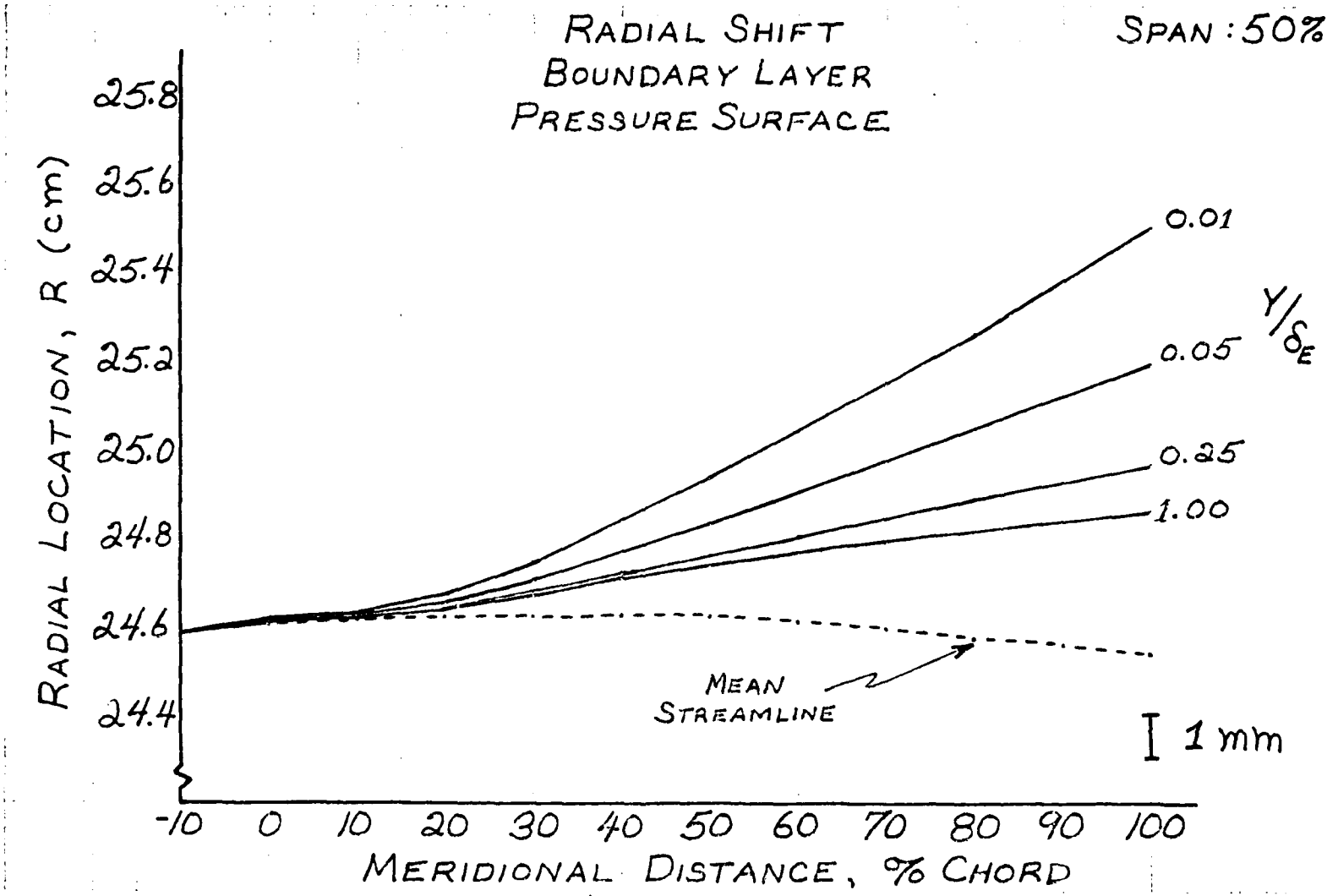

a). 50% SPAN.

FIGURE 15. PRESSURE SURFACE BOUNDARY LAYER

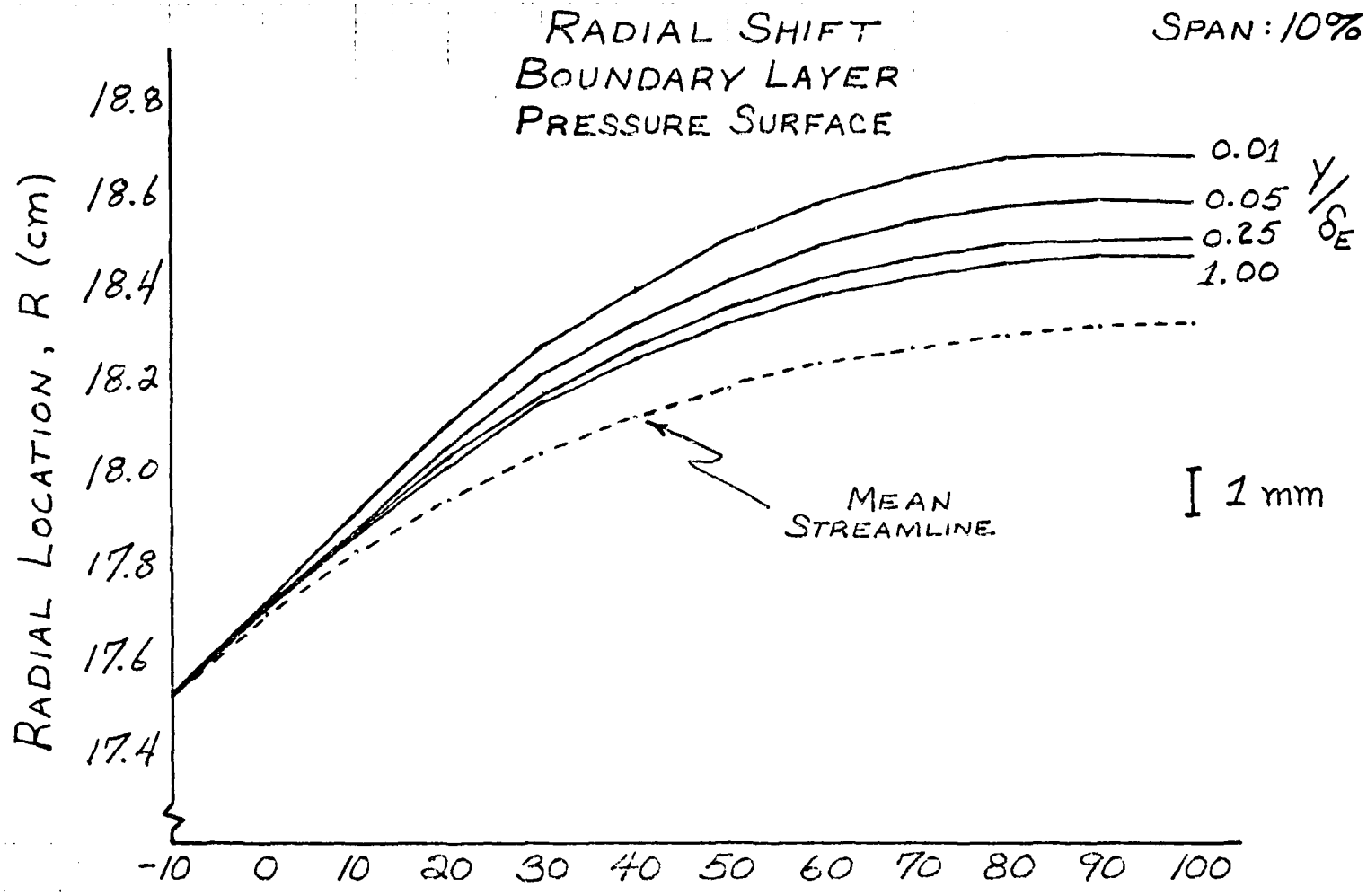

b). 10% SPAN.

FIGURE 15. PRESSURE SURFACE BOUNDARY LAYER MERIDIONAL TRAJECTORY.

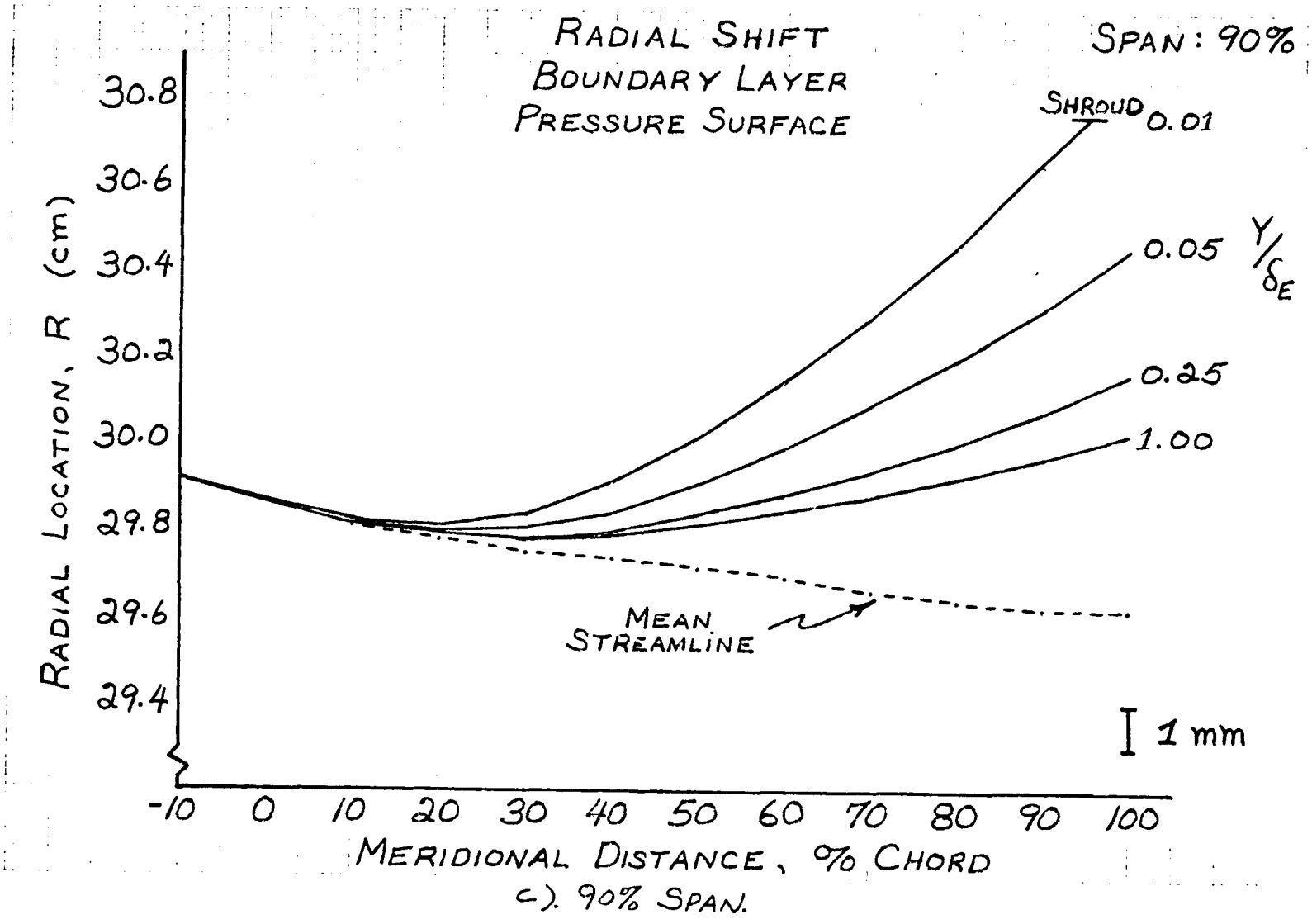

c). 90% SPAN.

FIGURE 15. PRESSURE SURFACE BOUNDARY LAYER

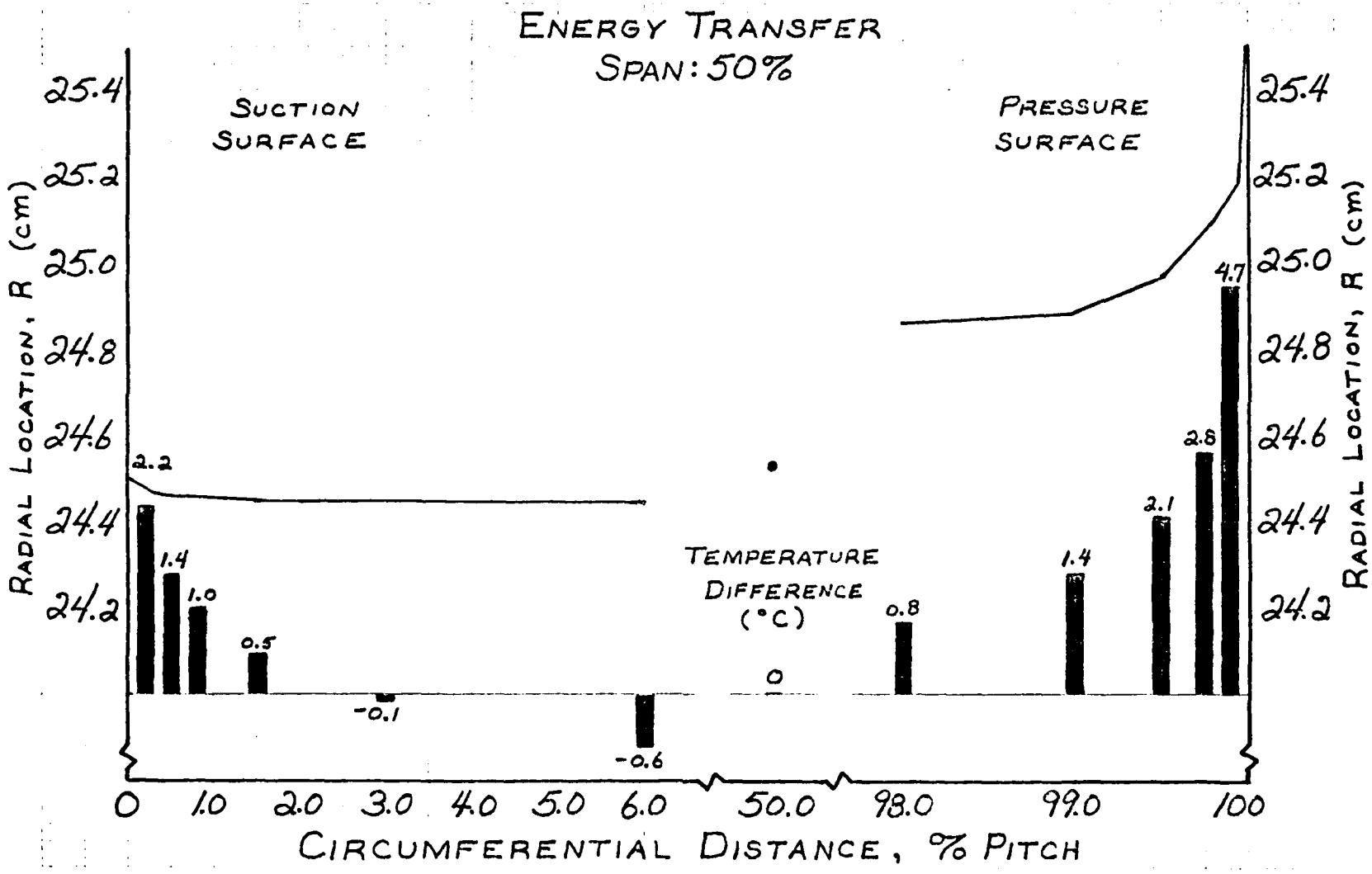

a). 50% SPAN.

FIGURE 16. CIRCUMFERENTIAL TOTAL TEMPERATURE VARIATIONS.

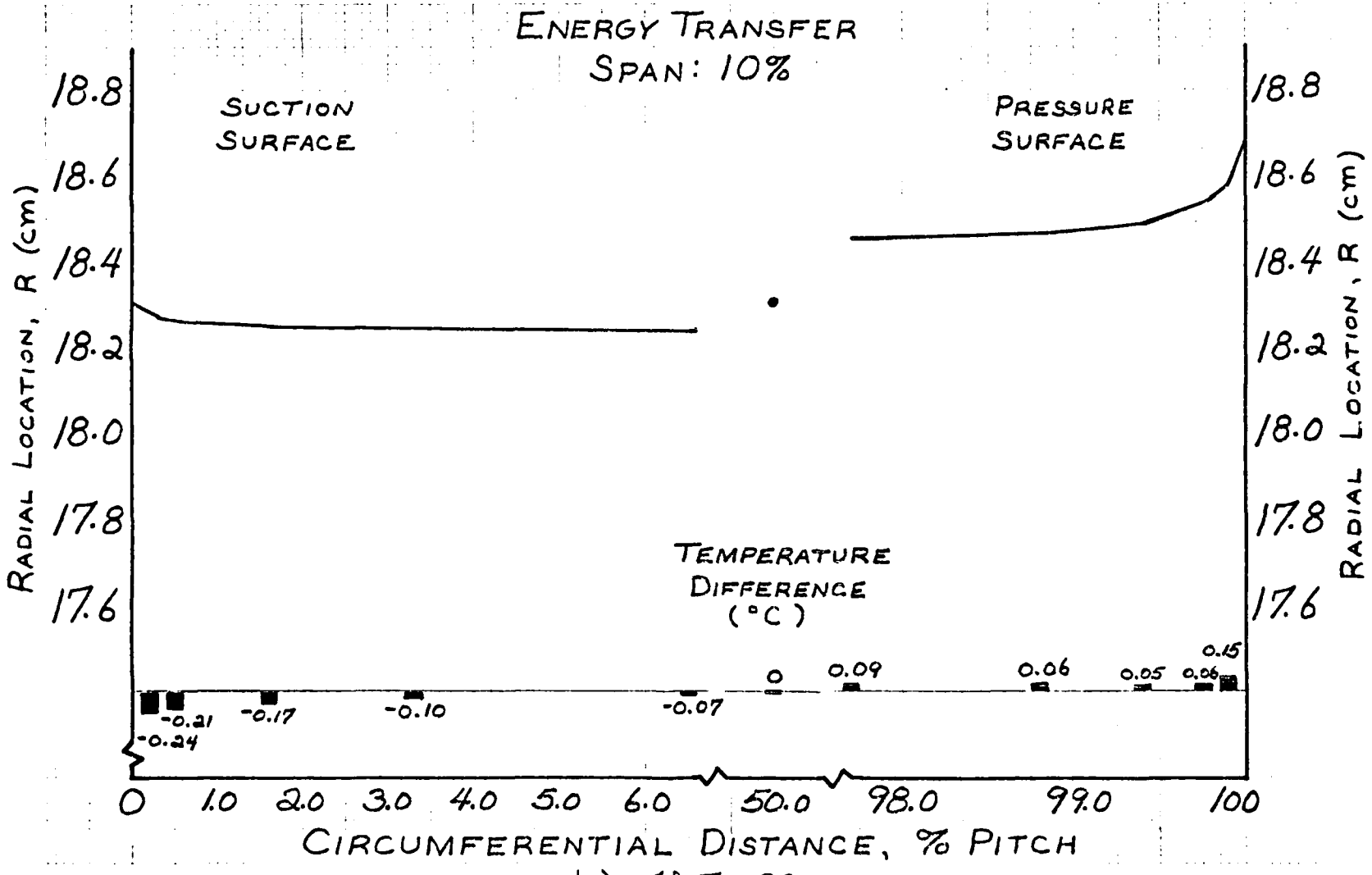

b). 10 % SPAN.

FIGURE 16. CIRCUMFERENTIAL TOTAL TEMPERATURE

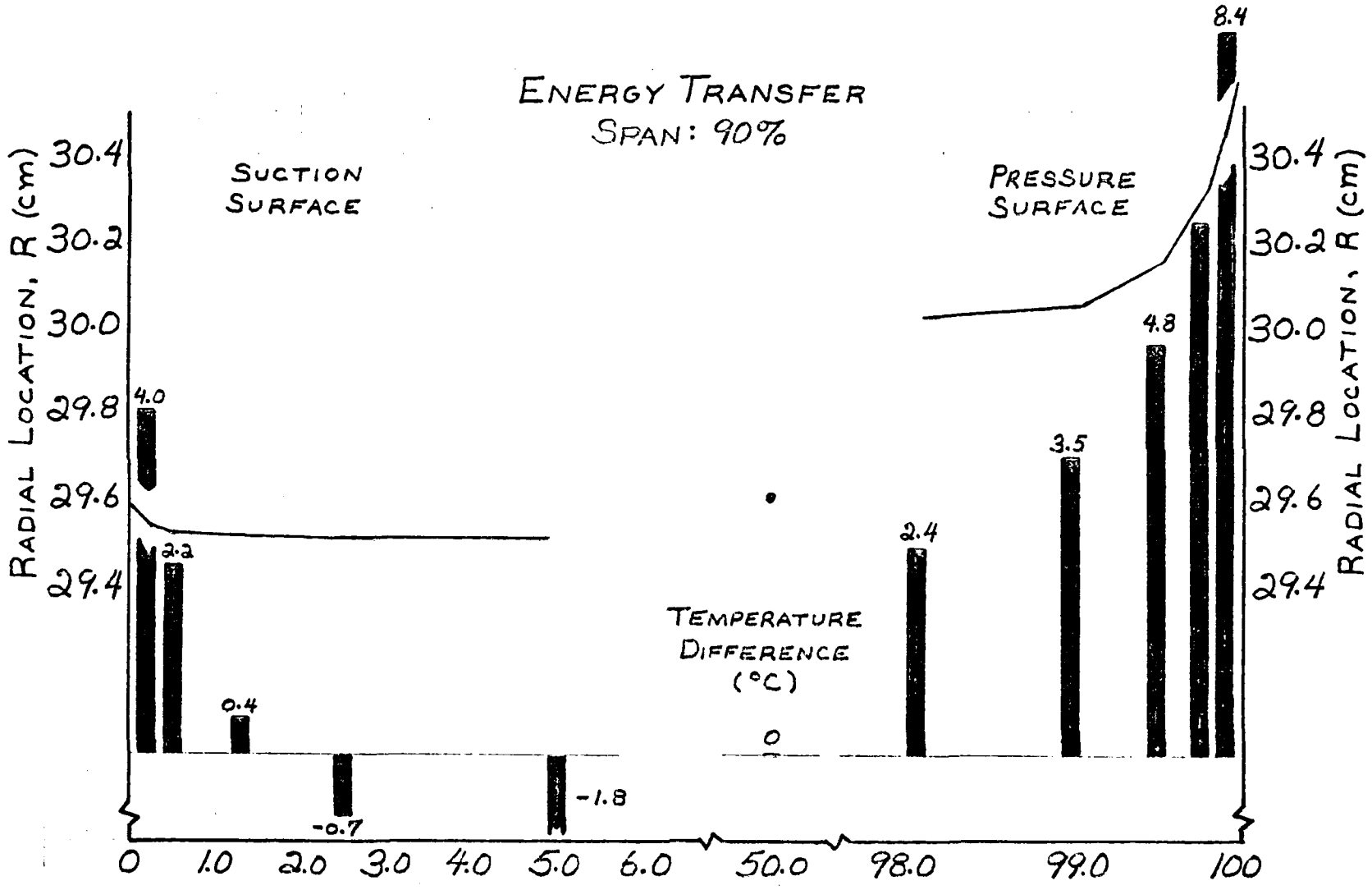

c). 90% SPAN.

FIGURE 16. CIRCUMFERENTIAL TOTAL TEMPERATURE VARIATIONS.

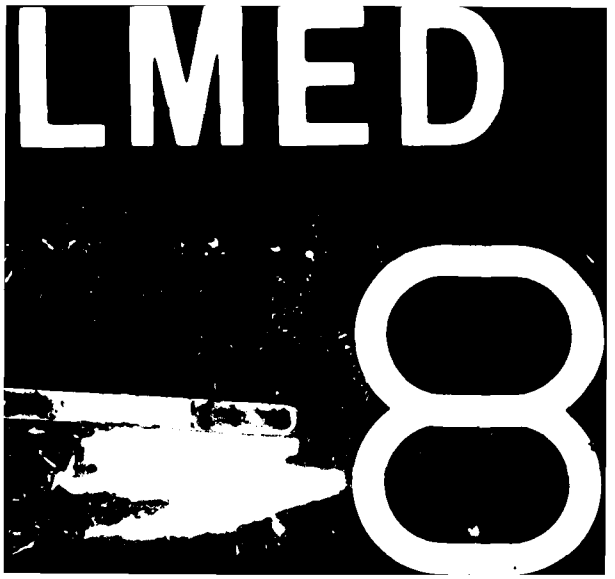
LMED
8